REPORT DOCUMENTATION PAGE

Form Approved OMB No. 0704-0188

1. REPORT DATE *(DD-MM-YYYY)*	2. REPORT TYPE	3. DATES COVERED *(From – To)*
03-10-2002	Final Report	21 June 2000 - 21-Jun-01

4. TITLE AND SUBTITLE

Comparison of Atmospheric Transmittance Measurements in the 0.4-0.7micro-m, 1.3-5.5micro-m and 8-12micro-m Spectral Regions with MODTRAN: Considerations for long path geometries applicable for Theatre Defense.

5a. CONTRACT NUMBER
F61775-00-WE013

5b. GRANT NUMBER

5c. PROGRAM ELEMENT NUMBER

6. AUTHOR(S)

Dr. Adam Devir

5d. PROJECT NUMBER

5d. TASK NUMBER

5e. WORK UNIT NUMBER

7. PERFORMING ORGANIZATION NAME(S) AND ADDRESS(ES)

IARD - Institute for Advanced Research and Development
Industry Park Tel-Hanan
Nesher, POB 271 20 302
Israel

8. PERFORMING ORGANIZATION REPORT NUMBER

N/A

9. SPONSORING/MONITORING AGENCY NAME(S) AND ADDRESS(ES)

EOARD
PSC 802 BOX 14
FPO 09499-0014

10. SPONSOR/MONITOR'S ACRONYM(S)

11. SPONSOR/MONITOR'S REPORT NUMBER(S)
SPC 00-4013

12. DISTRIBUTION/AVAILABILITY STATEMENT

Approved for public release; distribution is unlimited.

13. SUPPLEMENTARY NOTES

14. ABSTRACT

This report results from a contract tasking IARD - Institute for Advanced Research and Development as follows: The contractor will investigate atmospheric transmission modelling techniques. During the research, the contractor will take observations by infrared sensors deployed during tropospheric operations to detect objects on the Earth's surface from a manned aircraft or from an unmanned airborne vehicle (UAV) using long, near-horizontal viewing geometries. The contractor will begin by repeating measurements collected during a previous EOARD contract under desert conditions with additional instruments that will enable us to test the predictions of MODTRAN code in the 0.4-0.7 micro-m (the photopic region), and in the 1.3-5.5 micro-m and 8-12 micro-m spectral regions. The measurements proposed would be performed in Israel in the winter, summer and autumn 2000 with an infrared spectroradiometer having both high signal-to-noise ratio and high spectral resolution. The wide range of absolute humidities and air temperatures will help in the validation of the MODTRAN code with special attention to the negative temperature dependence of the water continuum in the 8-12 micro-m spectral region. The spectroradiometer will be adapted to make the measurements in 1.3-3.0 micro-m spectral region without saturation of its detector. An additional spectroradiometer will measure the slant path visibility in the 0.4-0.7 micro-m photopic spectral region. The autumn measurements will be synchronised with slant path visibility measurements that will be done in the framework of MEIDEX experiment on NASA STS-107 (November 2000).

15. SUBJECT TERMS
EOARD, Atmospheric Propagation

16. SECURITY CLASSIFICATION OF:			17. LIMITATION OF ABSTRACT	18, NUMBER OF PAGES	19a. NAME OF RESPONSIBLE PERSON
a. REPORT	b. ABSTRACT	c. THIS PAGE			David M. Burns, Lt Col, USAF
UNCLAS	UNCLAS	UNCLAS	UL	82	19b. TELEPHONE NUMBER *(Include area code)* +44 (0)20 7514 4955

IARD 61-02 (105-1-2)

Unclassified

Research Report

Comparison of Atmospheric Transmittance Measurements in the 3-5 μm and 8-12 μm Spectral Regions with MODTRAN 4.1 Long Path Geometry – Fourth Field Test

Adam D. Devir

IARD – Institute for Advanced Research & Development

August 2002

00-WE013 004013

Contract F61775-~~98-WE082~~, Project SPC-~~98-4042~~, EOARD, USAF.

Comparison of Atmospheric Transmittance Measurements in the 3-5 μm and 8-12 μm Spectral Regions with MODTRAN4.1 Long Path Geometry – Fourth Field Test	
Date: 22/07/02	Authors: Dr. A. D. Devir
Classification: Unclassified	Checked by: Prof. A. Lessin
Requested by: EOARD USAF	Approved by: Dr. Y. Bushlin
Order number: Contract F61775-98-WE082, Project SPC-98-4042, EOARD, USAF, Item 0002	Report type: Final Research Report
Distribution: EOARD USAF	Language: English
Remarks:	Reference: IARD 61-02 (105-1-2)

ABSTRACT

This work was performed as a part of the contract **F61775-98-WE082** "***Comparison of Atmospheric Transmittance Measurements in the 3-5μm and 8-12μm Spectral Regions with MODTRAN: Consideration for long path geometries***", in accordance with the item 0002 of the project SPC-98-4042.

Radiance measurements conducted during tropospheric operations to detect objects on the Earth's surface from a manned aircraft or from an unmanned airborne vehicle (UAV) will involve long, near-horizontal viewing geometries. The computer code MODTRAN is widely used for the prediction of the propagation of infrared radiation through the lower atmosphere.

This program was undertaken by the IARD to test and validate the predictions of the MODTRAN code for the 3-5μm and 8-12μm spectral regions under semi-arid desert conditions with well defined meteorological parameters.

The first stage of the project included preparation and performing field-test experiments. The final stage includes analysis of received experimental data and performing parametric calculations of atmospheric transmittance by code MODTRAN 4.1.

This document describes results of the performed analysis and comparison of the theoretical predictions of MODTRAN 4.1 to the experimental results that were obtained in the fourth field test that was carried out in the Negev in 14-16/7/02. The test results show rather very good agreement between the MODTRAN 4.1 predictions and the experimental data. However the MODTRAN code doesn't follow the changes in the visibility as the experimental data. It is imperative to improve the accuracy by which the water profile is measured in th test site – radiosonde and ground clamping are not accurate sufficiently.

Principal investigator: **Dr.** Adam D. Devir

IARD–Institute for Advanced Research & Development

CONTENTS

1. INTRODUCTION

Objective

The purpose of this research was to refine space atmospheric transmittance measurements in the 3-5 and 8-12 μm spectral regions and to compare them with the latest predictions of the MODTRAN code. Past experimental work [1,2] had demonstrated that the computer code MODTRAN 4.1, widely used for the prediction of the propagation of infrared radiation through the lower atmosphere, gives rather good agreement with experimental results.

The results of the studies reported herein have a strong impact on the use of this validated code to predict data obtained from IR sensors to be deployed for observation and detection of objects located on the Earth's surface. These sensors can be located either on manned aircraft or on unmanned airborne vehicle (UAV). The fact that some of these observation are planned to be made in very long near horizontal optical paths requires the validity of this code at the extreme of its potential use.

Early atmospheric transmittance measurements at slant paths to space using the sun as a radiation source were conducted in Israel already in June 1990. These measurements were made in the 3-5μm and 8-12μm spectral region with spectral resolution of $\Delta\lambda/\lambda=0.04$. The instrument used was a circular-variable-filter (CVF) spectroradiometer. The comparison of the experimental results with MODTRAN predictions showed good agreement in the 3-5μm spectral region but poorer agreement in the 8-12μm spectral region [1].

Following these early measurements EOARD supported a more intensive campaign of field tests of atmospheric transmittance measurements in long near-horizontal path geometries under desert conditions, if possible. This campaign took take place in Israel in two winters and one summer: November 1998 - January 1999, March 2001 and May 2002. During these periods we managed to make three field tests. The tests that took place in Mitzpe' Ramon (altitude 850m) in the southern part of Israel (the Negev). The results of these tests were published in three research reports that were submitted to EOARD in June 1999 (IARD 15-99), in June 2001 (IARD 40-01) and in June 2002 (IARD 57-02) all under Contract

F61775-98-WE082, Project SPC-98-4042, EOARD, USAF.

This report summarises the fourth field test that took place in July 2002 with special emphasis on the validation of the role of the aerosols on the slant visibility. This test was a part of MEIDEX - the scientific test of the Tel Aviv University, Department of Geophysics and Planetary Sciences, with ISA - the Israeli Space Agency, that was planned with NASA in the framework of FREESTAR payload during STS-107. Unfortunately, the launch of STS-107 was postponed from July 19, 2001 to the next fall and thus we were compelled to execute the last field test in July without the space shuttle support because we couldn't postpone the last field test under this contract beyond August 2002.

A general view of the experimental set-up in this site is shown in Figure 1. The SR-5000 spectroradiometer (with its new optical design) and the "Green" radiometers that were used to measure the visibility (see report IARD 40-01) are shown boresighted on single manually operated pan&tilt head while the teodolite is located on a different pedestal (not shown in this figure).

In this field-test we made good atmospheric transmittance measurements during July 14th, 15th and 16th. However, we had to spend more days during this test waiting for good visibility conditions and no indications for thin cirrus clouds.

2. THE FIELD TEST

The Experimental Set-up

The experimental set-up in this field-test (See Figure 1) and is based on the SR-5000 spectroradiometer made by CI and a special visible radiometer (called "Green" radiometer) that was already used in the second test.

A) The SR-5000 spectroradiometer

For the actual radiometric measurement of the sun we used the SR-5000 spectroradiometer that has a spectral resolution of $\Delta\lambda/\lambda=0.02$ (according to the manufacturer). This is a CVF spectroradiometer with a Newtonian optics with 5" aperture (12.5cm) and focal length of 20" (51cm) - F#=4.0. The main advantages of this completely computerised spectroradiometer are its ruggedness, its suitability for field experiments and its simple and easy modes of operation. The SR-5000 can make a complete spectral scan within a predetermined time (from 0.1sec to 64sec). We decided to operate it at an optimal scan rate of 2sec/scan. The corresponding chopper (50% duty cycle) frequency was chosen to be 800Hz. The SR-5000, the CVF and the CMT detector used in this test were the same that was used in the third field-test (see details in report IARD 57-02).

B) **The visibility radiometer**

The role of the visibility radiometer was already explained in the second report. However it will be brought also here for the integrity of this report.

The atmospheric transmittance depends on the aerosol attenuation (scattering and - to less extent - absorption) as well as on the molecular attenuation, we wanted to validate separately the contribution of the aerosol attenuation. Usually the aerosol attenuation is derived from the visibility through the relation VIS=3.912/β, where β is the extinction coefficient (km^{-1}) in the 0.55μm spectral region (the centre of the photopic band). We usually establish the visibility values from the reading of a visibility meter that measures the visibility from the number of photons that are scattered from a well-defined scattering volume. This instrument was checked by us and was found to have an error of $0.02km^{-1}$ in β (see Figure 2). As a result it cannot operate properly when high values of visibility. WE also used specific landmarks (located horizontally at distances from 10km to 80-90km) to check the readings of this instrument.

In order to use validated visibility values in the MODTRAN code, we obtained them from the measured transmittance in slant paths between the sun and the experimental site with actual measurements. For this purpose we had built a special radiometer (named by us as the "Green" radiometer – see IARD 40-01) that measured the attenuation of the atmospheric aerosols. In the design of this radiometer we had two goals: We wanted to use similar calibration methods for both this radiometer and the SR-5000 and we wanted to avoid that any absorption by molecular species will affect its readings.

Since in the calibration stage and in the measurement stage the radiation source (the calibration blackbody and the sun, respectively) fill the FOV, we had to compensate for the large difference between the spectral radiance (temperatures) of these two blackbody sources. To accomplish this we made an attenuating mask from a metal plate dark painted in its internal face that had few small aperture-holes arranged symmetrically around the clear aperture of the radiometer. This plate was placed in front of the aperture of the radiometer

during the measurements of the sun that is considered to radiate as blackbody at 5900K. This mask was removed during the calibration stage. This mask enabled us to accomplish the first goal.

To accomplish the second goal we had checked the upper part of the visible and the near IR (0.5-1.0μm) spectral regions for atmospheric "windows" in which the atmospheric transmittance is affected only by scattering of aerosols (that depend on the Visibility) and on the known molecular (Rayleigh) scattering. The only wavelength "window" that was found is the 0.86-0.88μm band (see Figure 3). This "window" is not spectrally far from the photopic region - used to define the visibility - and being in the NIR it enables to make an attenuating mask with reasonable attenuation factor. The spectral transmittance of the filter that finally was chosen (CW=869nm, FWHM=10nm) is shown in Figure 4. This "window" enabled us to work with attenuating mask that has attenuation factor of 138.

The designed radiometer is based on Newtonian optics with aperture of 15cm (6") and a focal length of 61cm (24") (F#4). A fast mechanical chopper operating at 870Hz chops the incoming radiation before it enters a field stop with diameter of 0.3mm or 0.5mrad. The radiation from this field stop passes the filter and then falls on a Si detector. A digital lock-in amplifier (model SR830 DSP) was used to measure the radiometric signal of the sun and the calibration blackbody.

Since the measurement of the sun is done with the "Green" focused to infinity therefore we calibrated it with a combination of an off-axis collimator and a blackbody at 1200C (1473K). In this calibration the radiometer was left aligned to infinity but the total reflectance of the optics of the off-axis collimator was taken into account. This value was taken from the data sheet of the collimator (0.92) and lately measured by us as 0.917.

The slant path transmittance can be expressed as:

(1) $$\tau=[V_m(\theta)V_c]\cdot[<P(1473K)>_{filter}\cdot 0.92]/[<P(5900)>_{filter}/138]$$

Where V_c is the signal measured during the calibration, $V_m(\theta)$ is the signal measured with the sun at zenith angle θ and $<P(T)>_{filter}$ is Planck's function for temperature T(K) weighted by the filter transmittance.

The measurement theory

The atmospheric transmittance measurements with the SR-5000 are based on a very simple theory because both the calibration process of the spectroradiometer by external blackbody and the measurements of the sun are made with full FOV. A full FOV means that the angular dimension of the measured object is larger than the angular dimension of the FOV. In this configuration the dependence of the measured signal on the measurement distance is only through the effect of the atmospheric transmittance and the actual size of the FOV (see below). In our tests the calibration was done from a distance of about 15m. This distance is sufficient small so that the angular dimension of the aperture of the blackbody (diameter = 22.2mm or 1.48 mrad) was larger than the FOV (0.5mrad).

It can be shown that during the calibration the measured signal $V_c(\lambda)$ can be expressed as:

$$(2) \qquad V_c(\lambda) = K \cdot FOV_c^2 \cdot \{P(T_c, \lambda) \cdot \tau_c(L_c, \lambda) - P(T_{ibb}, \lambda)\} \cdot A_{rad} \cdot F(\lambda) \cdot R(\lambda)$$

Where: $V_c(\lambda)$ is the measured signal (V).

K is a proportionality constant (Volt/Watt).

$P(T_c, \lambda)$ is Planck's function at $T_c = 1273K$ (Watt/str·cm^2·μm)

$\tau_c(L_c, \lambda)$ is the atmospheric transmittance for the calibration distance L_c.

L_c is the calibration distance (cm).

$P(T_{ibb}, \lambda)$ is Planck's function at the temperature of the internal blackbody.

FOV_c is the angular dimension of the FOV of the SR-5000 during the calibration stage (mrad).

A_{rad} is the clear aperture of the SR-5000 (cm^2).

$F(\lambda)$ is the spectral transmittance of the CVF

$R(\lambda)$ is the relative response of the InSb/CMT detector.

Calculation shows that the radiance of the internal blackbody (T_{ibb}=300K) which is the second term in the { } in Eq. 2 is very small compared to radiance of the calibration blackbody (T_c=1273K) which is the first term in { } and therefore can be neglected. Hence Eq. 2 can be rewritten as:

(3) $$V_c(\lambda) = K \cdot FOV_c^2 \cdot P(T_c, \lambda) \cdot \tau_c(L_c, \lambda) \cdot A_{rad} \cdot F(\lambda) \cdot R(\lambda)$$

The signal obtained during the measurement of the sun - $V_m(\lambda)$ - can be expressed as:

(4) $$V_m(\theta, \lambda) = K \cdot FOV_m^2 \cdot A_{rad} \cdot F(\lambda) \cdot R(\lambda) \cdot \{P(T_s, \lambda) \cdot \tau_m(\theta, \lambda) + I_{scatt}(\lambda) + [1-\tau_m(\theta, \lambda)] \cdot P(T_{amb}, \lambda) - P(T_{ibb}, \lambda)\}$$

Where: $V_m(\theta, \lambda)$ is the measured signal as a function of the zenith angle θ (V).

$P(T_s, \lambda)$ is Planck's function at T_s = 5900K[3] (Watt/str·cm^2·μm).

$\tau_m(\theta, \lambda)$ is the ground-to-space atmospheric transmittance for zenith angle θ.

$P(T_{ibb}, \lambda)$ is Planck's function at the temperature of the internal blackbody.

FOV_m is the angular dimension of the FOV of the SR-5000 during the measurement of the sun (mrad).

The second term, which is the solar radiance scattered into the FOV (by the atmosphere and by internal surfaces located in the SR-5000) was measured (by measuring the sky very close to the solar disk) to be is very small compared to the first term (see below).

The third term (the path radiance) and the fourth term (the radiance of the internal blackbody) tend to cancel each other as can be seen from rearranging the terms that appear in Eq. (4):

(4A) $$V_m(\theta, \lambda) = K \cdot FOV_m^2 \cdot A_{rad} \cdot F(\lambda) \cdot R(\lambda) \cdot \{\tau_m(\theta, \lambda) \cdot [P(T_s, \lambda) - P(T_{amb}, \lambda)] + [P(T_{amb}, \lambda) - P(T_{ibb}, \lambda)]\}$$

Since $P(T_s, \lambda) >> P(T_{amb}, \lambda)$ and since $P(T_{amb}, \lambda) \approx P(T_{ibb}, \lambda)$ then Eq. (4A) can be rewritten without the second and the third terms as:

(5) $$V_m(\theta, \lambda) = K \cdot FOV_m^2 \cdot A_{rad} \cdot F(\lambda) \cdot R(\lambda) \cdot P(T_s, \lambda) \cdot \tau_m(\theta, \lambda)$$

From Eqs. (5) and (3) we obtain that the ground-to-space atmospheric transmittance for zenith angle θ - $\tau_m(\theta, \lambda)$ - can be expressed as:

(6) $$\tau_m(\theta, \lambda) = \tau_c(\lambda) \cdot [V_m(\theta, \lambda)/V_c(\lambda)] \cdot [P(T_c, \lambda)/P(T_s, \lambda)] \cdot [FOV_c/FOV_m]^2$$

The last term is due to the fact that the FOV of the spectroradiometer is determined by the equation:

(7) $$FOV = \pi \cdot (d/v)^2/4$$

Where **d** is the diameter of the field stop and **v** is the distance between the field stop and the primary mirror. During the measurement of the sun is measured the SR-5000 is focused to infinity so that v = f. However, during the calibration stage the SR-5000 was focused to distance L_c =15.8 and not to infinity. Simple calculation show us that $v = f \cdot [L_c/(L_c - f)]$.
For f = 50.8cm (20") and L_c = 1580cm one obtains that v = 52.5cm. Hence, one obtains that:

(8) $$[FOV_c/FOV_m]^2 = [f/v]^2 = [(L_c - f) / L_c]^2 = 0.937$$

A reasonable 5cm error in the measured calibration distance L_c (that was always between 15.3m and 15.0m) will yield only a negligible relative error of 0.02% in the value of $[FOV_c/FOV_m]^2$.

For each zenith angle we made 25 successive measurements. From the average of these 25 measurements - $V'_m(\lambda)$ we subtracted the offset/background signal in order to produce the true signal – $V_m(\lambda)$. Similar average and subtraction was made on the calibration signal - $V'_c(\lambda)$ - to obtain the true calibration signal – $V_c(\lambda)$. The true calibration and measurements signals were introduced to Eq. 6.

3. THE RESULTS

A) The visibility data

The morning of the first day of the field test - 14/2/02 we had problems with the experimental set-up. The evening we managed to solve all the set-up problems and good visibility conditions allowed us to acquire good atmospheric transmittance data (see Figure 5).

The morning of the second day of the field test - 15/2/02 was characterised by high and low clouds that made all transmittance measurements impossible (see Figure 6). The evening was characterised by fairly good visibility (see Figure 7)

Both the morning and the evening of the third day of the field test - 16/2/02 were characterised by good visibility conditions (see Figures 8 and 9, respectively).

All measure visibility data were backed by visual observation of mountains that were located 20-35km from us.

B) The other meteorological data

The radiosonde profiles of the air pressure (in mb) - $P_{air}(h)$, air temperature (in C) - $T_{air}(h)$ and water vapour density (in gr/m^3) - $\rho_{water}(h)$ that were measured at 2AM and 2PM (for altitudes up to 10000m) were averaged to calculate the data for MODTRAN profiles. The profiles of the water vapour and the air temperatures are shown in Figures 10 and 11, respectively. The exact meteorological conditions along the day (that are used as input to MODTRAN 4.1) are to be calculated from the radiosonde data that is clamped to the ground meteorological conditions for the actual air temperature - T_{air}(at h>850), water vapour content - ρ_{water}(at h>850) and the pressure P_{air}(at h>850).

We measured the ground (h=850m) meteorological parameters (T, RH) in these two days. The pressure was not measured due to bubble that was in the mercury column of the barometer. As a results we used the radiosonde data without clamping. Since the parameters T and RH did not change much during the 2:20 hours in which the sun moved between the horizon and zenith angle of 60°, their average (± STD) were summarised as shown in Table 1.

Date	Time	P(mb)	T(K)	ρ_{water} (gr/m^3)
14/7	Evening	N/A	301.0±1.2	11.13±0.38
15/7	Evening	N/A	301.1±1.9	15.26±0.17
16/7	Morning	N/A	295.3±2.0	10.65±0.41
16/7	Evening	N/A	302.9±1.7	13.14±0.38

Table 1: The average ground meteorological conditions

Since the major contribution to the STD was due to inaccurate readings of the wet/dry temperatures, we decided to use the averages as representative meteorological conditions for these 2:20 hours.

These conditions were used for clamping the radiosonde profile to the ground temperature and absolute humidity (in gr/m^3) according to the following method. This clamped profile was obtained from the following equations:

(8) $$T_{air,\ ground\ clamped}(h) = T_{air,\ sonde}(h) + \Delta T$$

(9) $$\rho_{water,\ ground\ clamped}(h) = \rho_{water,\ sonde}(h) \cdot K$$

Where:

$$\Delta T = T_{ground}(h=850m) - T_{air,\ sonde}(h=850m)$$

$$K = \rho_{ground}(h=850m) / \rho_{water,\ sonde}(h=850m)$$

The values of the clamping factors ΔT, K and G are shown in table 2:

Date	Time	G	ΔT (K)	K
14/7	Evening	N/A	7.5	0.86
15/7	Evening	N/A	7.3	1.25
16/7	Morning	N/A	0.7	0.79
16/7	Evening	N/A	7.6	0.89

Table 2: The clamping factors

Using these parameter to clamp the radiosonde data of T and ρ from Mitzpe' Ramon ground level (h=0.85 km) up to altitude of h=10 km (and above it to use the Israel/July profile), produced the profiles we used for the predictions of MODTRAN 4.1. These profiles are shown in Tables 3-6.

HEIGHT (km)	PRESS (mb)	TEMP (K)	Water (gr/m^3)
0.1	999.4	306.1	2.12E+01
0.2	987.9	304.9	2.00E+01
0.3	976.4	303.9	1.87E+01
0.4	965.0	303.1	1.73E+01
0.5	953.7	302.4	1.58E+01
0.75	925.9	301.3	1.23E+01
0.85	915.0	301.0	1.11E+01
1	898.7	300.5	9.43E+00
1.25	872.1	299.7	7.70E+00
1.5	846.0	298.6	6.66E+00
2	795.7	296.3	5.10E+00
2.5	747.7	293.8	3.93E+00
3	702.0	291.2	3.03E+00
3.5	658.7	288.5	2.48E+00
4	617.3	285.8	1.96E+00
4.5	578.0	283.0	1.59E+00
5	540.8	280.2	1.28E+00
6	472.2	274.7	8.35E-01
7	410.4	269.1	5.35E-01
8	355.6	263.0	3.39E-01
9	306.8	256.6	2.09E-01
10	264.2	250.0	1.31E-01
15	123.6	211.3	1.00E-03
20	55.1	209.3	4.50E-04
30	10.8	233.0	3.50E-04
40	2.6	256.0	3.00E-05
50	0.7	265.0	3.00E-06
100	0.0	244.7	1.00E-09

Table 3: The meteorological profile of 14/7/02 – Evening

HEIGHT (km)	PRESS (mb)	TEMP (K)	Water (gr/m^3)
0.1	999.4	306.3	2.90E+01
0.2	987.9	305.0	2.74E+01
0.3	976.4	304.0	2.56E+01
0.4	965.0	303.2	2.37E+01
0.5	953.7	302.5	2.17E+01
0.75	925.9	301.4	1.68E+01
0.85	915.0	301.1	1.53E+01
1	898.7	300.6	1.29E+01
1.25	872.1	299.8	1.06E+01
1.5	846.0	298.7	9.13E+00
2	795.7	296.4	7.00E+00
2.5	747.7	293.9	5.39E+00
3	702.0	291.3	4.15E+00
3.5	658.7	288.6	3.40E+00
4	617.3	285.9	2.68E+00
4.5	578.0	283.1	2.18E+00
5	540.8	280.3	1.75E+00
6	472.2	274.8	1.15E+00
7	410.4	269.2	7.34E-01
8	355.6	263.1	4.65E-01
9	306.8	256.8	2.86E-01
10	264.2	250.1	1.79E-01
15	123.6	211.3	1.00E-03
20	55.1	209.3	4.50E-04
30	10.8	233.0	3.50E-04
40	2.6	256.0	3.00E-05
50	0.7	265.0	3.00E-06
100	0.0	244.7	1.00E-09

Table 4: The meteorological profile of 15/7/02 - Evening

HEIGHT (km)	PRESS (mb)	TEMP (K)	Water (gr/m^3)
0.1	999.4	300.4	2.03E+01
0.2	987.9	299.1	1.91E+01
0.3	976.4	298.1	1.79E+01
0.4	965.0	297.3	1.65E+01
0.5	953.7	296.7	1.52E+01
0.75	925.9	295.6	1.17E+01
0.85	915.0	295.3	1.07E+01
1	898.7	294.8	9.02E+00
1.25	872.1	293.9	7.37E+00
1.5	846.0	292.9	6.37E+00
2	795.7	290.5	4.89E+00
2.5	747.7	288.1	3.76E+00
3	702.0	285.5	2.90E+00
3.5	658.7	282.8	2.37E+00
4	617.3	280.0	1.87E+00
4.5	578.0	277.3	1.52E+00
5	540.8	274.4	1.22E+00
6	472.2	268.9	8.00E-01
7	410.4	263.3	5.12E-01
8	355.6	257.3	3.25E-01
9	306.8	250.9	2.00E-01
10	264.2	244.3	1.25E-01
15	123.6	211.3	1.00E-03
20	55.1	209.3	4.50E-04
30	10.8	233.0	3.50E-04
40	2.6	256.0	3.00E-05
50	0.7	265.0	3.00E-06
100	0.0	244.7	1.00E-09

Table 5: The meteorological profile of 16/7/02 – Morning

HEIGHT (km)	PRESS (mb)	TEMP (K)	Water (gr/m^3)
0.1	999.4	308.0	2.50E+01
0.2	987.9	306.7	2.36E+01
0.3	976.4	305.7	2.20E+01
0.4	965.0	304.9	2.04E+01
0.5	953.7	304.3	1.87E+01
0.75	925.9	303.2	1.45E+01
0.85	915.0	302.9	1.31E+01
1	898.7	302.4	1.11E+01
1.25	872.1	301.5	9.09E+00
1.5	846.0	300.5	7.86E+00
2	795.7	298.1	6.02E+00
2.5	747.7	295.7	4.64E+00
3	702.0	293.1	3.57E+00
3.5	658.7	290.4	2.93E+00
4	617.3	287.6	2.31E+00
4.5	578.0	284.9	1.88E+00
5	540.8	282.1	1.51E+00
6	472.2	276.5	9.86E-01
7	410.4	270.9	6.32E-01
8	355.6	264.9	4.01E-01
9	306.8	258.5	2.47E-01
10	264.2	251.9	1.54E-01
15	123.6	211.3	1.00E-03
20	55.1	209.3	4.50E-04
30	10.8	233.0	3.50E-04
40	2.6	256.0	3.00E-05
50	0.7	265.0	3.00E-06
100	0.0	244.7	1.00E-09

Table 6: The meteorological profile of 16/7/02 - Evening

We used a rural aerosol model since it is the most suitable one for the region involved as long as the desert aerosol model is not recommended. The final transmittance values were scanned (convoluted) with a Gaussian slit-function with FWHM=2.0%, 2.5% and 3% of the wavelength. As can be seen from Figures 11-13 the best convolution was obtained for FWHM=3%. We'll use this value for all presentation of the MODTRAN results.

The results from the measurements made at all zenith angles in the evening of 14/7/02 are shown in Figures 14 to 29.

The results from the measurements made at all zenith angles in the evening of 15/7/02 are shown in Figures 30 to 46.

The results from the measurements made at all zenith angles in the morning of 16/7/02 are shown in Figures 47 to 63.

The results from the measurements made at all zenith angles in the evening of 16/7/02 are shown in Figures 64 to 81.

4. DISCUSSION OF THE RESULTS

The results show few distinctive features.

- In this field-test we obtained very good fit between the experimental data and the predictions of MODTRAN. Such fit was not found in the previous tests and is due to the good and stable weather conditions that occurred during this period of the year.
- The best fit between the experimental results and the predictions were found in the 3-5μm spectral region that is not affected by the water absorption (molecular and continuum) as the 8-12μm spectral region. This fit in the 3-5μm spectral region was found in low and high zenith angles (see especially in the evening of the 15/7) indicating that we had good visibility measurements. The fit in the 8-12μm spectral region was not so good indicating that this region is more susceptible to the humidity profile as well as to the occurrence of invisible thin layers of cirrus clouds that we could not see.

  An example of the problem of the water/cirrus absorption in this spectral region can be found in the changing fit that we see in the 8-12μm spectral region during the 2:20 hours that we made the measurements in the evening of the 15/7. When the zenith angle of the sun was was 65° there was a slight drop in the visual (870nm) transmittance and the measured visibility dropped from a value of ~31km (that can be aaroximated from the values at 60° and 70°) to the value of 25km. This drop (that was probably caused by very thin cloud) did not affect the good fit that was between the experimental data and the predictions of the MODTRAN code in the 3-5μm spectral region at 65° as well as at 60° and 70°. However, This drop in the visibility reduced the experimental data in the 8-12μm spectral region by noticable amount of ~5% from its exact matching with the MODTRAN predictions that is found at zenith angles of 60° and 70°.
- Analyzing two sets of data from two different days indicated something unusual about the sensitivity of the MODTRAN code to the visibility values especially when measured at high ground altitudes. We compared the measured data and the prediction of the MODTRAN code at zenith angles of 85° and 80° for two days: the evening of the 14/7 and the morning of the 16/7. The comparison is shown in Figures 82 and 83 respectively.

In Figure 82 we see that the experimental data in these two days almost fit each other as well as the MODTRAN predictions. This result was expected since
A) The integrated water density along the optical path in these two days was almost identical. This can be seen from figures 84 and 85 that show the transmittance of the water vapor and the transmittance of the water continuum, respectively.
B) The visibility values in these two days for zenith angle of 85° was 50km.

In Figure 83 we see that the experimental data in these two days does not fit each other while the MODTRAN predictions almost fit. The fit in the MODTRAN predictions is expected because though the integrated water density along the optical path in these two days was almost identical (see figures 84 and 85), the visibility during these two measurements were not identical. The visibility in these two days for zenith angle of 80° was 40km for the morning of the 16/7 and 50km for the evening of the 14/7.
We hardly believe that while the enhanced visibility values (14/7 evening) create a difference of ~30% in the experimental results (Figure 83) there is no indication to this in the MODTRAN predictions that predict only a change of (3.5±1.0)% in the aerosol transmittance – see Figure 86.

5. ERROR ANALYSIS

The validity of the experimental results depends on the error in the experimental data as well as in the parameters that affect the predicted transmittance values. The measured transmittance values are expressed according to Eq. (5):

$$\tau_m(\theta, \lambda)= \tau_c(\lambda)\cdot[V_m(\theta, \lambda)/V_c(\lambda)]\cdot[P(T_c, \lambda)/P(T_s, \lambda)]\cdot[FOV_c/FOV_m]^2$$

From this equation it is quite easy to calculate the relative error of the measured transmittance:

$$\begin{aligned}\Delta\tau_m(\theta, \lambda)/\tau_m(\theta, \lambda) = {} & \Delta V_m(\theta, \lambda)/V_m(\theta, \lambda) + \\ & \Delta V_c(\lambda)/V_c(\lambda) + \\ & \Delta P(T_c, \lambda)/P(T_c,\lambda) + \\ & ERR_{FOV}\end{aligned}$$

For the sake of simplicity, we'll calculate the average value of $<\Delta\tau_m(\theta, \lambda)/\tau_m(\theta, \lambda)>$ in two spectral regions: 3-5μm and 8-12μm.

It was already shown that the expected relative error in the term $[FOV_c/FOV_m]^2$ is equal to a negligible value of $ERR_{FOV} = 0.02\%$.

The relative error in the calibration blackbody can be calculated from its temperature stability. According to the data sheet that is better than 2K at $T_c = 1273K$. This yield an averaged relative error - $<\Delta P(T_c, \lambda)/P(T_c, \lambda)>$ - of 0.48% in the 3-5μm and 0.26% in the 8-12μm.

The relative error in the calibration signal was calculated from all calibrations that were done in 14-16/7/02. The averaged relative error - $<\Delta V_c(\lambda)/V_c(\lambda)>$ - was calculated as 1.8% in the 3-5μm spectral region and 1.1% in the 8-12μm spectral region (excluding the absorption bands) as shown in figure 87.

The relative error in the measured signal $V_m(\theta, \lambda)$ was taken from the third test (see IARD 57-02). We had calculated from the measurement file that was done at zenith angle of 76^o in the evening of 11/5/02. Since each measured signal $V_m(\theta, \lambda)$ is average of 25 spectral scans (CVF scans), we calculated, the average values and the standard deviations of $V_m(\theta, \lambda)$. The averaged relative error - $<\Delta V_m(\lambda)/V_m(\lambda)>$ - was calculated as 1.2% in the 3-5μm spectral region and 0.9% in the 8-12μm spectral region.

From this analysis we can conclude that the averaged relative error of the measured transmittance - $\mathbf{<\Delta\tau_m(\theta, \lambda)/\tau_m(\theta, \lambda)>}$ - is equal to 2.2% in the 3-5μm spectral region and 1.4% in the 8-12μm spectral region.

The averaged relative error of the calculated transmittance - $\mathbf{<\Delta\tau(\theta, \lambda)/\tau(\theta, \lambda)>}$ - was calculated from the sensitivity of the calculation to different input parameters. There are two input parameter that could have rather large error [(1)] > one is the visibility that was measured by us and the other is the water density along our optical path. Our experimental results showed good agreement between the measured transmittance at 870nm and the predicted values. In view of this data we can conclude that we can derive from the measured slant path transmittance at 870nm the value of the horizontal visibility. This value is to be used for the prediction of the aerosol extinction at longer wavelength. Therefore, we have no reason to have an error in the visibility. However we had already indicated (see the results of the evening of 15/7) that though we have excellent fit between the experimental data and the MODTRAN predictions at low and high zenith angles, this fit is reduced at certain zenith angles. The only explanation for this is a change in the water profile due either to cirrus clouds or to local variations in the water density/ The only way to resolve this problem is either to use a radio water sounder or to make transmittance measurements in very stable atmospheric conditions.

6. CONCLUSIONS

1) The measured transmittance values in the 0.87μm spectral region show excellent agreement with the prediction of the MODTRAN 4.1 code (based on measured and observed visibility values) at all solar zenith angles (89^{o} to 60^{o}). This led us to apply the visibility values, obtained from the intersection of the predicted curves and the measured transmittance data, for the MODTRAN 4.1 predictions in the 3.0-13.5μm spectral region.
2) The measured transmittance values in the 3.0-13.5μm spectral region show very good agreement with the prediction of the MODTRAN 4.1 code at high elevation angles (close to the horizon) and low elevation angles.
3) The disagreement between the measured data and the MODTRAN prediction were caused probably by uncorrected water vapor densities along the optical path.
4) It seems to us that the sensitivity of the predicted aerosol transmittance to the ground (H=0.85km) measured visibility values is too low to explain experimental results. This needs a better analysis of the limits of the boundary layer at elevated terrain.

7. ACKNOWLEDGEMENT

We would like to thank the European Office of Aerospace Research and Development (EOARD) for its funding of this research.

We would like to thank the Mitzpe Ramon Field School and its personnel for their assistance and for supplying us the entire local infrastructure needed for these tests.

References

1. A. J. Ratkowski, G. P. Anderson, J. H. Chetwynd, R. M. Nadile, A. D. Devir and T. D. Conley, "A comparison of atmospheric transmittance measurements in the 3-5μm and 8-12μm spectral regions with MODTRAN: considerations for long near-horizontal path geometries", Proc SPIE, Vol. 3219, pp. 2-10, 1998.
2. A. J. Ratkowski, G. P. Anderson, and A. D. Devir, "Comparison of atmospheric transmittance measurements in the 3-5μm and 8-12μm spectral regions with MODTRAN: considerations for long near-horizontal path geometries" in "Optics in Atmospheric Propagation and Adaptive Systems III", Proc SPIE, Vol. 3866, pp. 11-22, 1999.
3. W. M. Gutman, W. A. Peterson, B. K. Matise, J. L. Manning and R. E. Soulon, "Atmospheric transmittance spectroscopy using the sun as the source", Appl. Optics, 29, pp.3213-3217, 1990.
4. D. Kryskowski and G. H. Suits, "Natural Sources" Ch. 3 in "Sources of Radiation" Vol. 1 of "The Infrared and Electro-Optical Systems Handbook", ERIM/SPIE 1993.

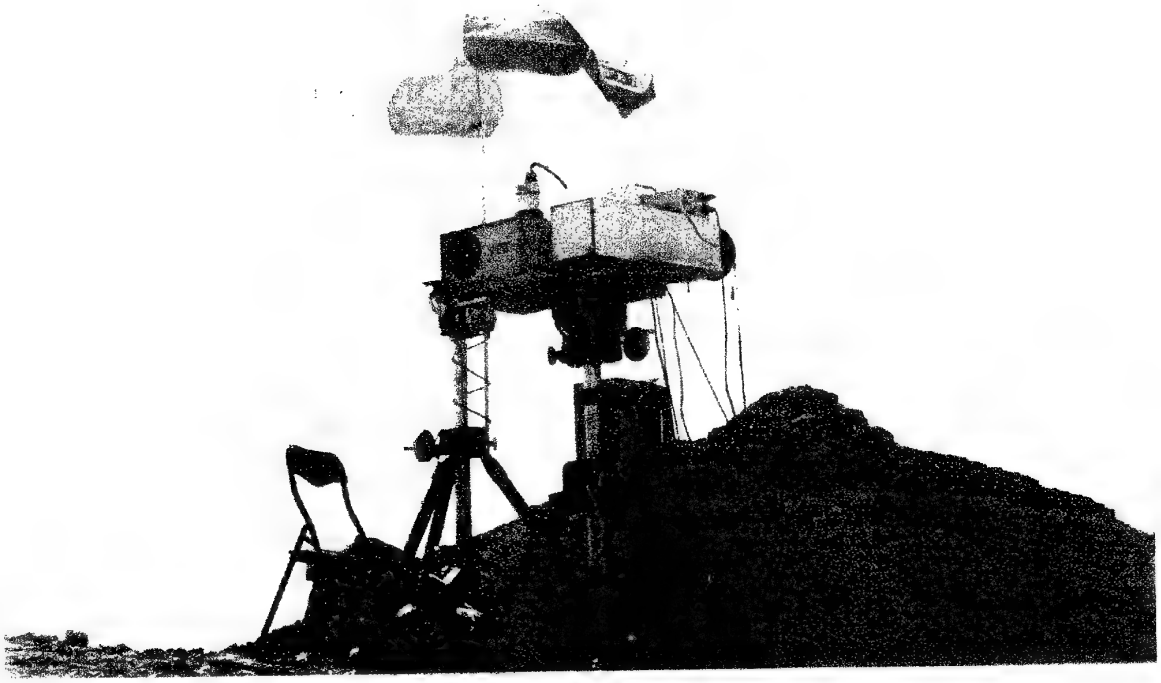

Figure 1: The experimental set-up in Mitzpe' Ramon

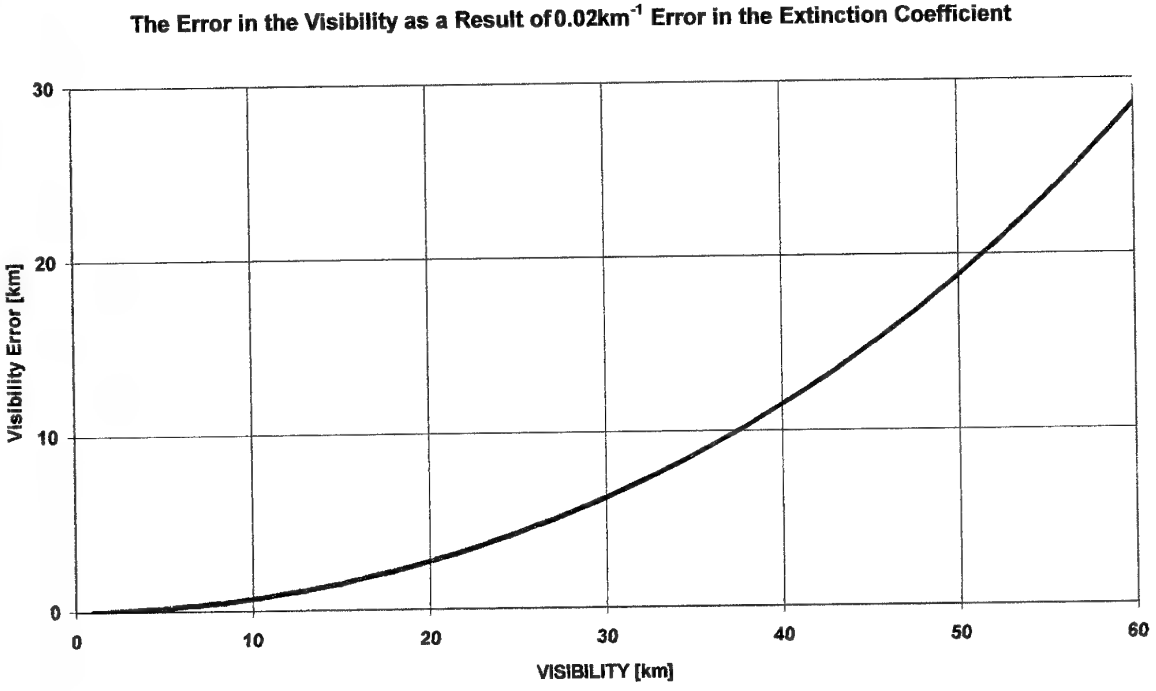

Figure 2: The effect of $0.02km^{-1}$ error in the extinction coefficient on the visibility

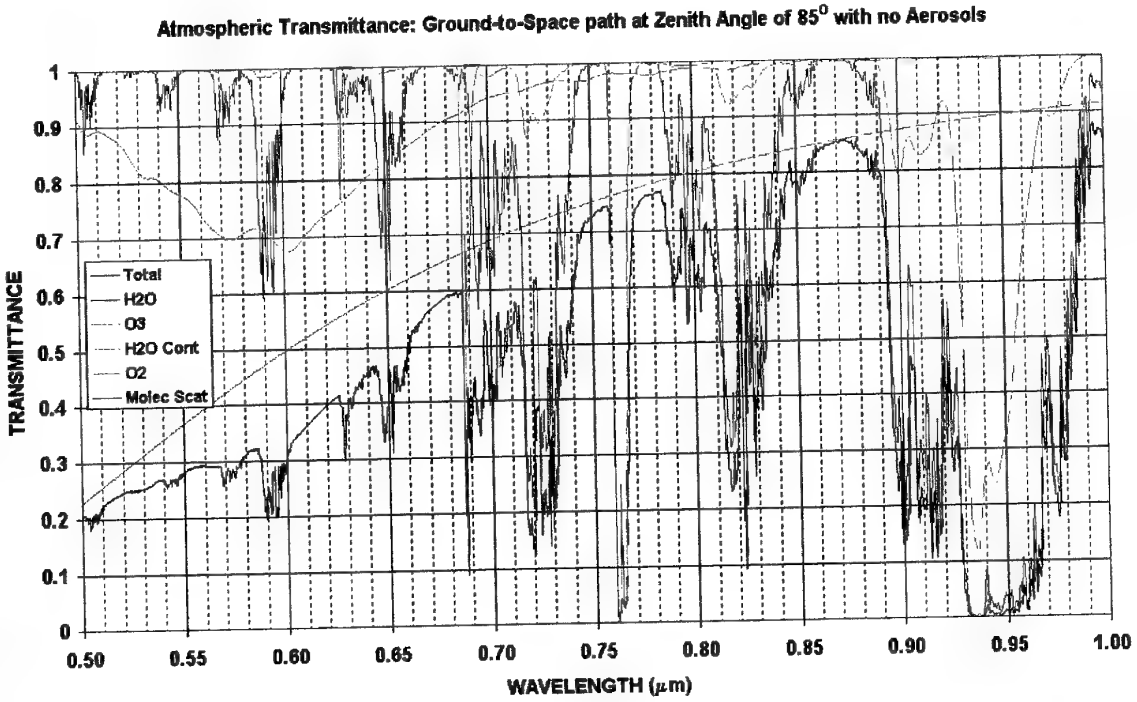

Figure 3: The absorption and scattering of different atmospheric species in the visible spectral region

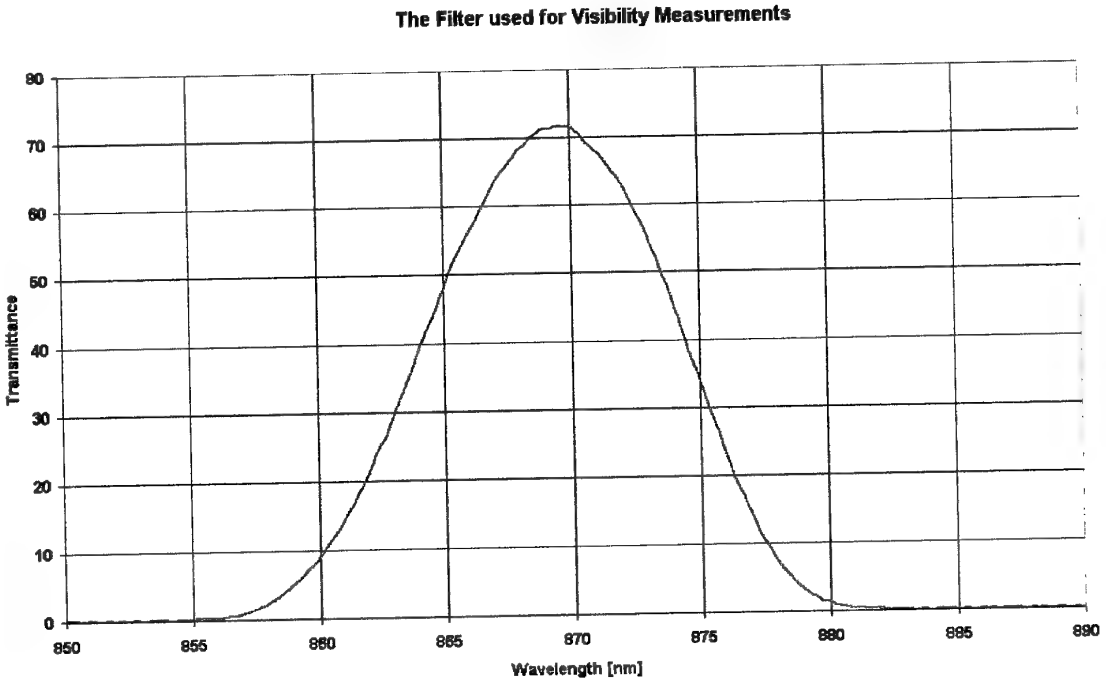

Figure 4: The transmittance of the filter used in the Visibility radiometer

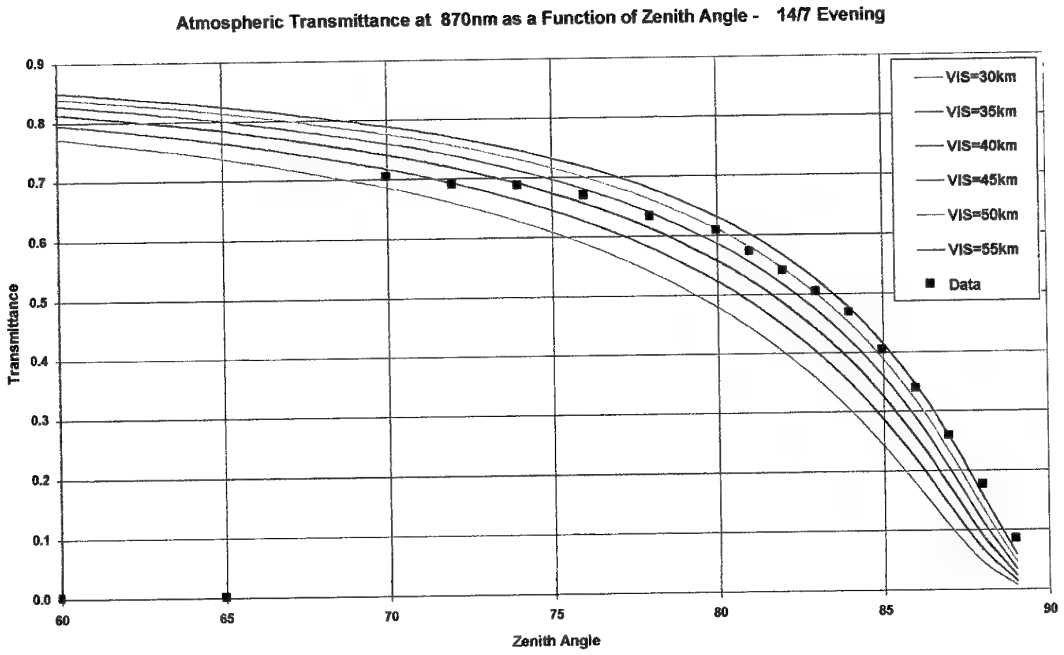

Figure 5: Comparison between the measured and predicted transmittance values at 870nm – evening 14/7.

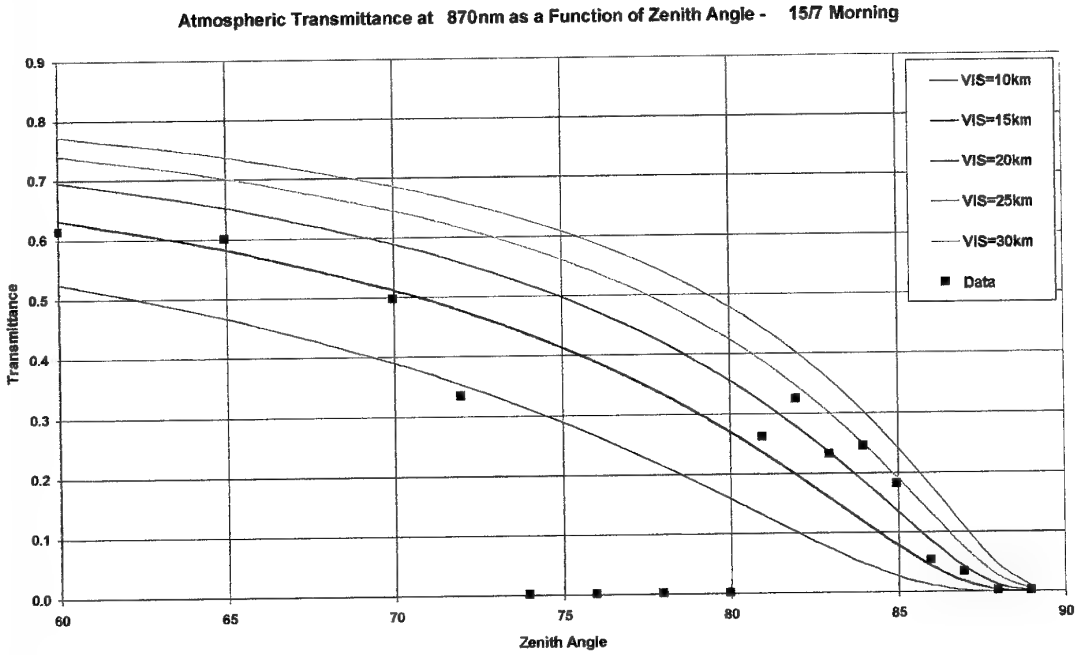

Figure 6: Comparison between the measured and predicted transmittance values at 870nm – morning 15/7.

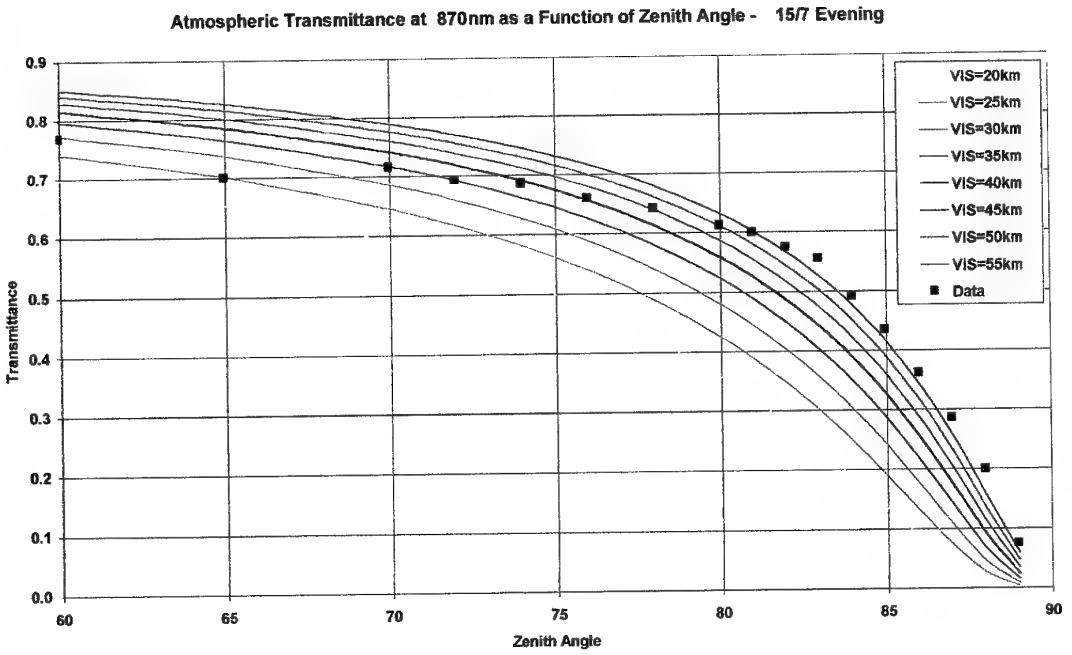

Figure 7: Comparison between the measured and predicted transmittance values at 870nm – evening 15/7.

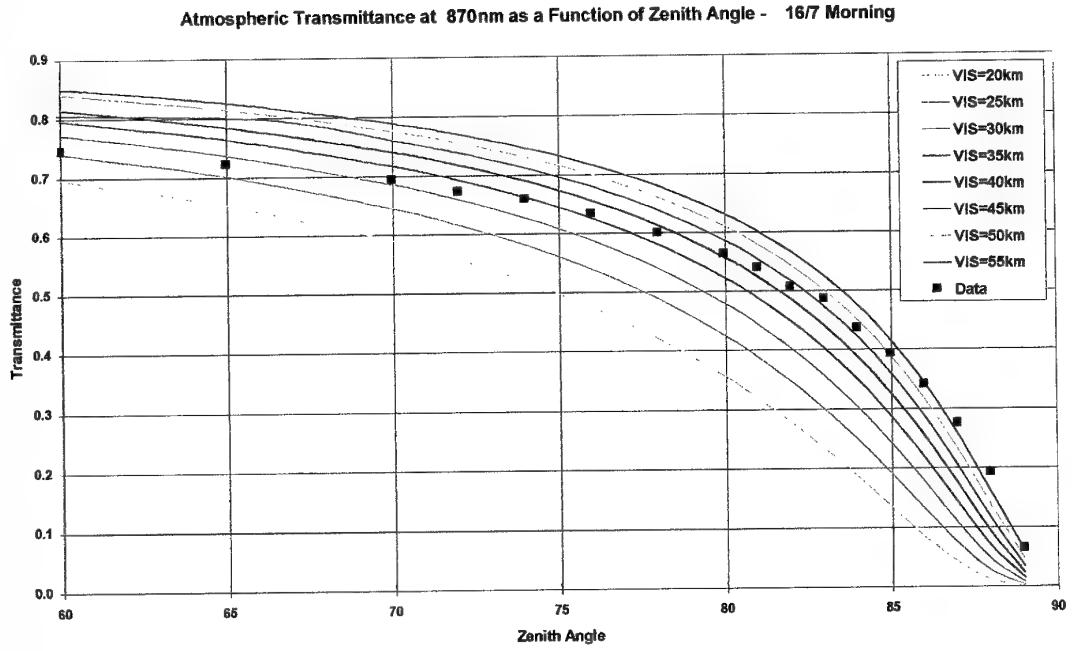

Figure 8: Comparison between the measured and predicted transmittance values at 870nm – morning 16/7.

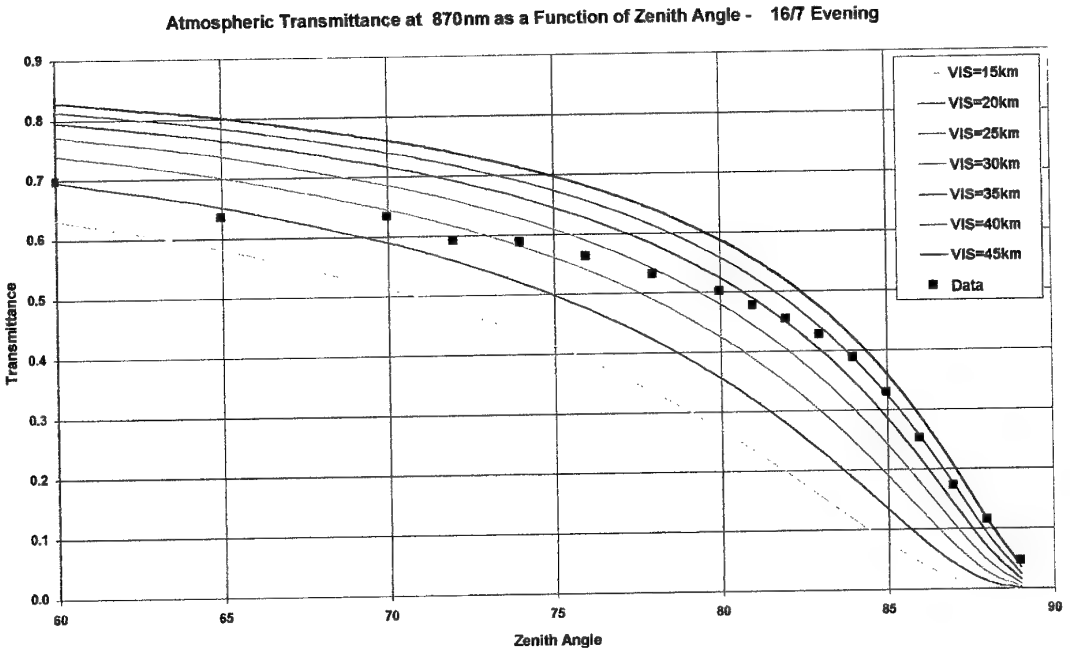

Figure 9: Comparison between the measured and predicted transmittance values at 870nm – evening 16/7.

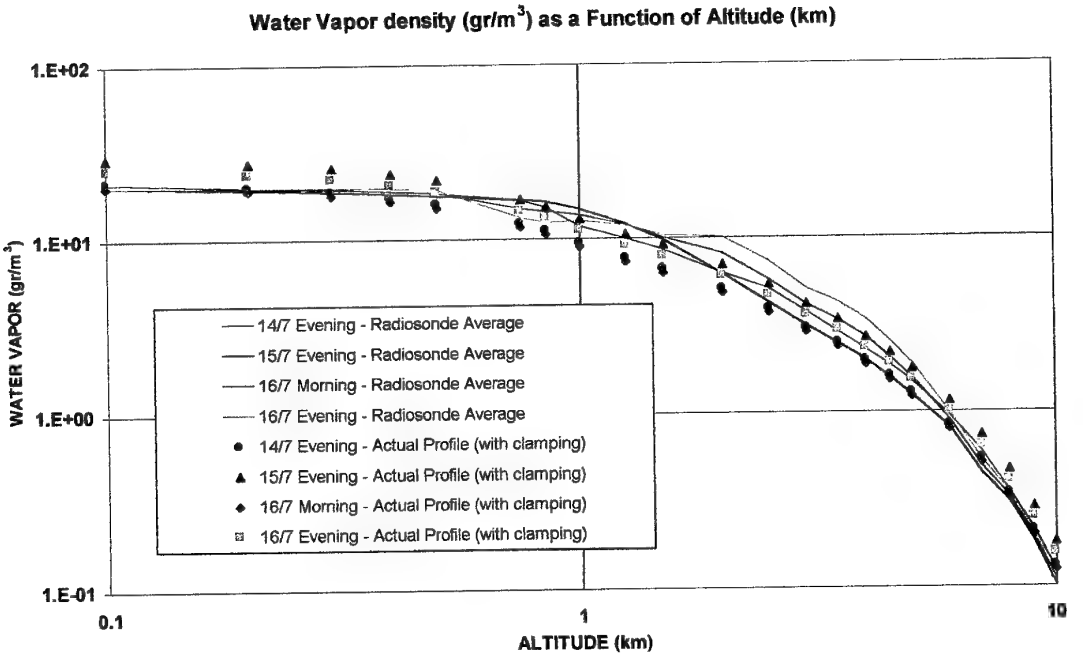

Figure 10: The air temperature (K) profile as measured by the radiosonde.

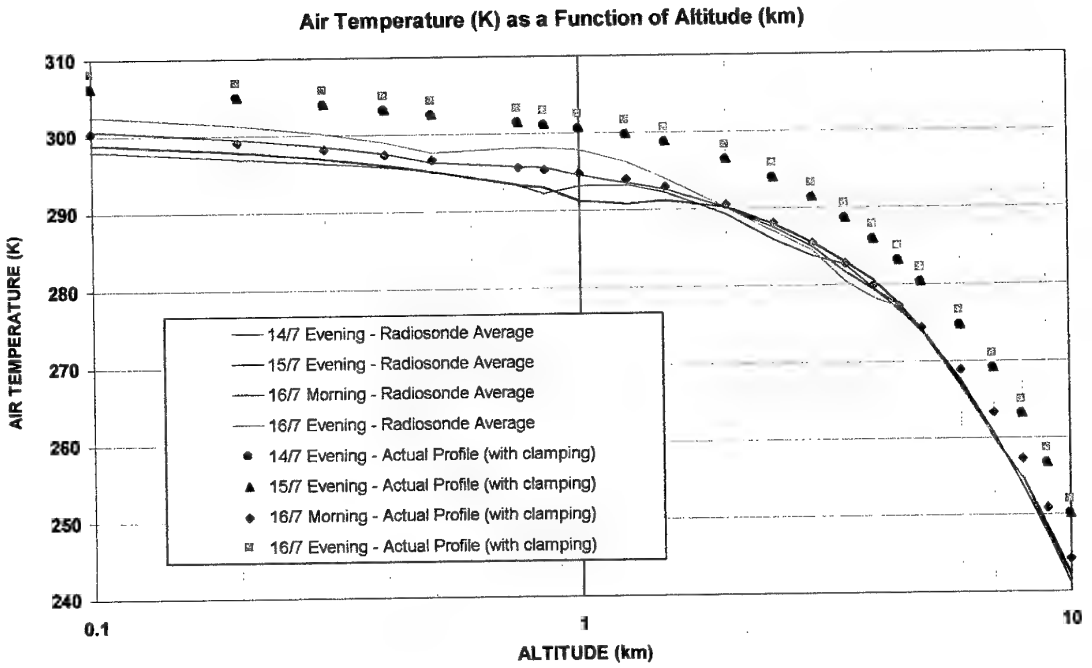

Figure 11: The water density (gr/m^3) profile as measured by the radiosonde.

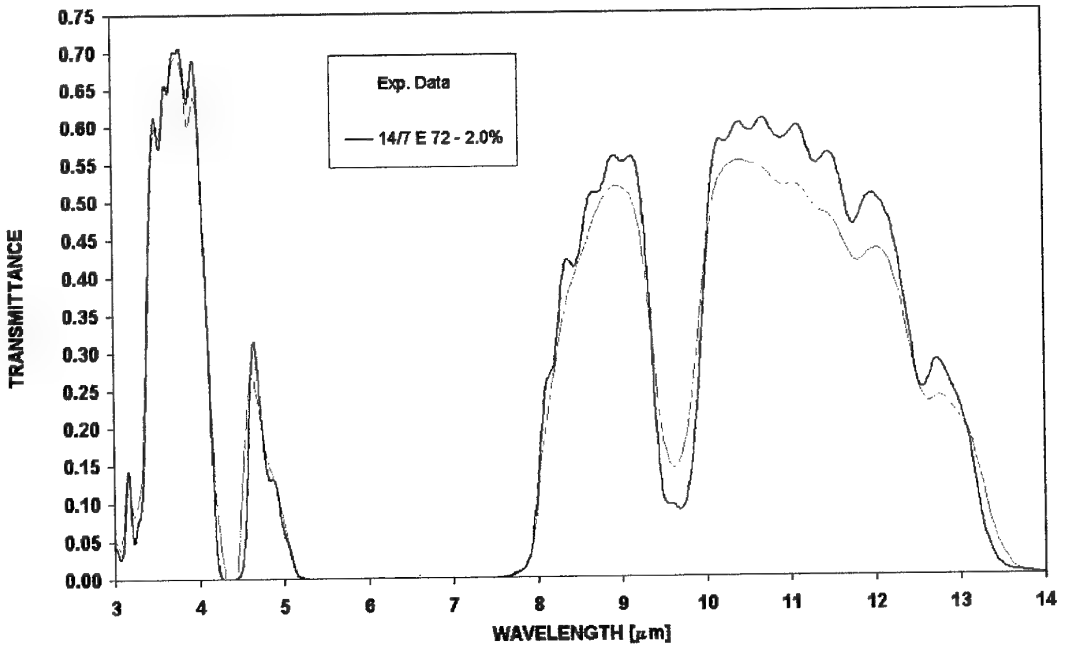

Figure 12: The experimentally measured transmittance data compared to the prediction of MODTRAN 4.1 for zenith angle of 72° convoluted with Gaussian slit with FWHM=2.0%.

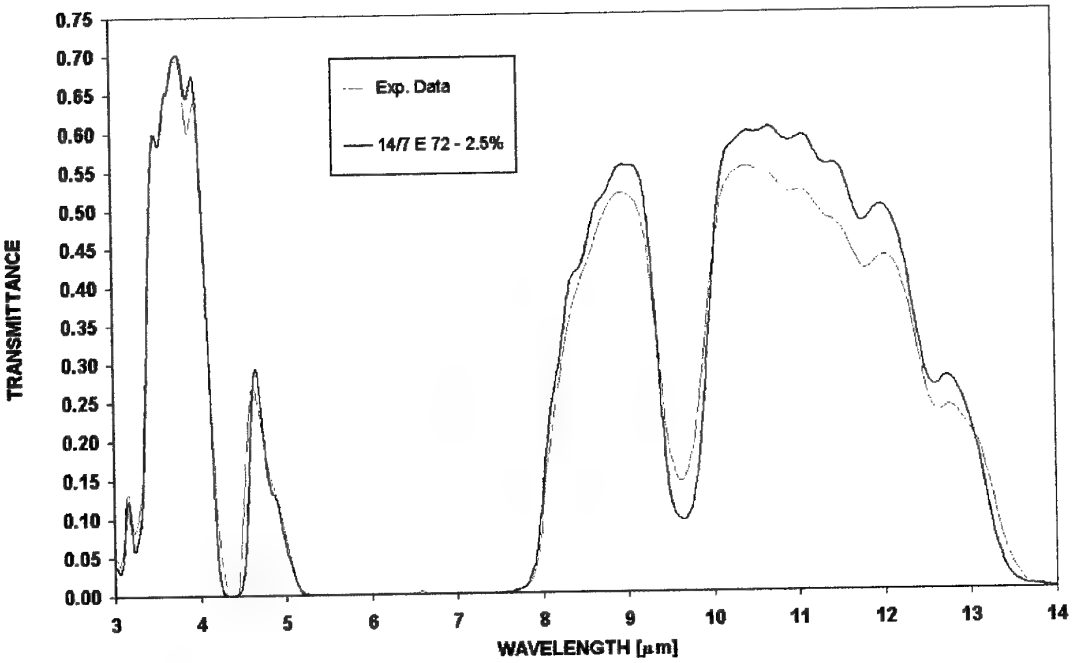

Figure 13: The experimentally measured transmittance data compared to the prediction of MODTRAN 4.1 for zenith angle of 72° convoluted with Gaussian slit with FWHM=2.5%.

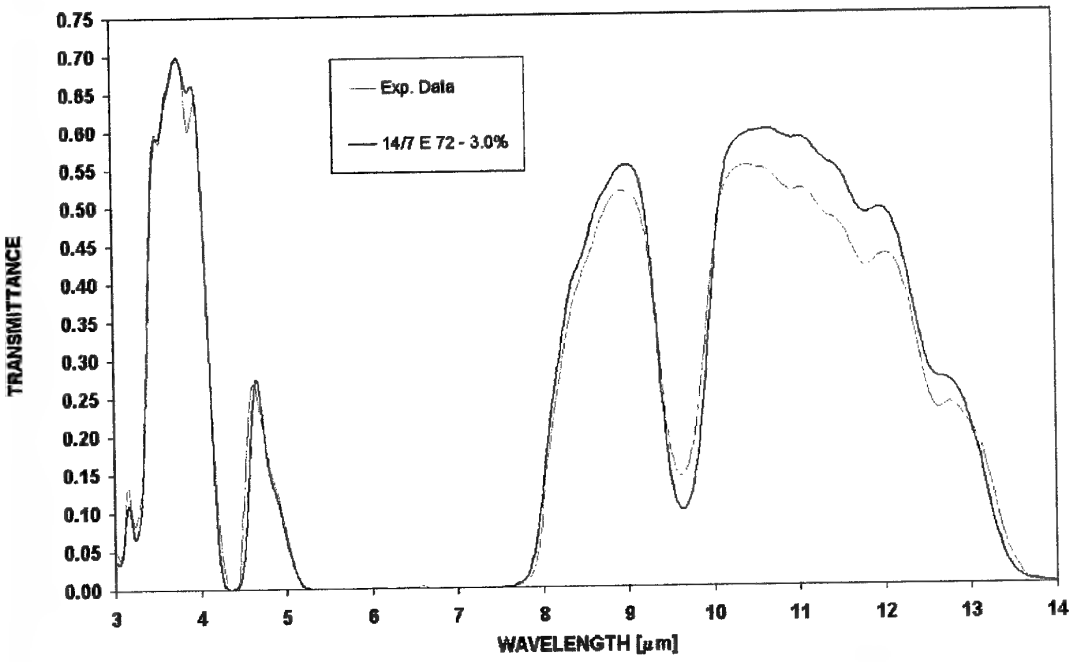

Figure 14: The experimentally measured transmittance data compared to the prediction of MODTRAN 4.1 for zenith angle of 72° convoluted with Gaussian slit with FWHM=3.0%.

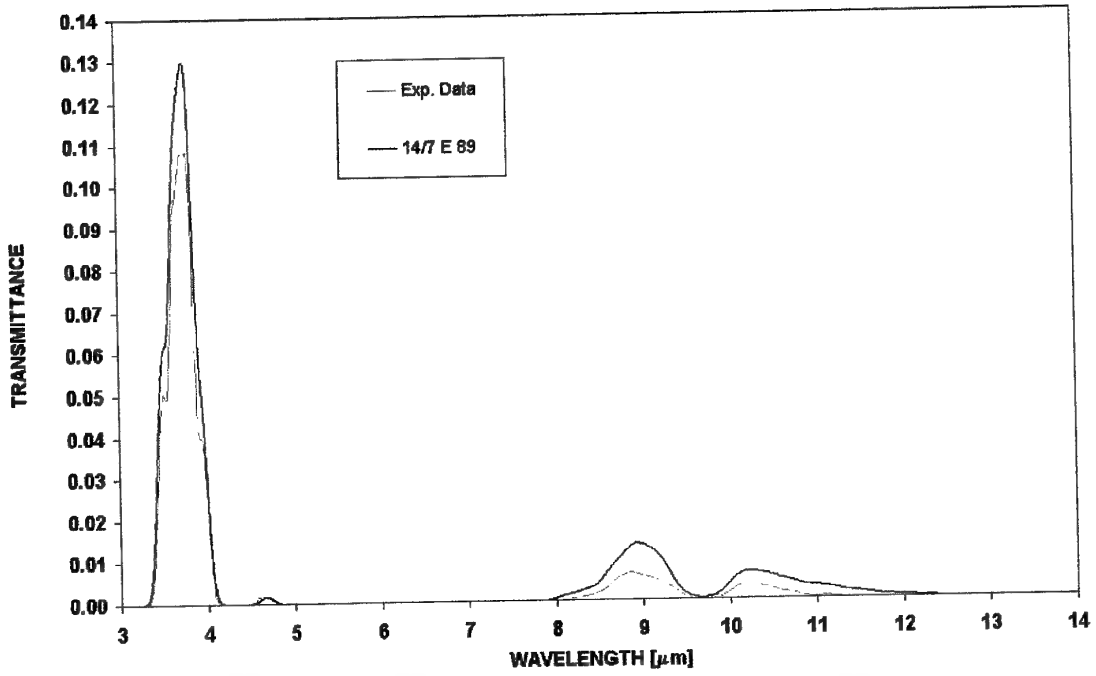

Figure 15: The measured transmittance (Exp. Data) compared to the prediction of MODTRAN 4.1 for zenith angle of 89° in the evening of 14/7/02.

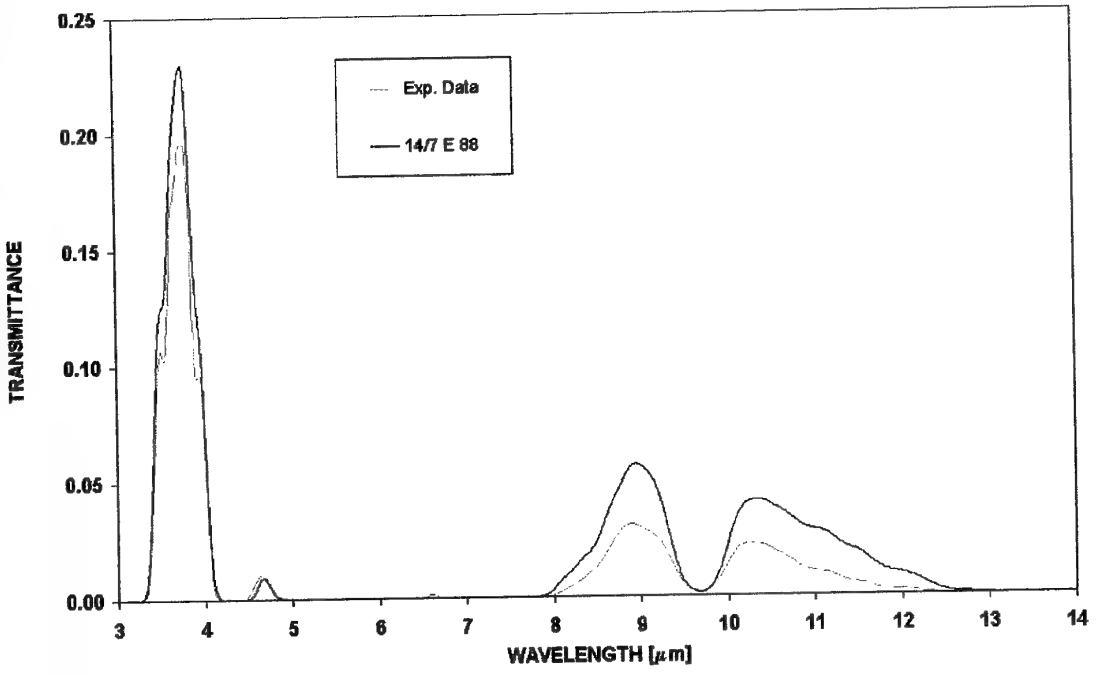

Figure 16: The measured transmittance (Exp. Data) compared to the prediction of MODTRAN 4.1 for zenith angle of 88° in the evening of 14/7/02.

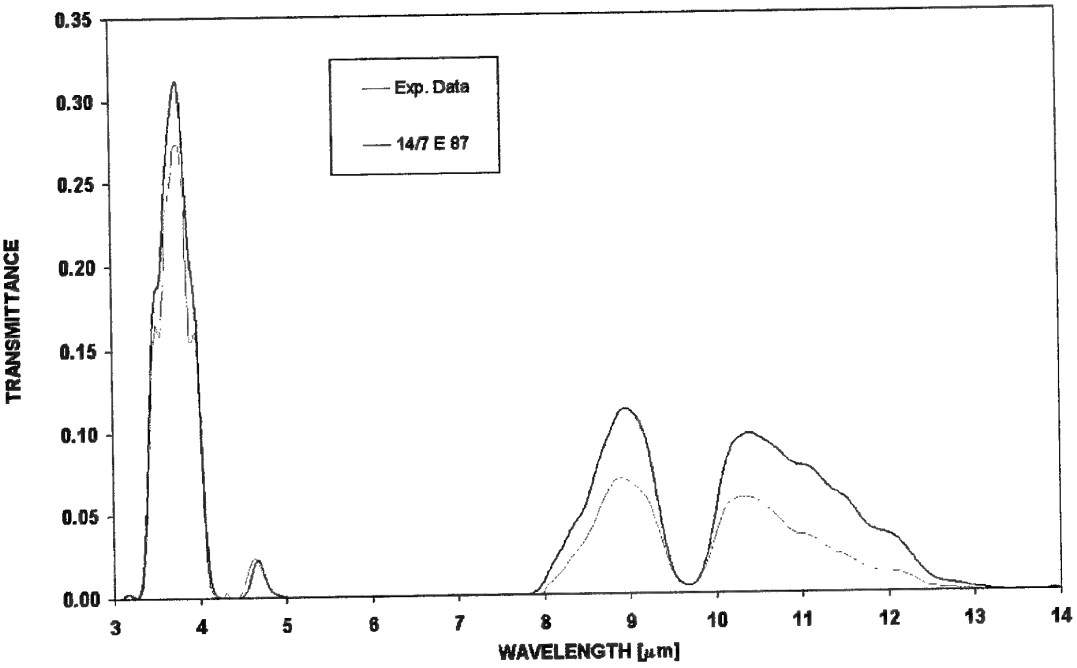

Figure 17: The measured transmittance (Exp. Data) compared to the prediction of MODTRAN 4.1 for zenith angle of 87° in the evening of 14/7/02.

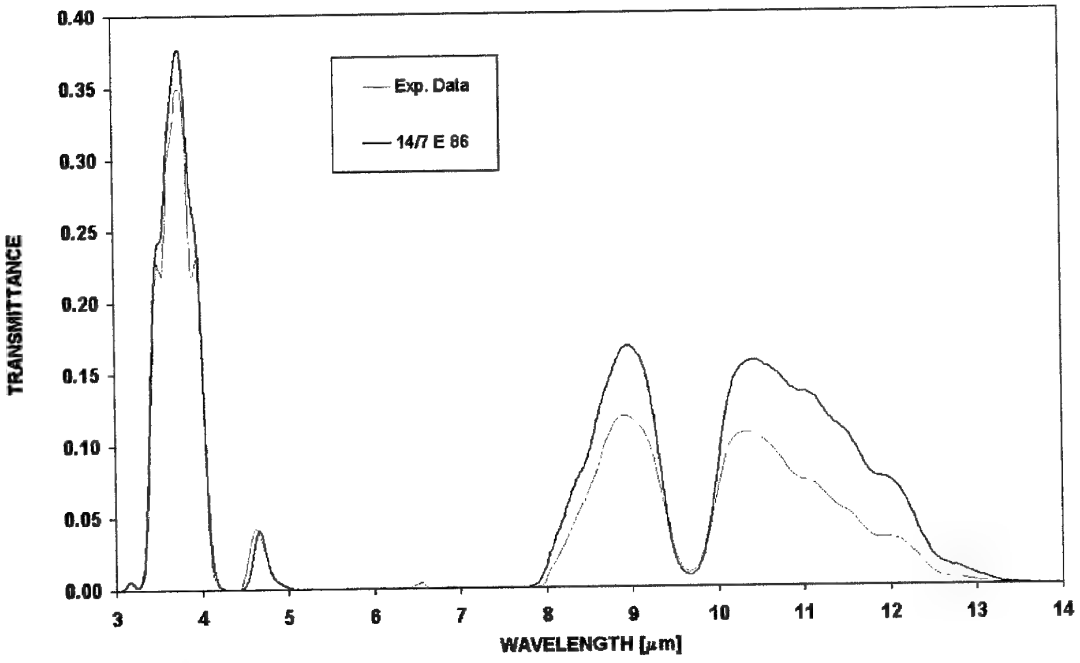

Figure 18: The measured transmittance (Exp. Data) compared to the prediction of MODTRAN 4.1 for zenith angle of 86° in the evening of 14/7/02.

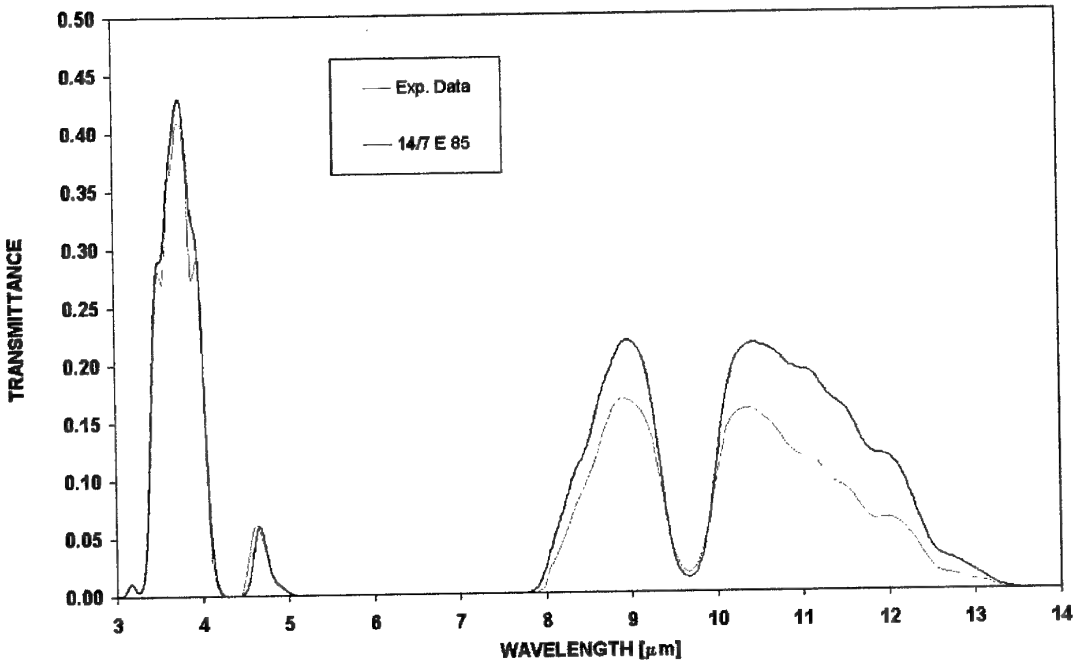

Figure 19: The measured transmittance (Exp. Data) compared to the prediction of MODTRAN 4.1 for zenith angle of 85° in the evening of 14/7/02.

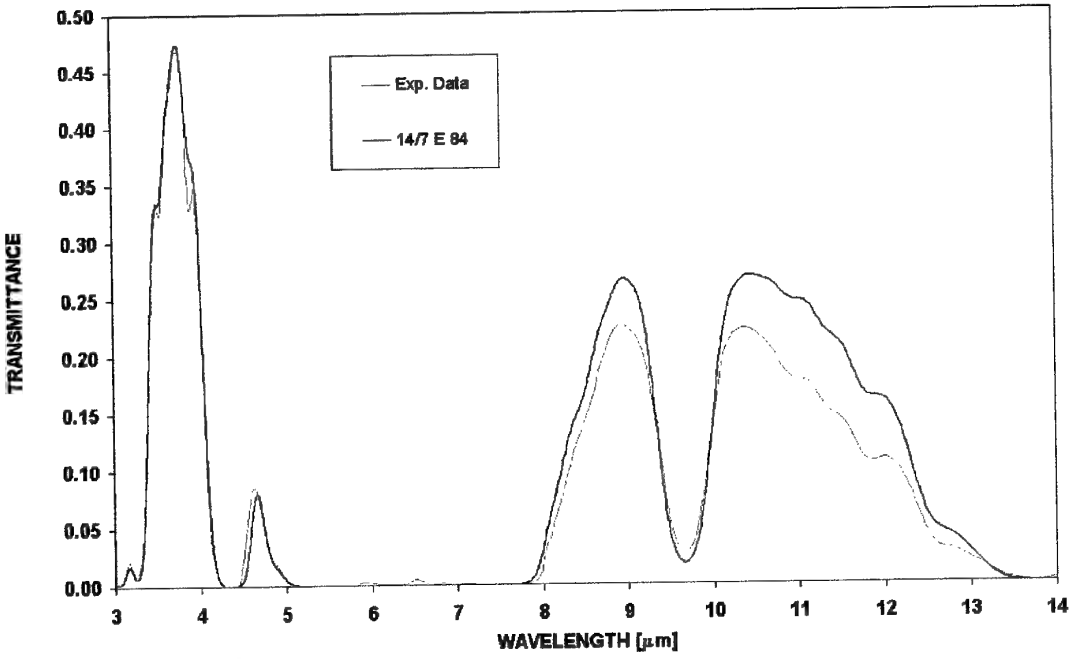

Figure 20: The measured transmittance (Exp. Data) compared to the prediction of MODTRAN 4.1 for zenith angle of 84° in the evening of 14/7/02.

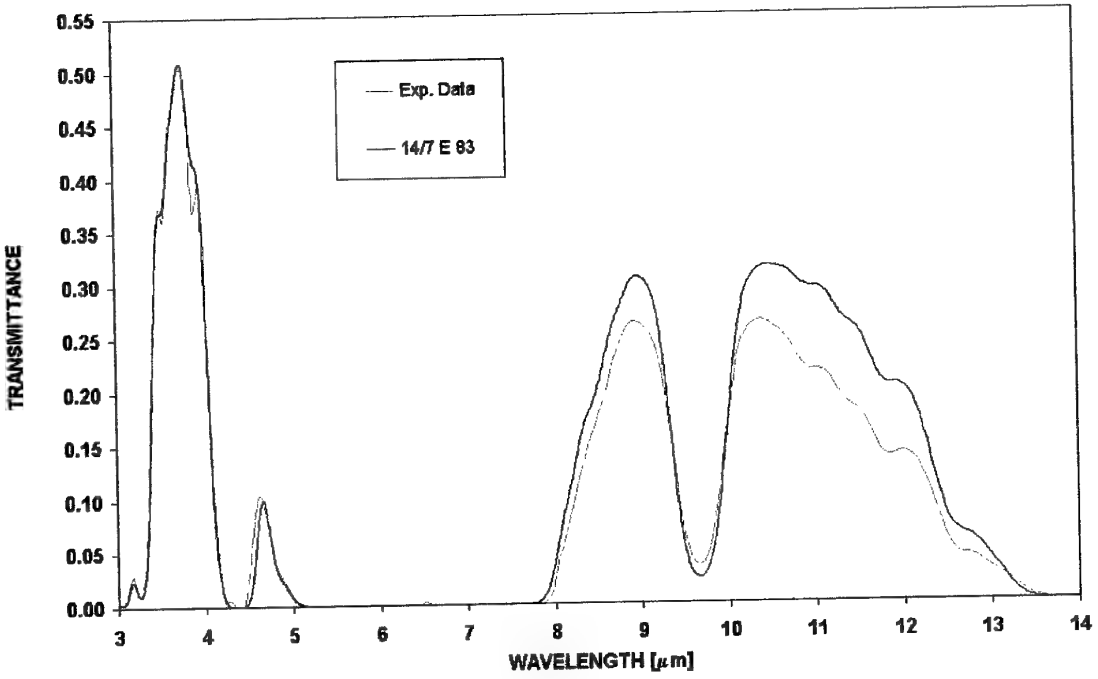

Figure 22: The measured transmittance (Exp. Data) compared to the prediction of MODTRAN 4.1 for zenith angle of 83° in the evening of 14/7/02.

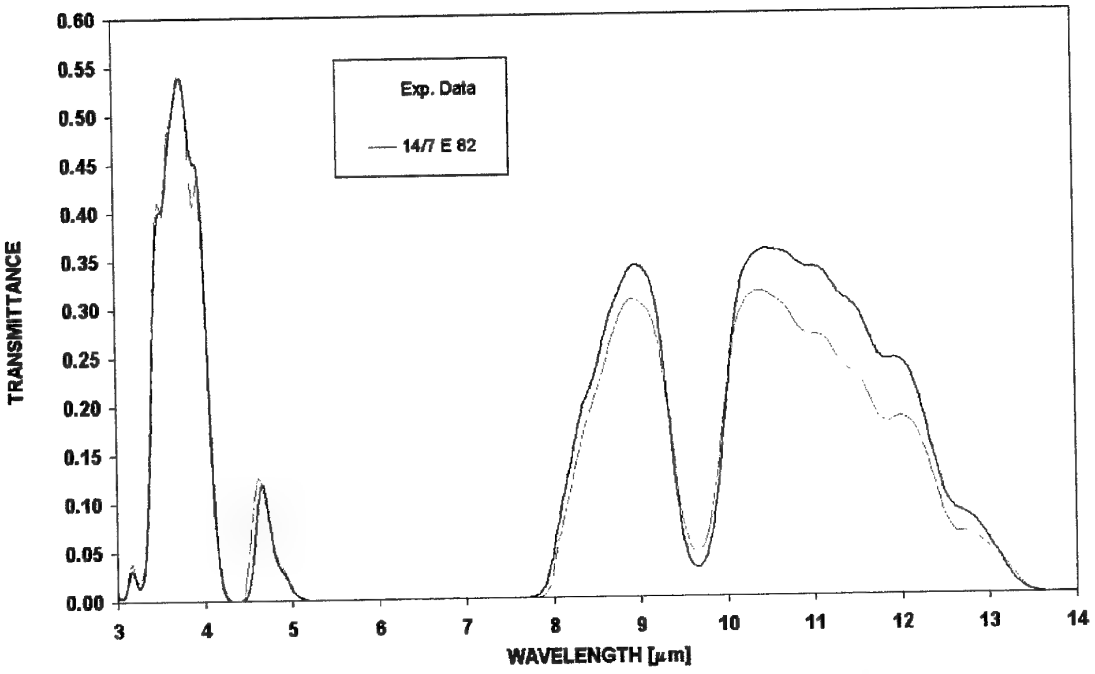

Figure 23: The measured transmittance (Exp. Data) compared to the prediction of MODTRAN 4.1 for zenith angle of 82° in the evening of 14/7/02.

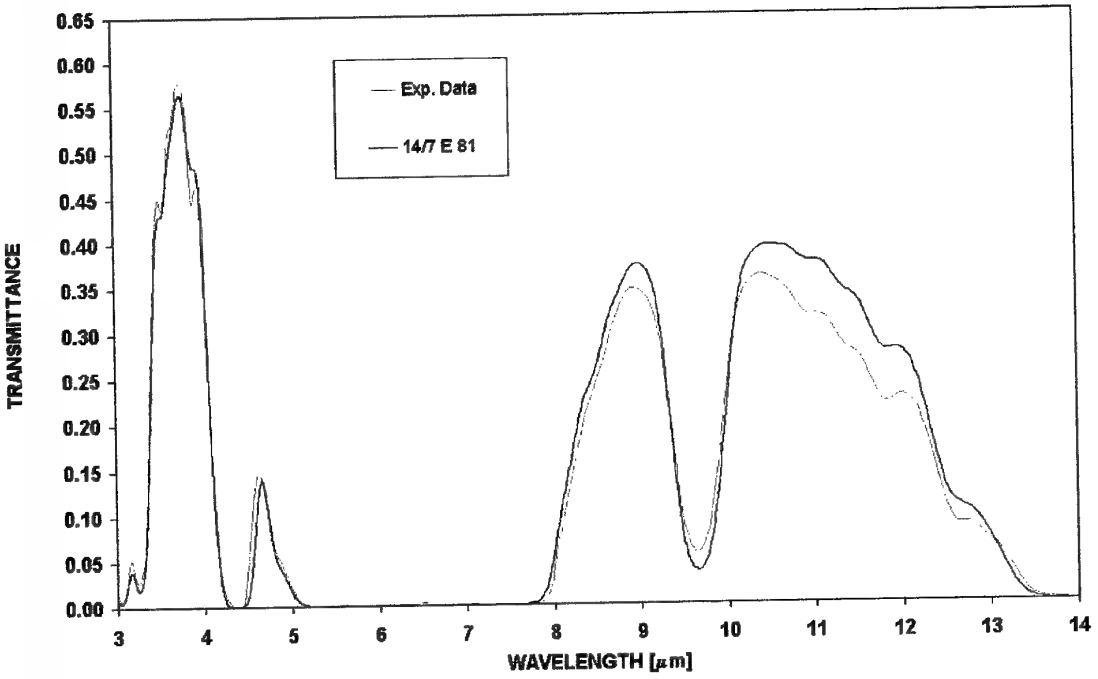

Figure 24: The measured transmittance (Exp. Data) compared to the prediction of MODTRAN 4.1 for zenith angle of 81° in the evening of 14/7/02.

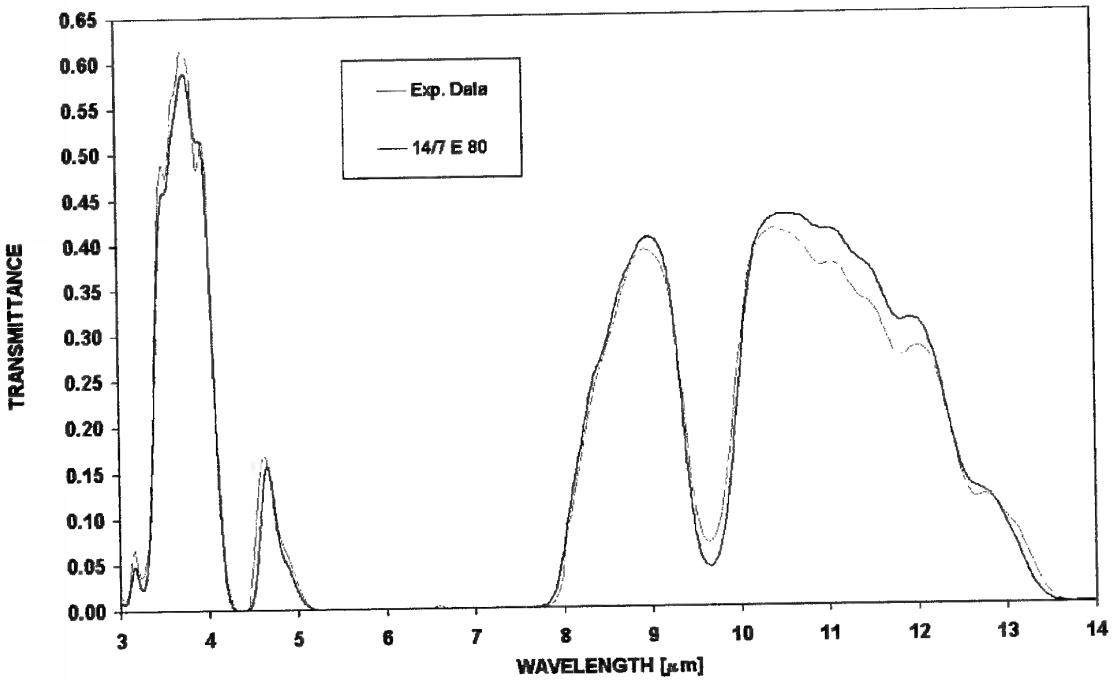

Figure 25: The measured transmittance (Exp. Data) compared to the prediction of MODTRAN 4.1 for zenith angle of 80° in the evening of 14/7/02.

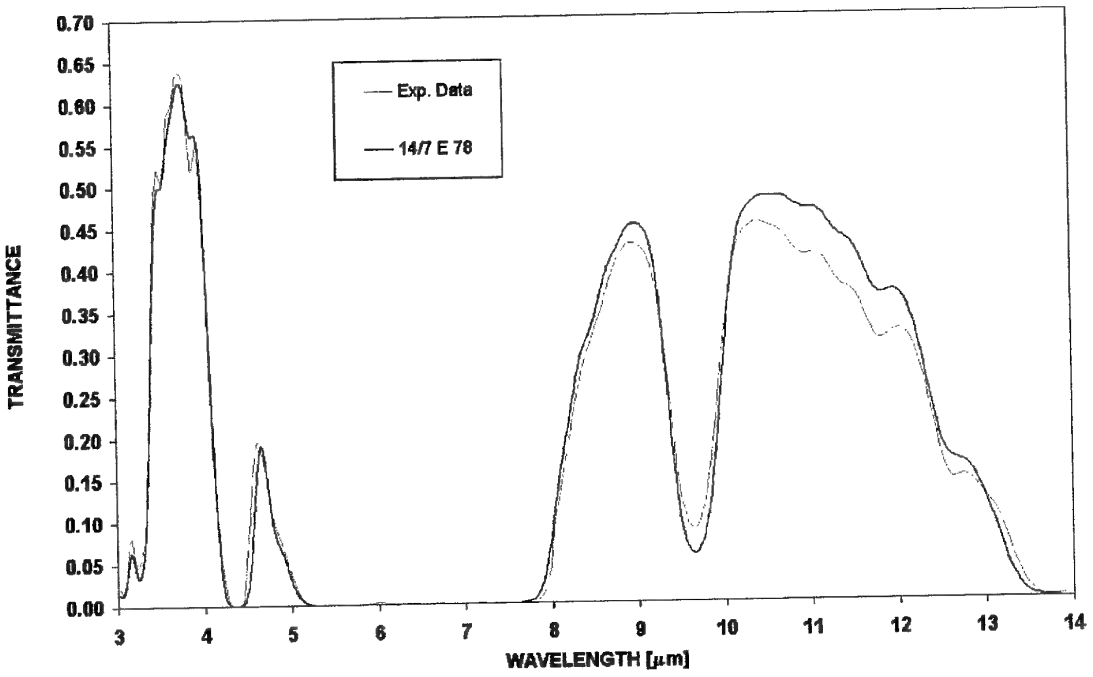

Figure 26: The measured transmittance (Exp. Data) compared to the prediction of MODTRAN 4.1 for zenith angle of 78° in the evening of 14/7/02.

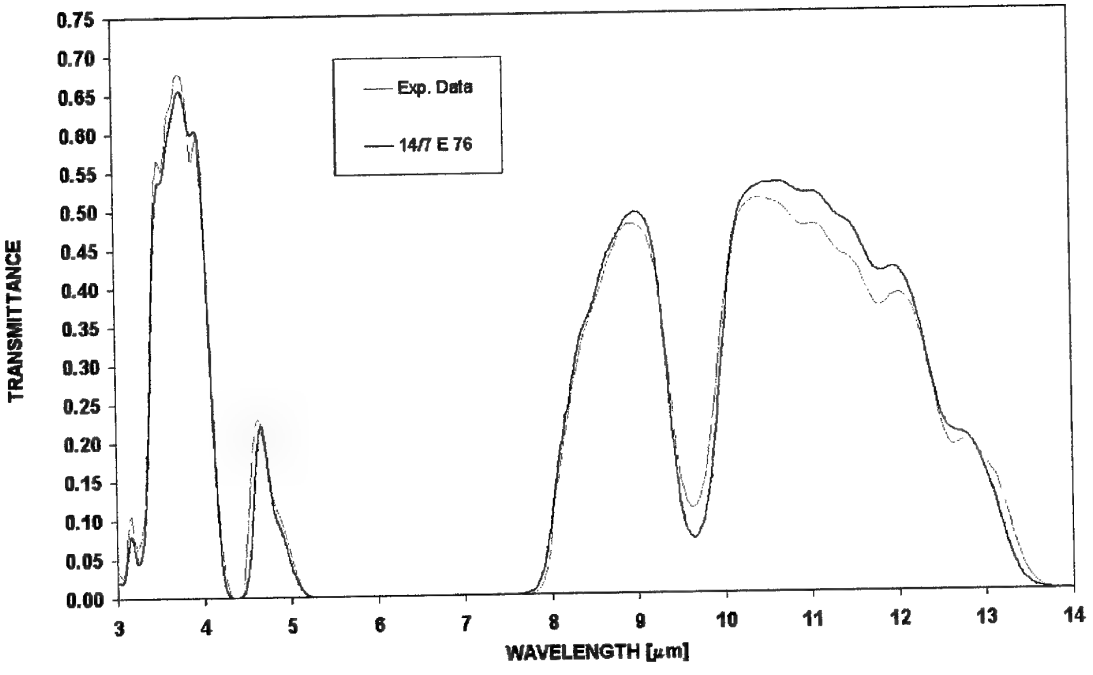

Figure 27: The measured transmittance (Exp. Data) compared to the prediction of MODTRAN 4.1 for zenith angle of 76° in the evening of 14/7/02.

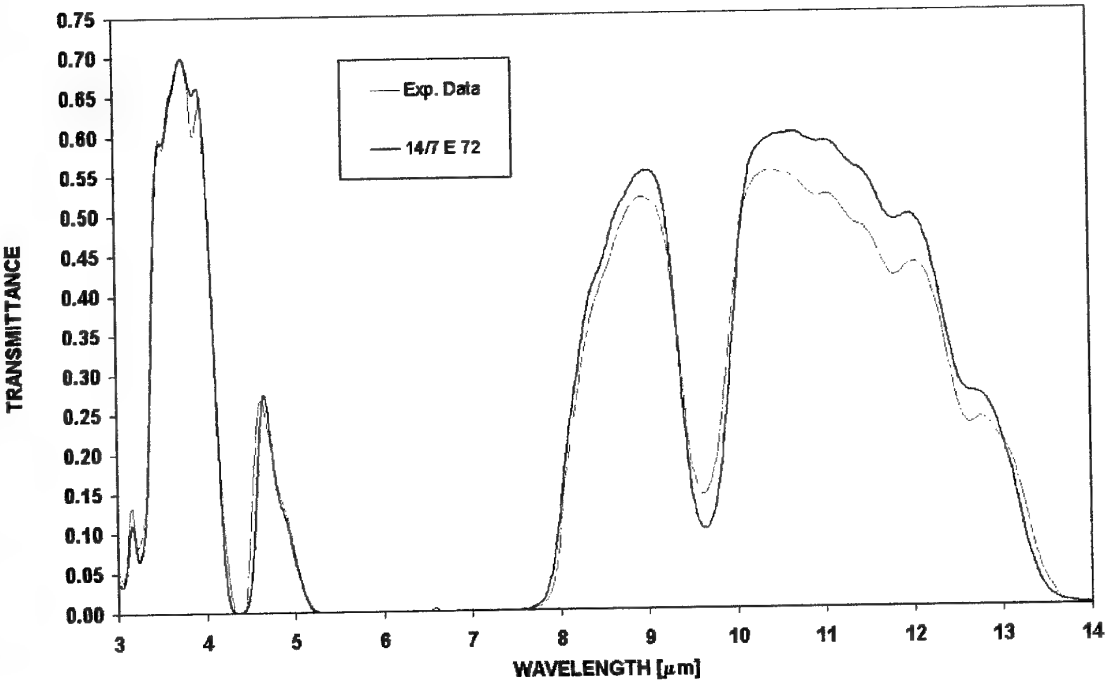

Figure 28: The measured transmittance (Exp. Data) compared to the prediction of MODTRAN 4.1 for zenith angle of 72° in the evening of 14/7/02.

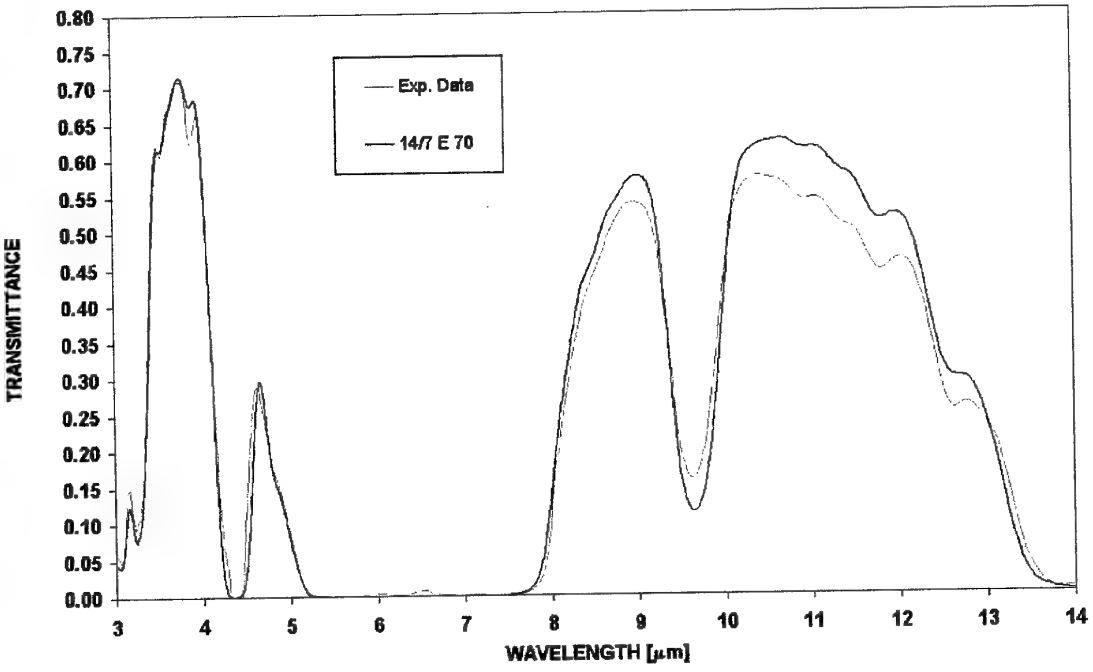

Figure 29: The measured transmittance (Exp. Data) compared to the prediction of MODTRAN 4.1 for zenith angle of 70° in the evening of 14/7/02.

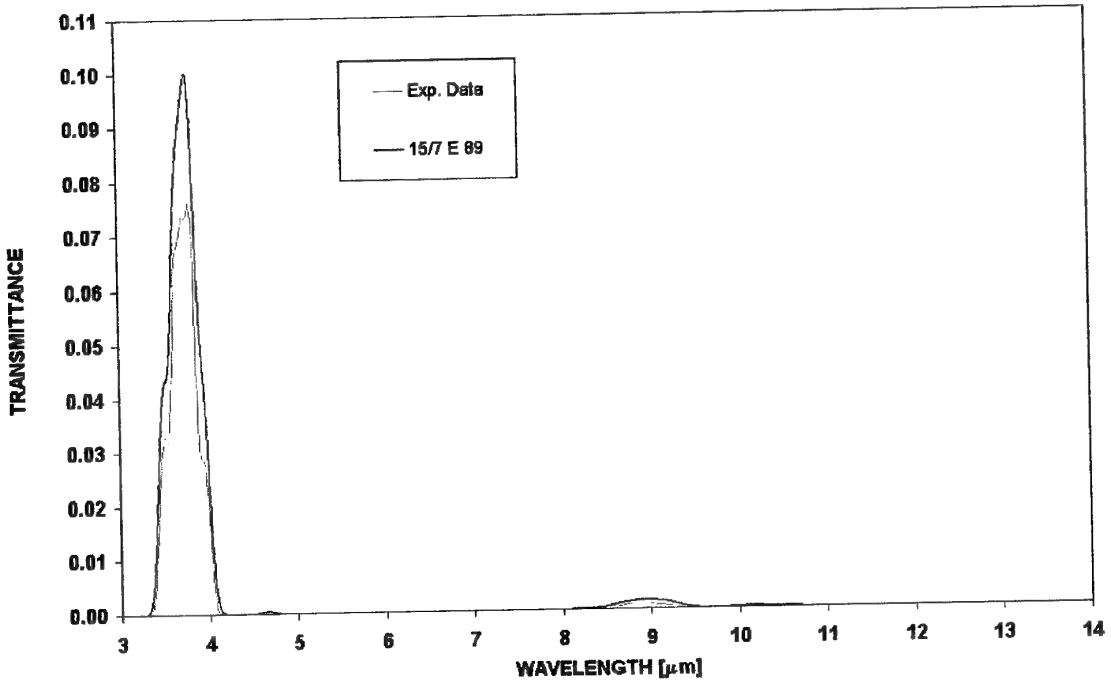

Figure 30: The measured transmittance (Exp. Data) compared to the prediction of MODTRAN 4.1 for zenith angle of 89° in the evening of 15/7/02.

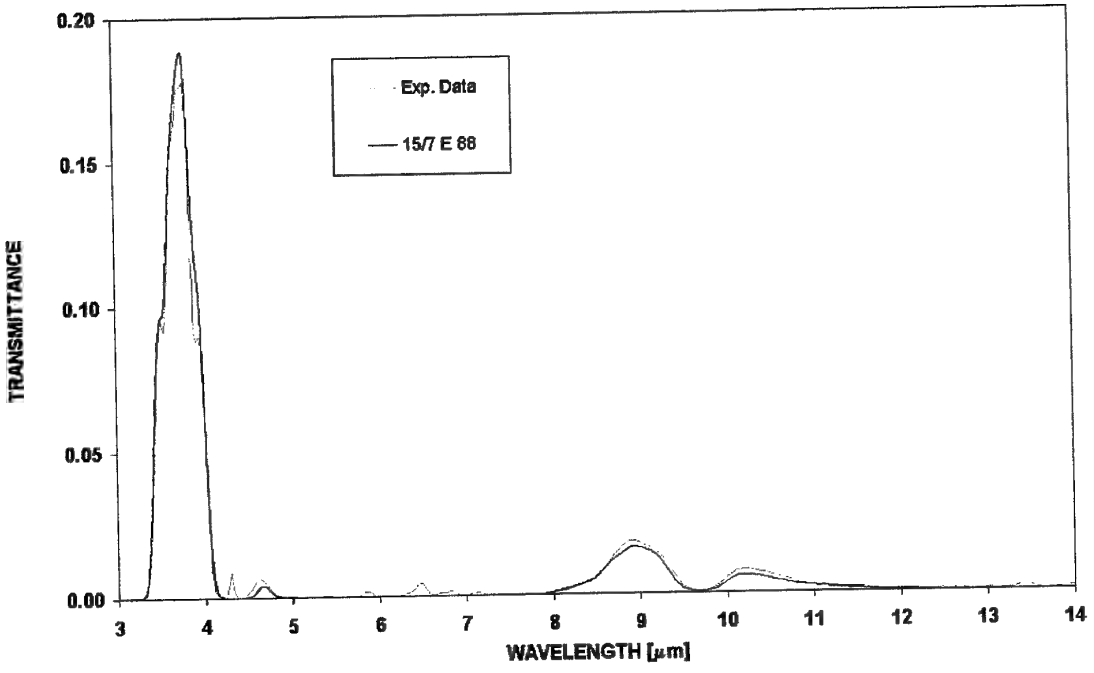

Figure 31: The measured transmittance (Exp. Data) compared to the prediction of MODTRAN 4.1 for zenith angle of 88° in the evening of 15/7/02.

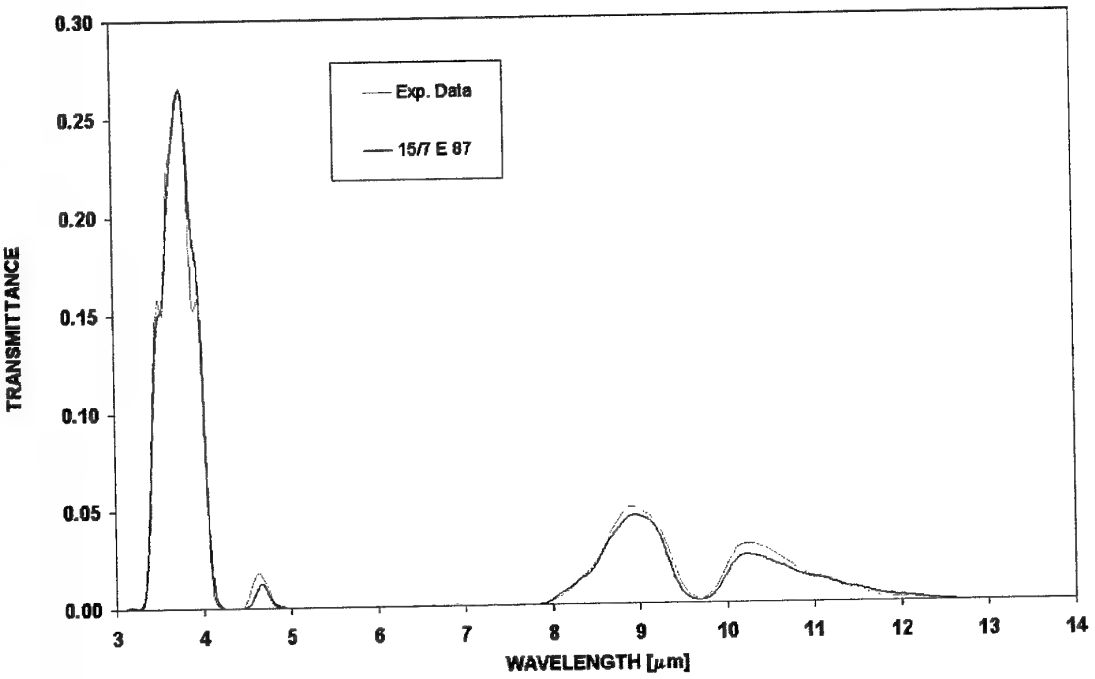

Figure 32: The measured transmittance (Exp. Data) compared to the prediction of MODTRAN 4.1 for zenith angle of 87° in the evening of 15/7/02.

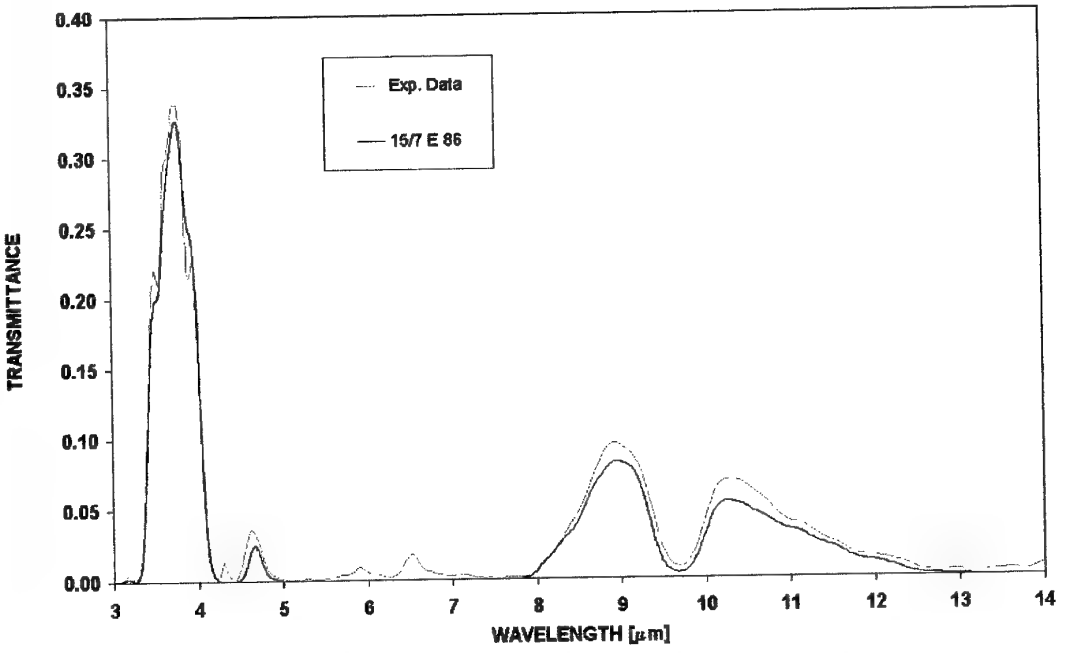

Figure 33: The measured transmittance (Exp. Data) compared to the prediction of MODTRAN 4.1 for zenith angle of 86° in the evening of 15/7/02.

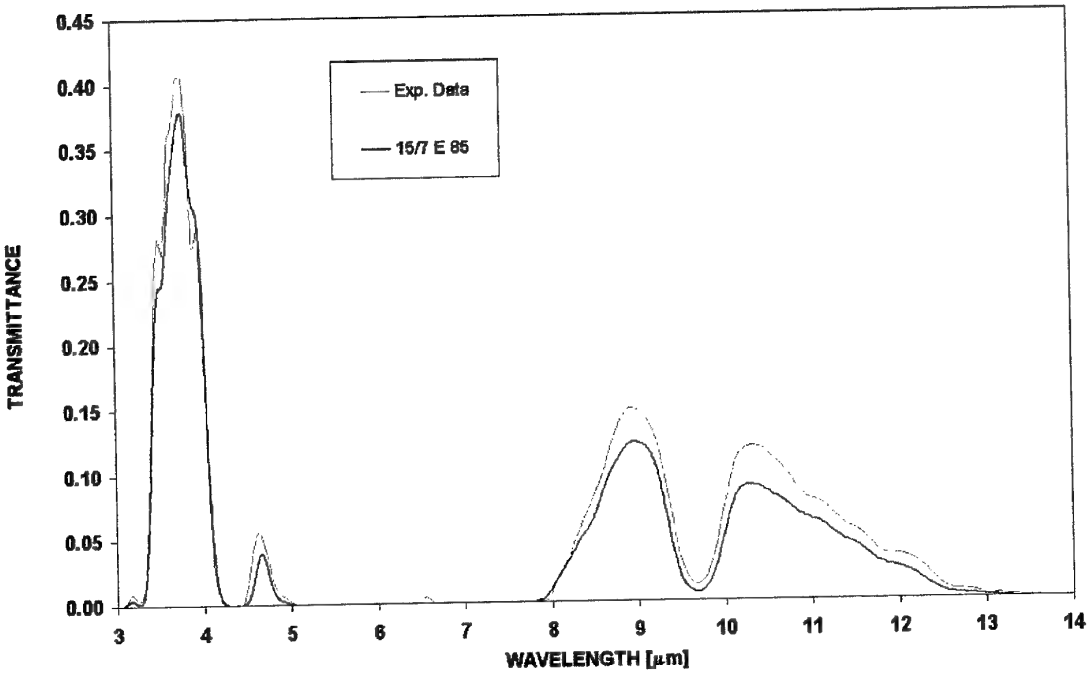

Figure 34: The measured transmittance (Exp. Data) compared to the prediction of MODTRAN 4.1 for zenith angle of 85° in the evening of 15/7/02.

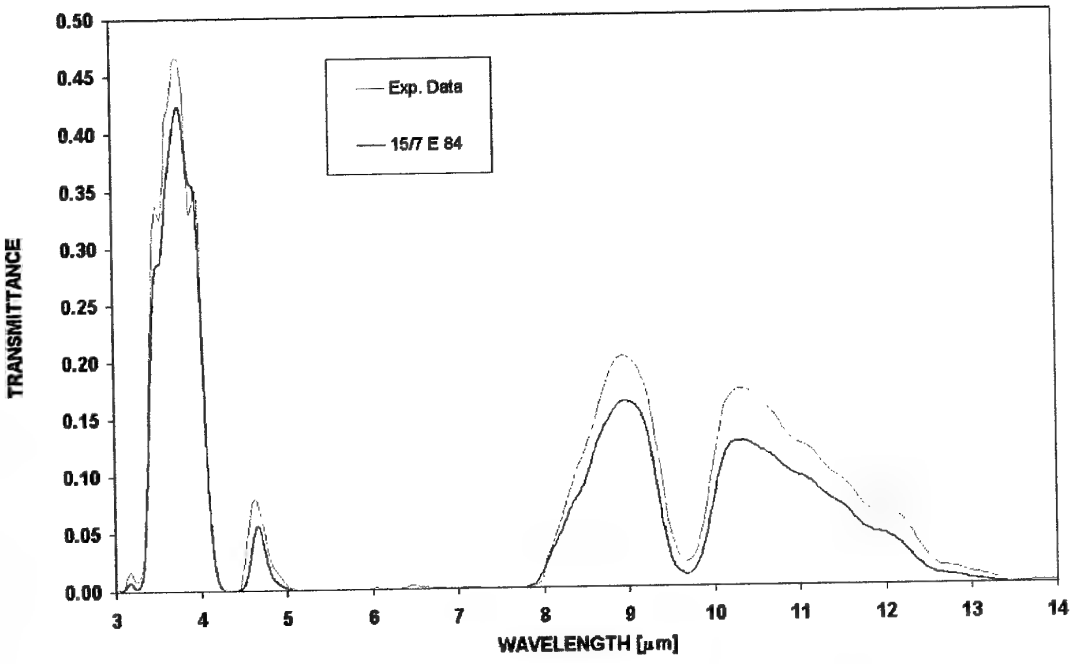

Figure 35: The measured transmittance (Exp. Data) compared to the prediction of MODTRAN 4.1 for zenith angle of 84° in the evening of 15/7/02.

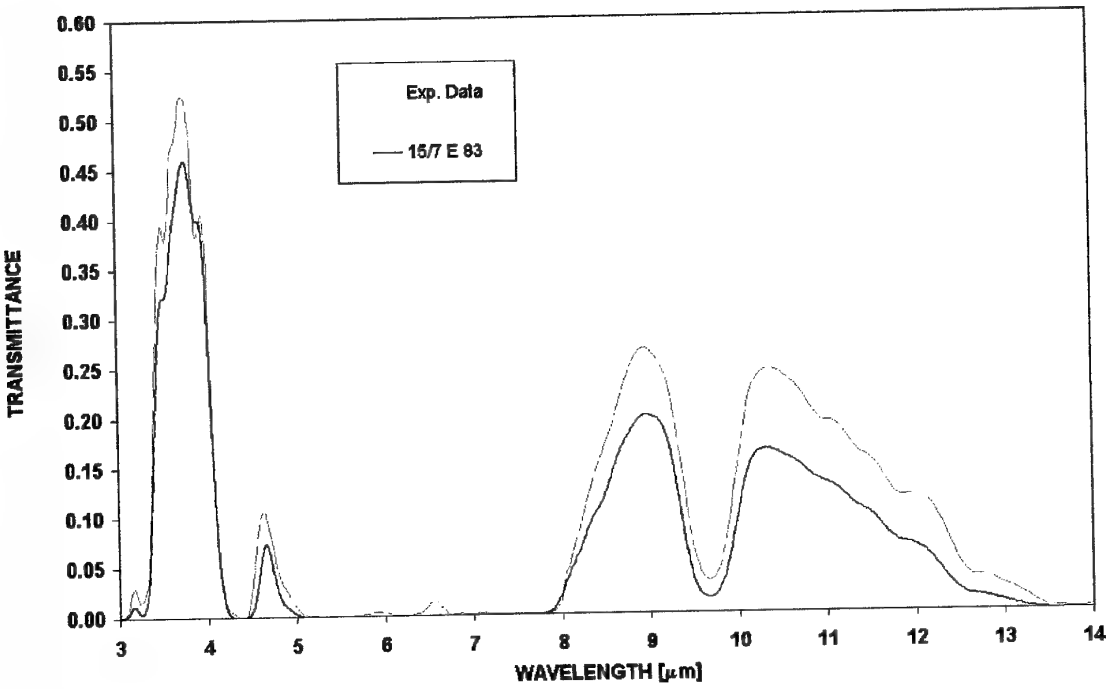

Figure 36: The measured transmittance (Exp. Data) compared to the prediction of MODTRAN 4.1 for zenith angle of 83° in the evening of 15/7/02.

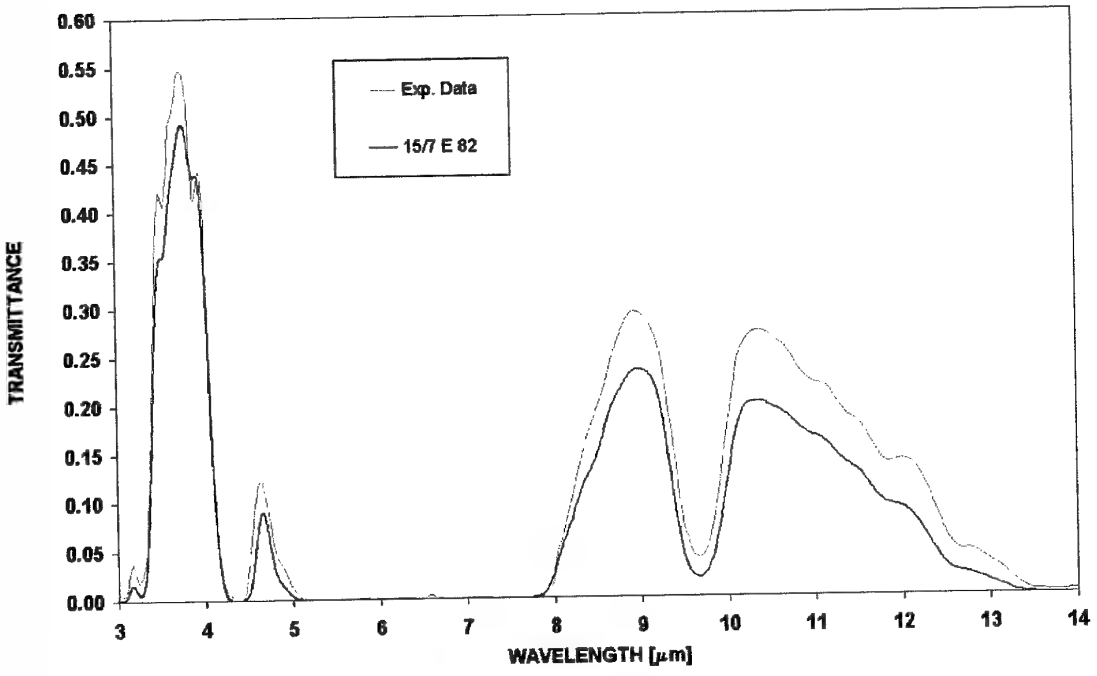

Figure 37: The measured transmittance (Exp. Data) compared to the prediction of MODTRAN 4.1 for zenith angle of 82° in the evening of 15/7/02.

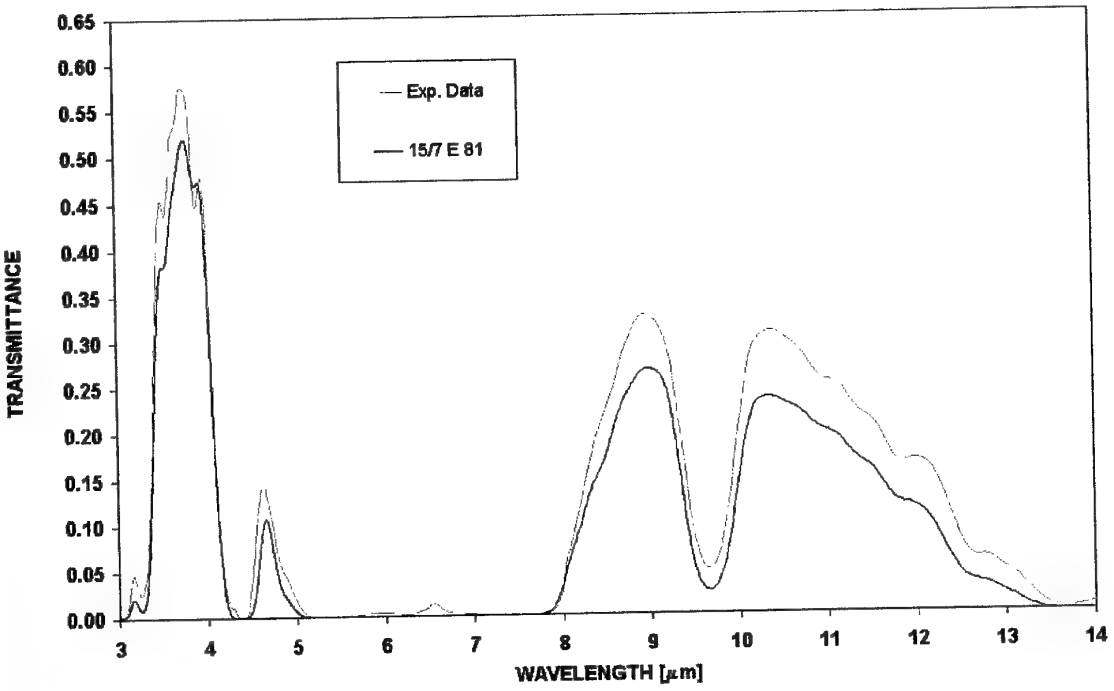

Figure 38: The measured transmittance (Exp. Data) compared to the prediction of MODTRAN 4.1 for zenith angle of 81° in the evening of 15/7/02.

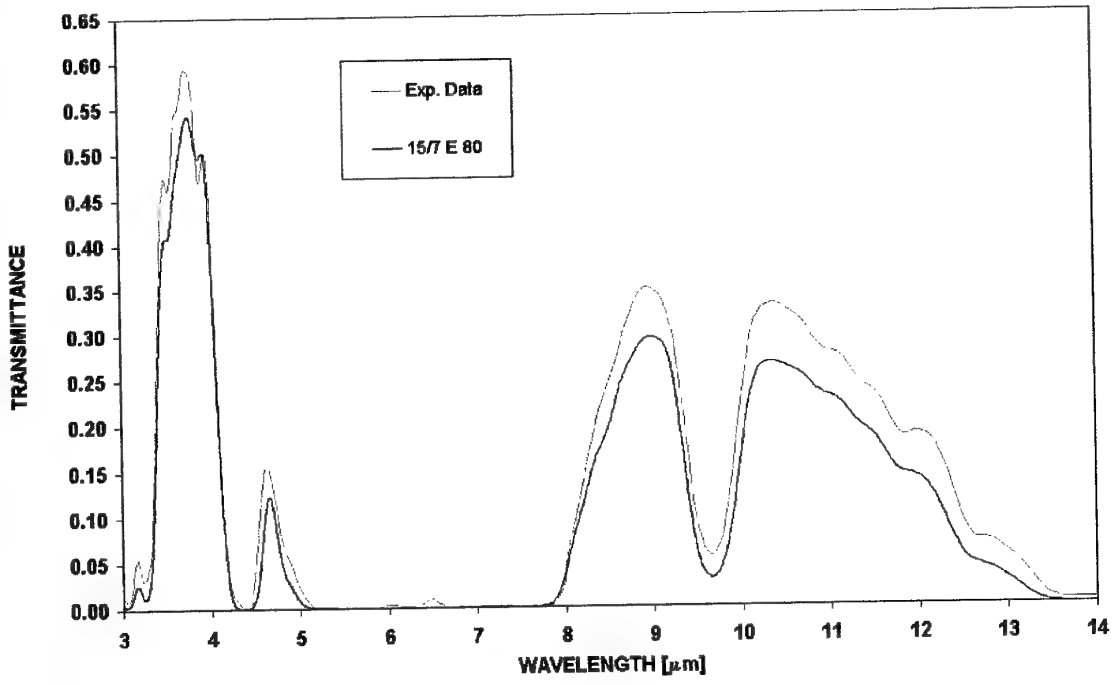

Figure 39: The measured transmittance (Exp. Data) compared to the prediction of MODTRAN 4.1 for zenith angle of 80° in the evening of 15/7/02.

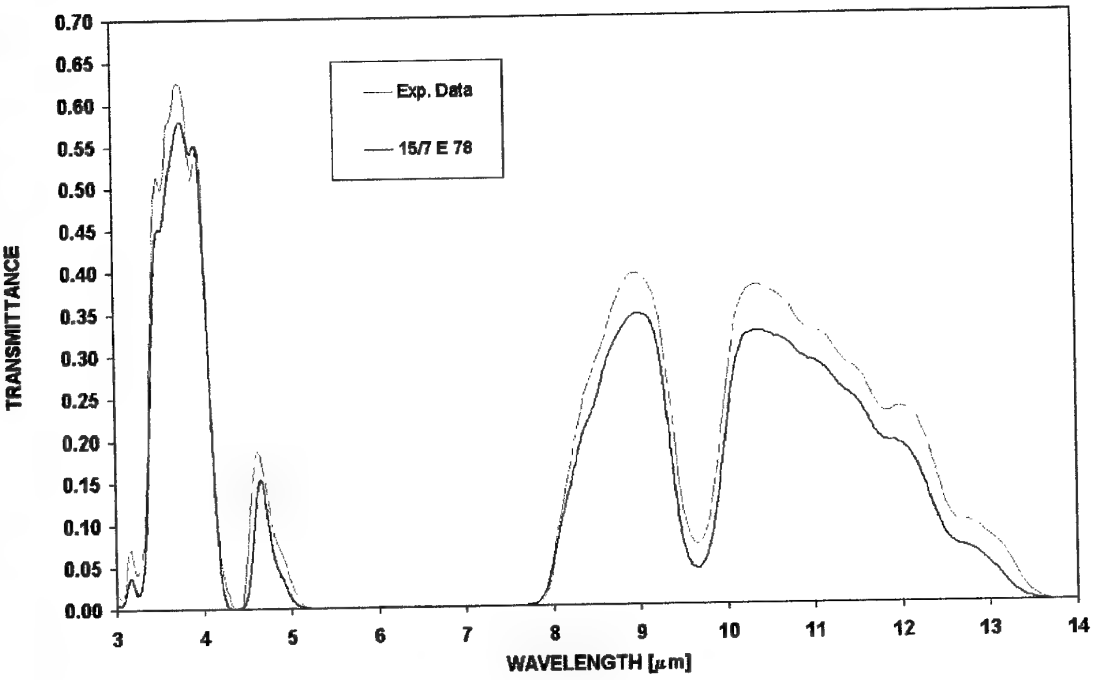

Figure 40: The measured transmittance (Exp. Data) compared to the prediction of MODTRAN 4.1 for zenith angle of 78° in the evening of 15/7/02.

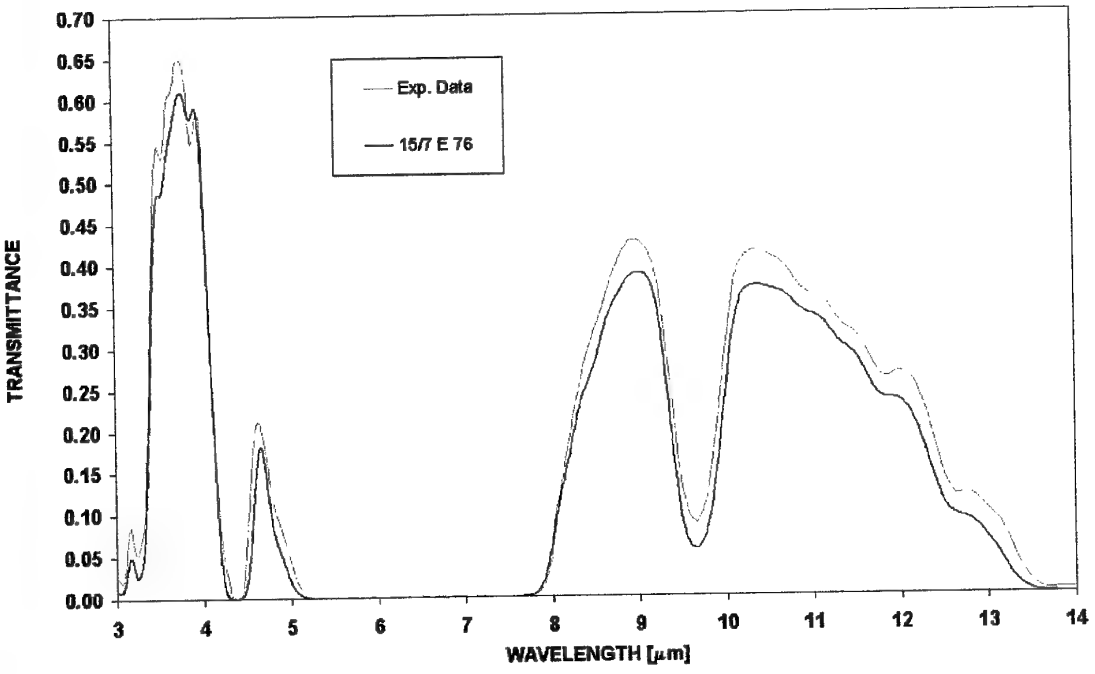

Figure 41: The measured transmittance (Exp. Data) compared to the prediction of MODTRAN 4.1 for zenith angle of 76° in the evening of 15/7/02.

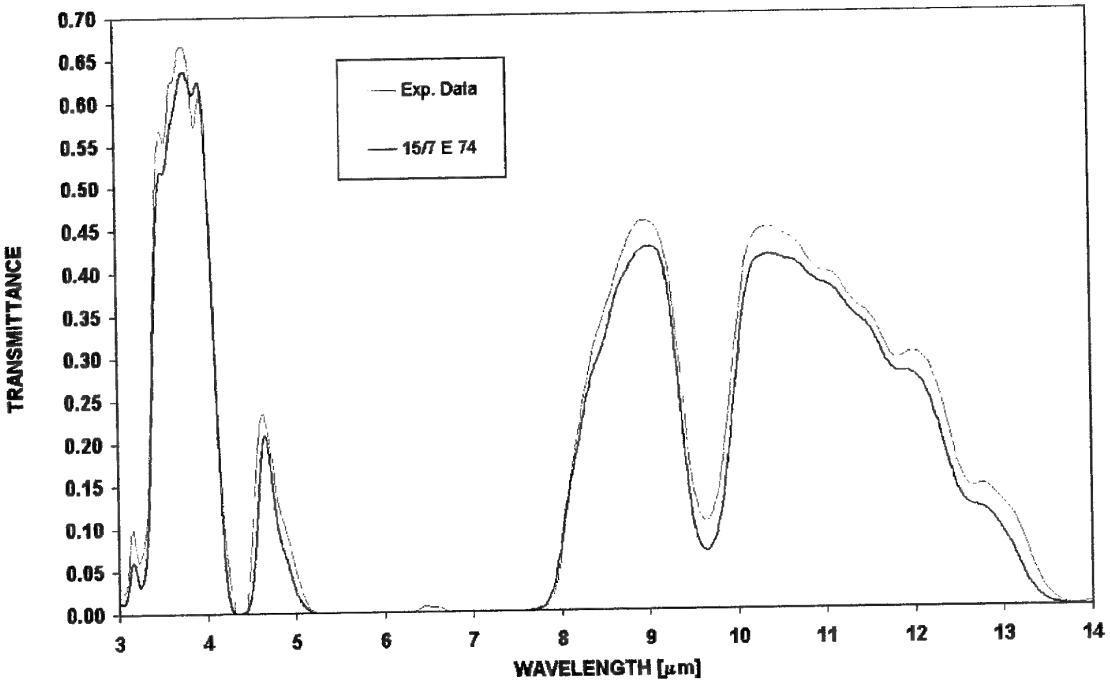

Figure 42: The measured transmittance (Exp. Data) compared to the prediction of MODTRAN 4.1 for zenith angle of 74° in the evening of 15/7/02.

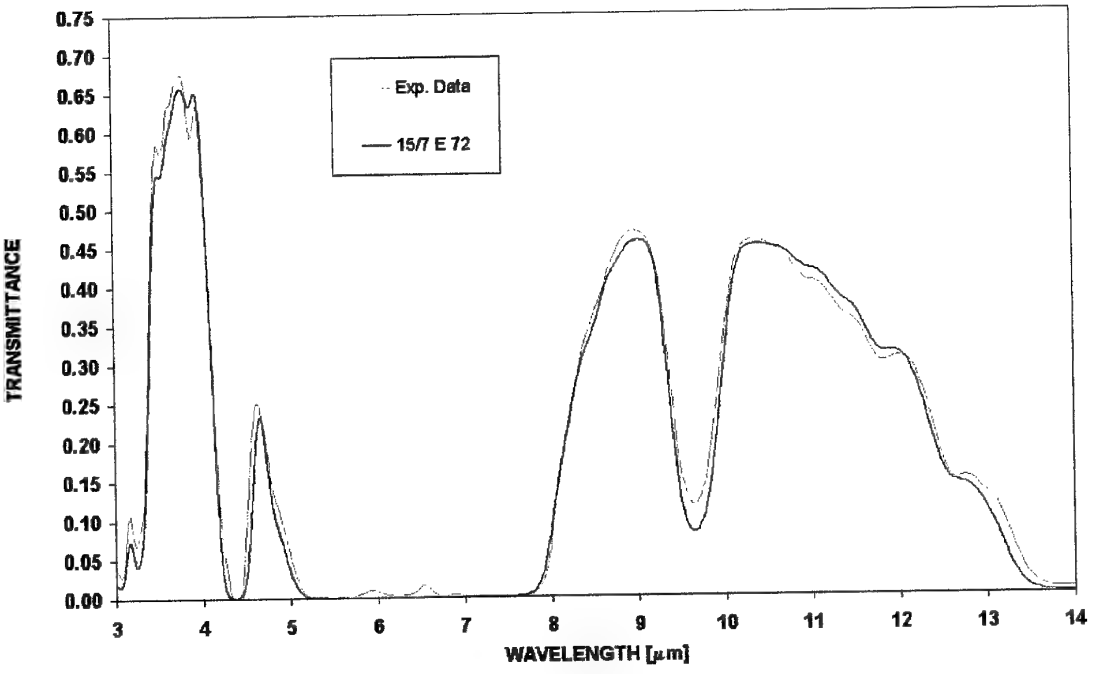

Figure 43: The measured transmittance (Exp. Data) compared to the prediction of MODTRAN 4.1 for zenith angle of 72° in the evening of 15/7/02.

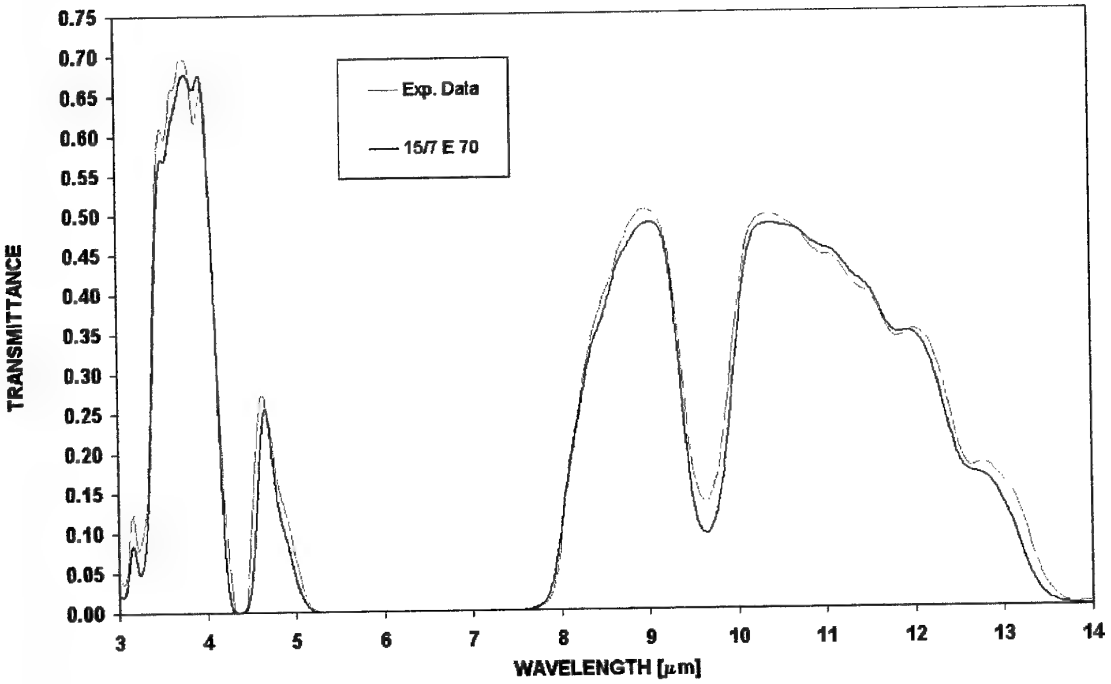

Figure 44: The measured transmittance (Exp. Data) compared to the prediction of MODTRAN 4.1 for zenith angle of 70° in the evening of 15/7/02.

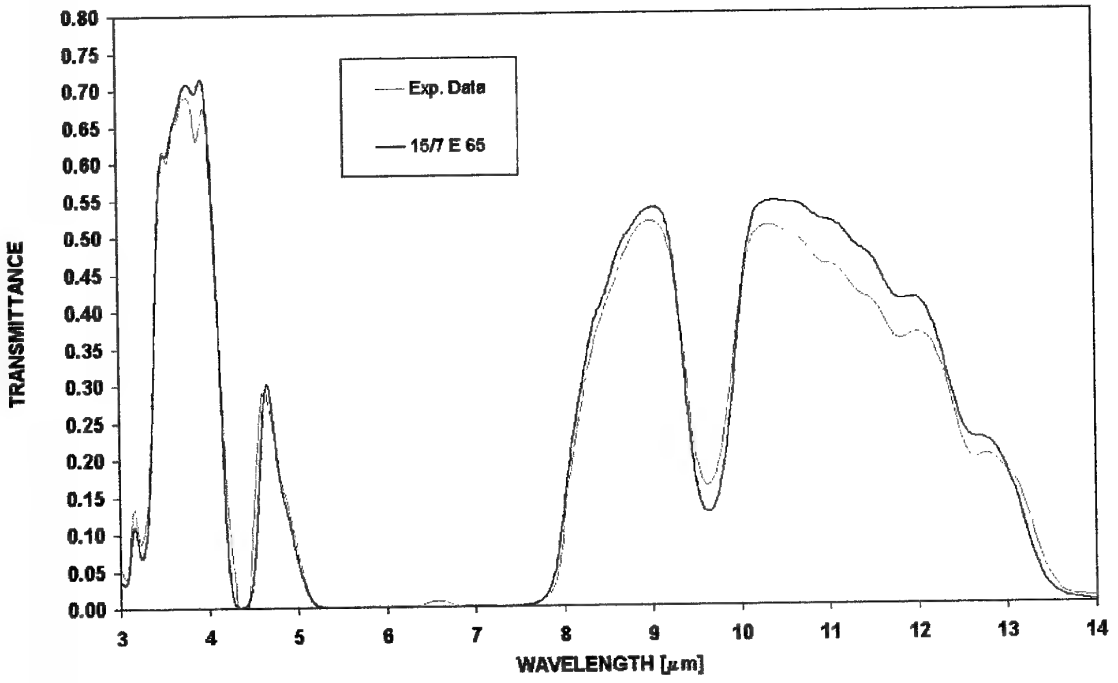

Figure 45: The measured transmittance (Exp. Data) compared to the prediction of MODTRAN 4.1 for zenith angle of 65° in the evening of 15/7/02.

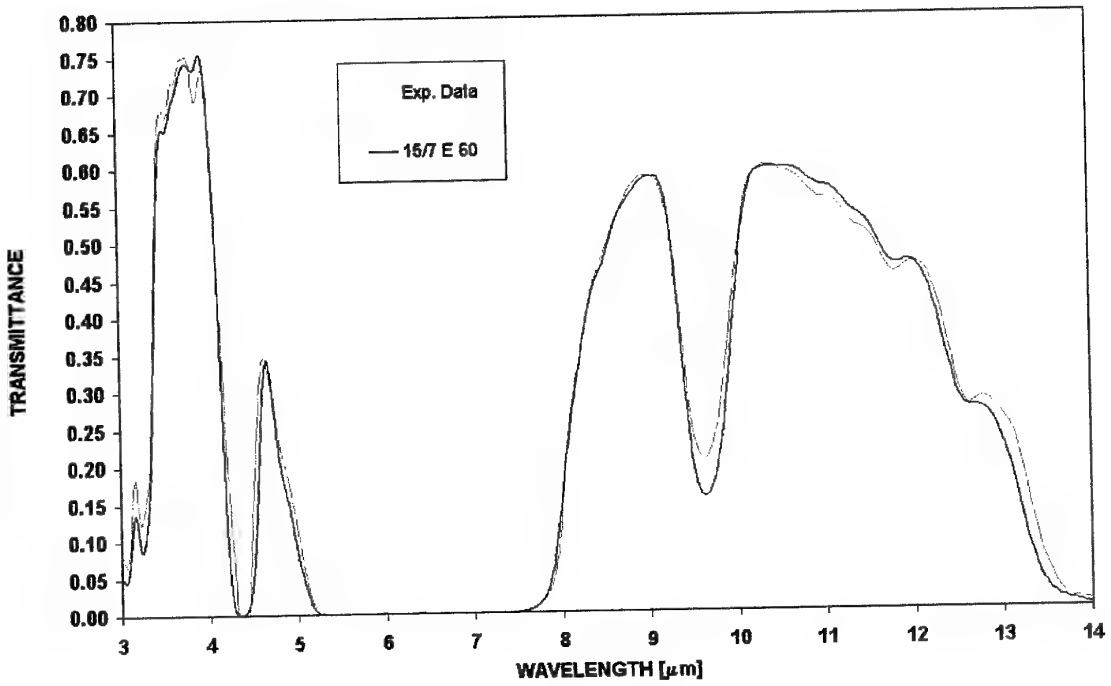

Figure 46: The measured transmittance (Exp. Data) compared to the prediction of MODTRAN 4.1 for zenith angle of 60° in the evening of 15/7/02.

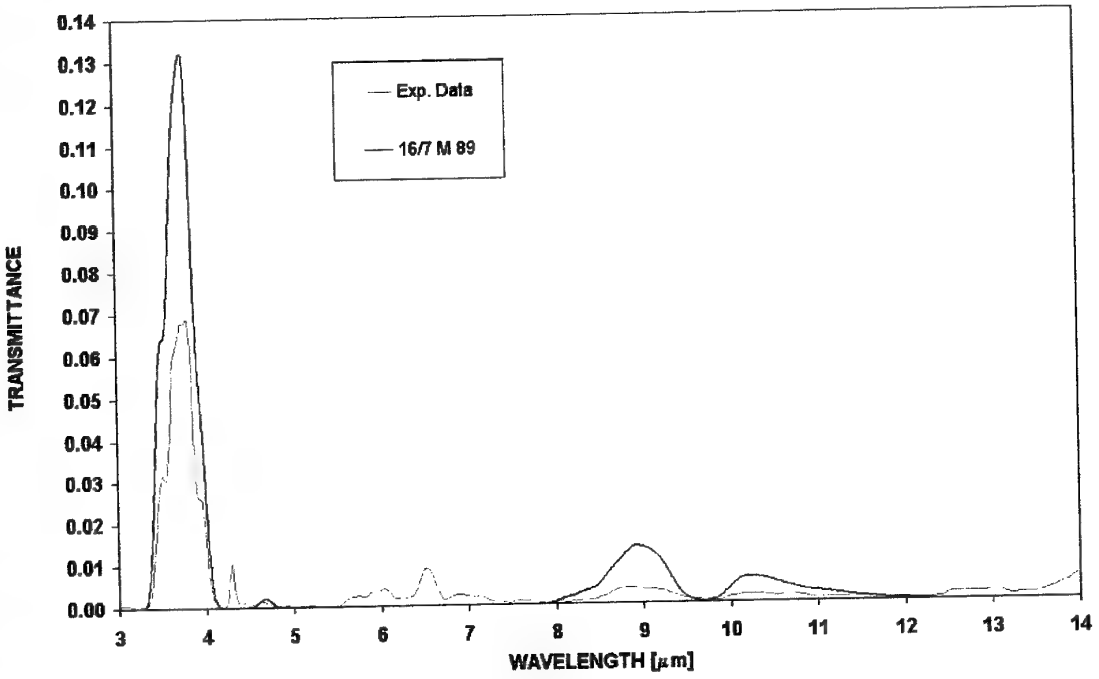

Figure 47: The measured transmittance (Exp. Data) compared to the prediction of MODTRAN 4.1 for zenith angle of 89° in the morning of 16/7/02

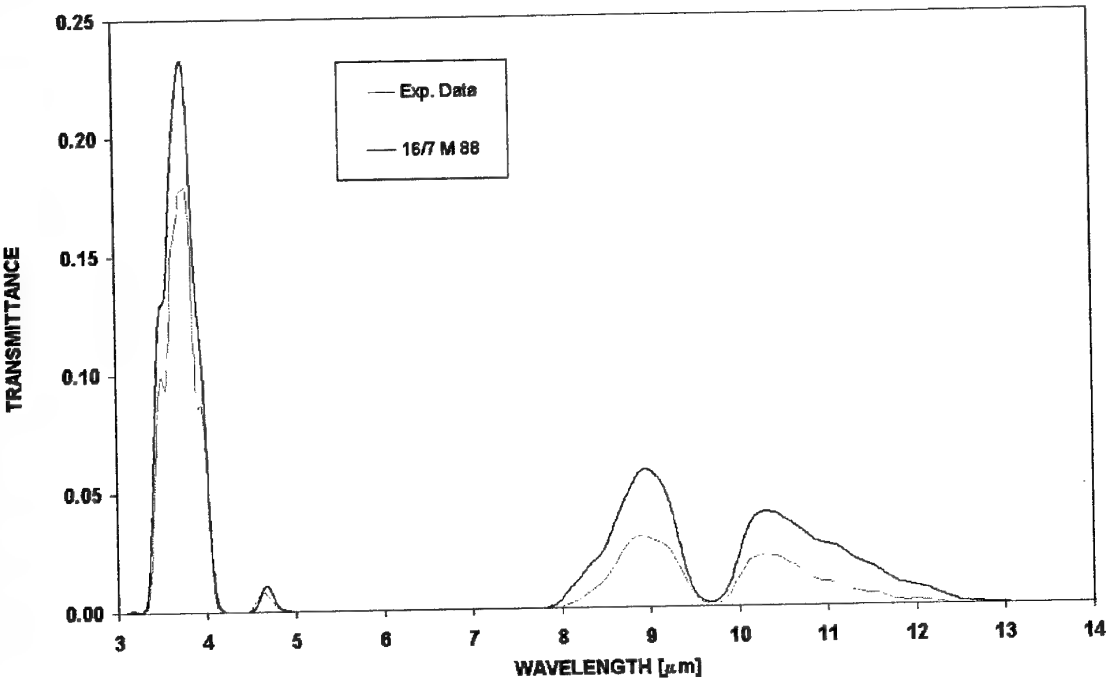

Figure 48: The measured transmittance (Exp. Data) compared to the prediction of MODTRAN 4.1 for zenith angle of 88° in the morning of 16/702.

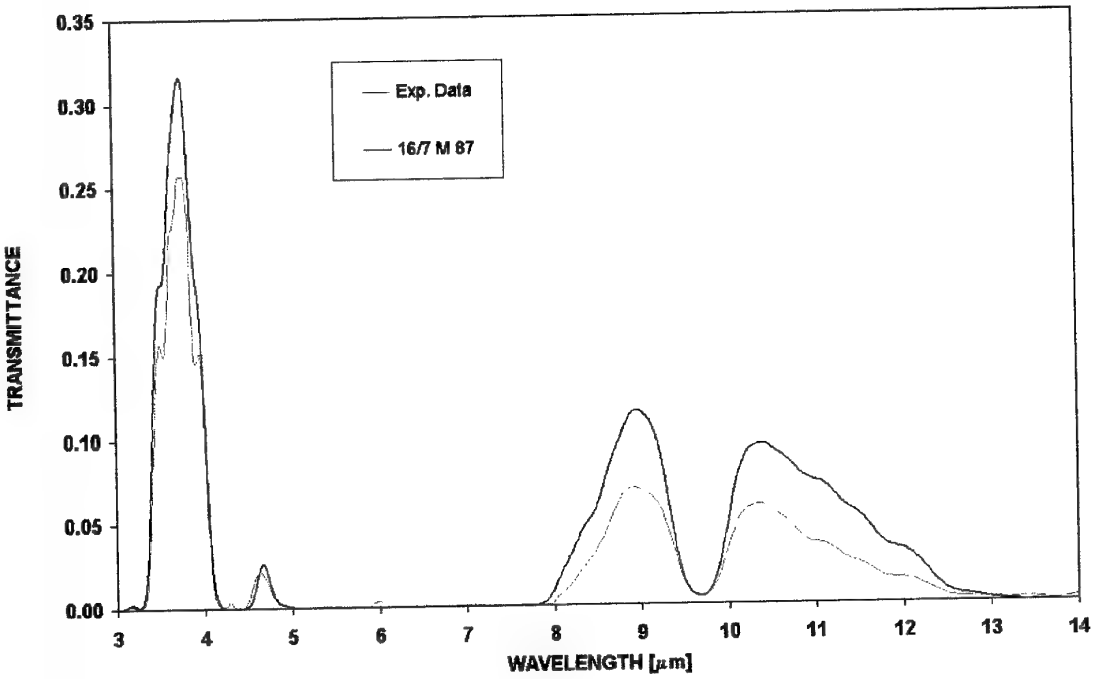

Figure 49: The measured transmittance (Exp. Data) compared to the prediction of MODTRAN 4.1 for zenith angle of 87° in the morning of 16/702.

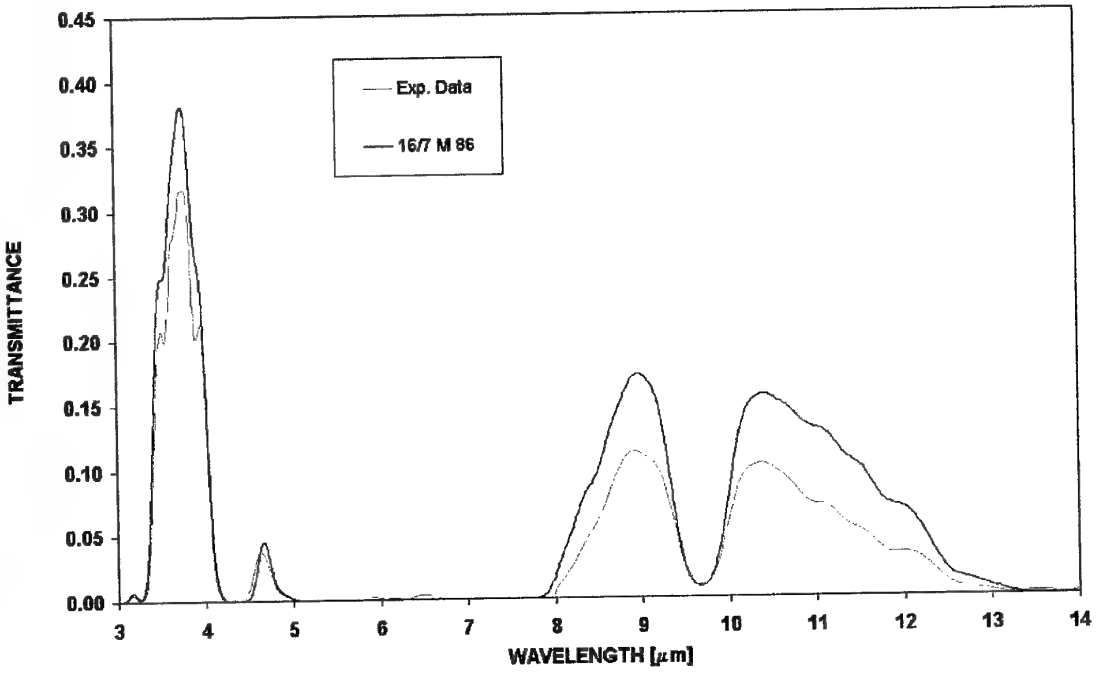

Figure 50: The measured transmittance (Exp. Data) compared to the prediction of MODTRAN 4.1 for zenith angle of 86° in the morning of 16/702.

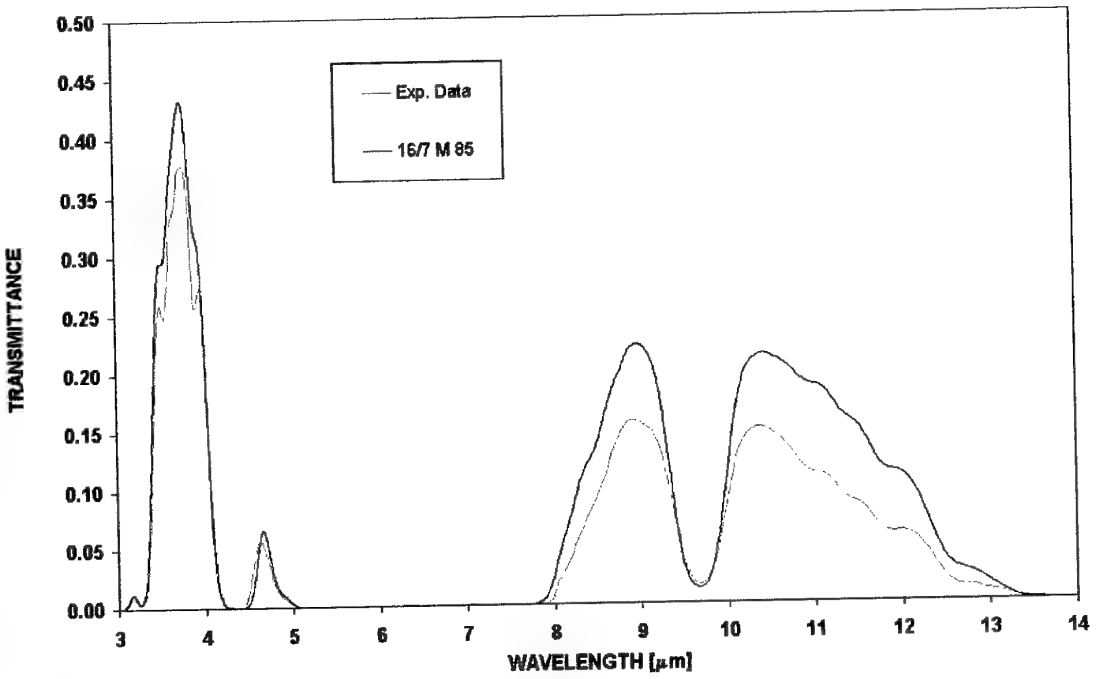

Figure 51: The measured transmittance (Exp. Data) compared to the prediction of MODTRAN 4.1 for zenith angle of 85° in the morning of 16/702.

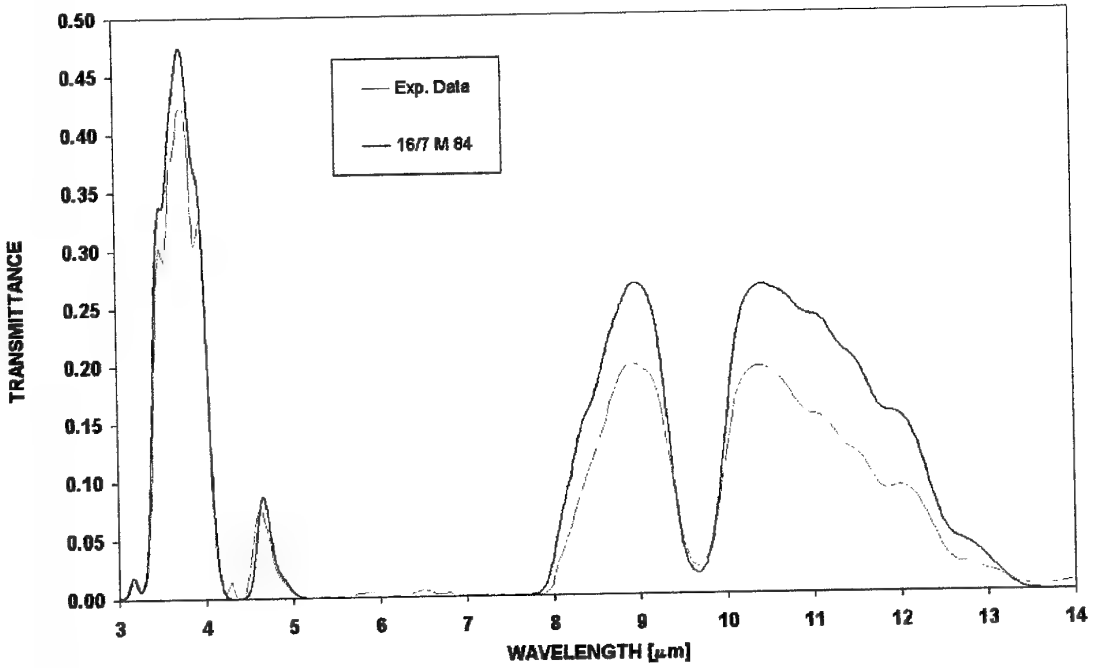

Figure 52: The measured transmittance (Exp. Data) compared to the prediction of MODTRAN 4.1 for zenith angle of 84° in the morning of 16/702.

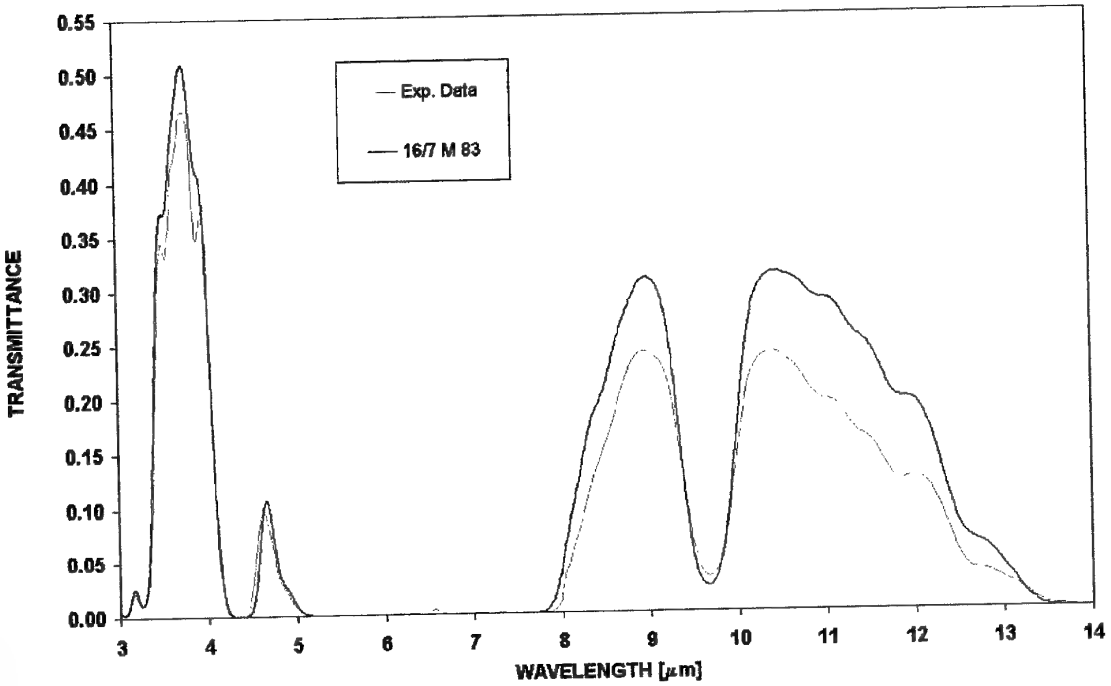

Figure 53: The measured transmittance (Exp. Data) compared to the prediction of MODTRAN 4.1 for zenith angle of 83° in the morning of 16/702.

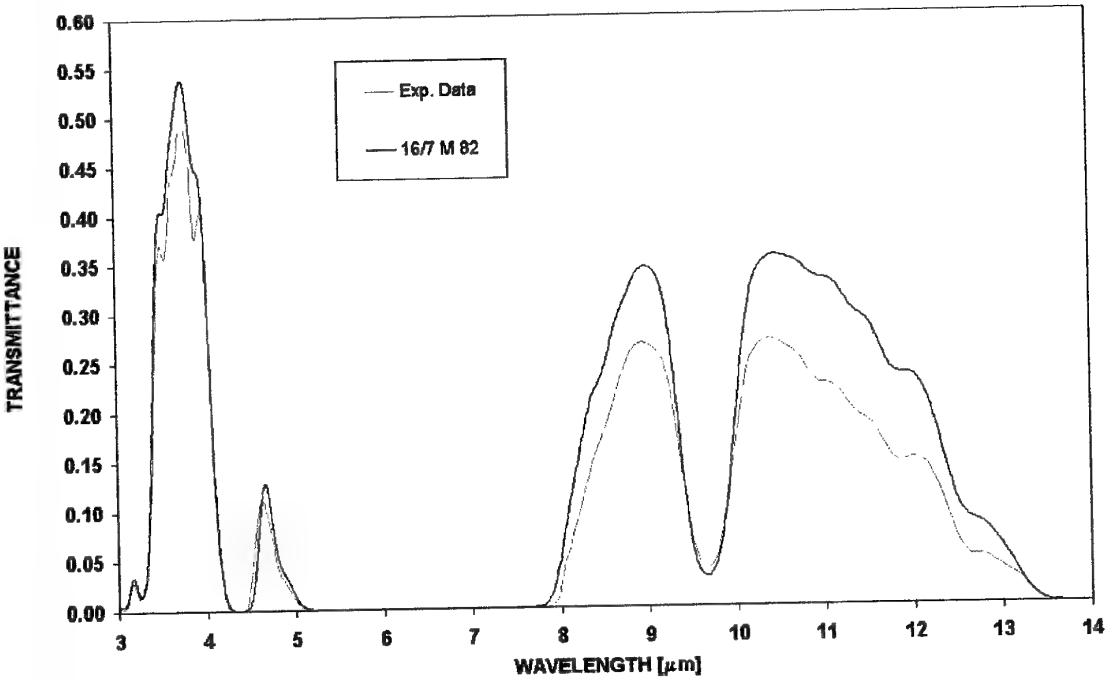

Figure 54: The measured transmittance (Exp. Data) compared to the prediction of MODTRAN 4.1 for zenith angle of 82° in the morning of 16/702.

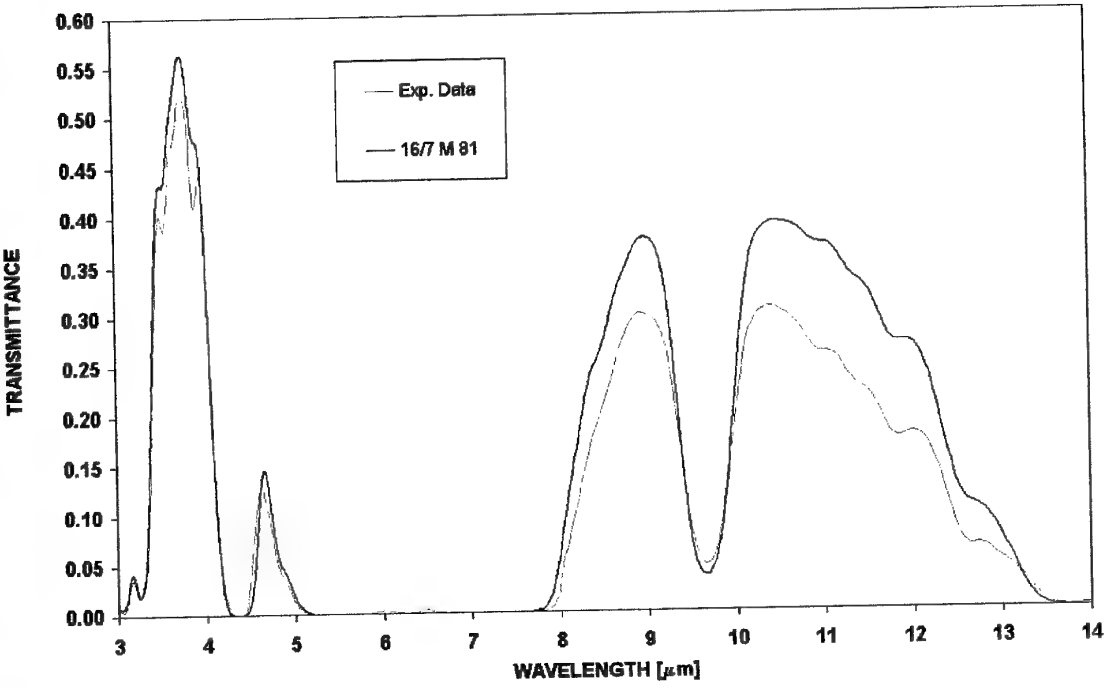

Figure 55: The measured transmittance (Exp. Data) compared to the prediction of MODTRAN 4.1 for zenith angle of 81° in the morning of 16/702.

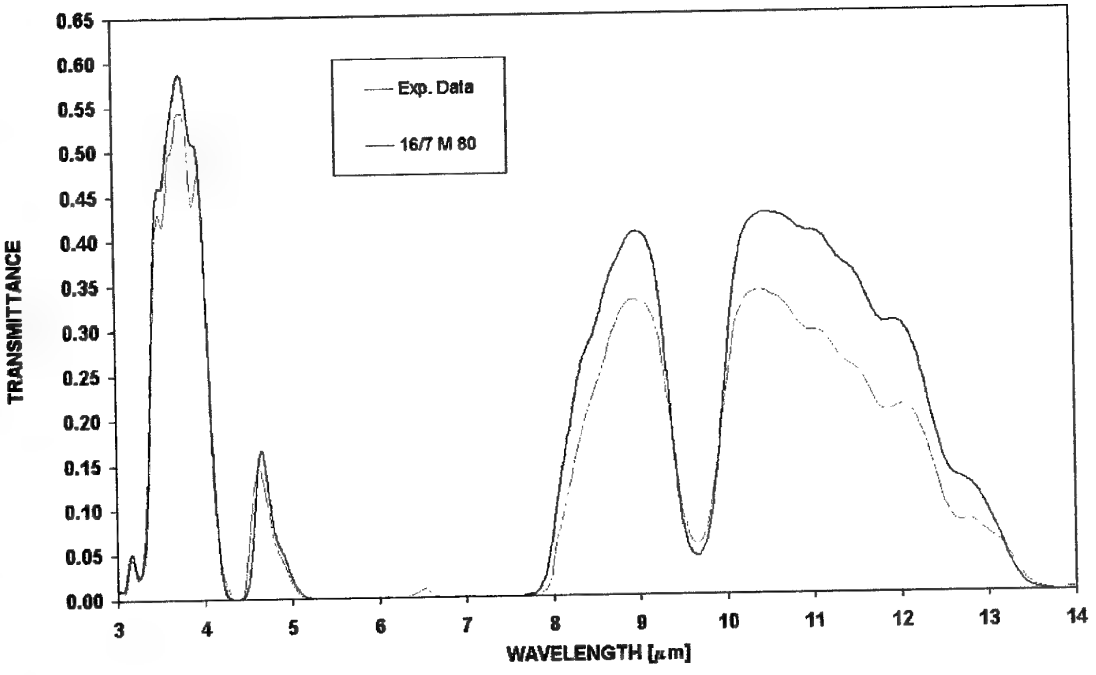

Figure 56: The measured transmittance (Exp. Data) compared to the prediction of MODTRAN 4.1 for zenith angle of 80° in the morning of 16/702.

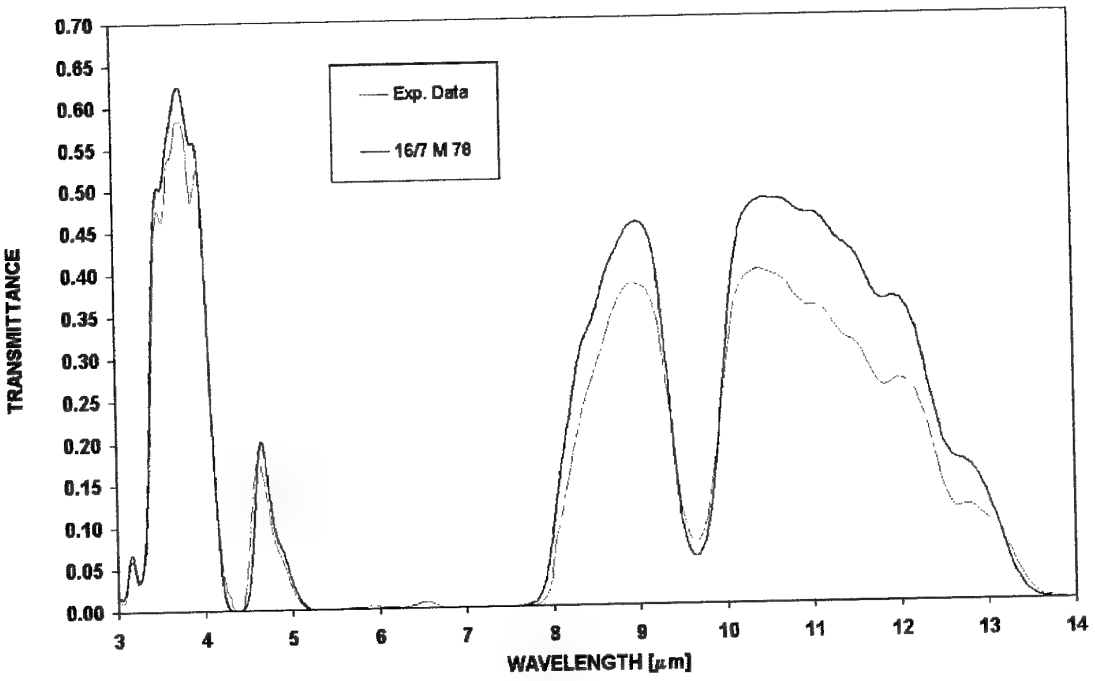

Figure 57: The measured transmittance (Exp. Data) compared to the prediction of MODTRAN 4.1 for zenith angle of 78° in the morning of 16/702.

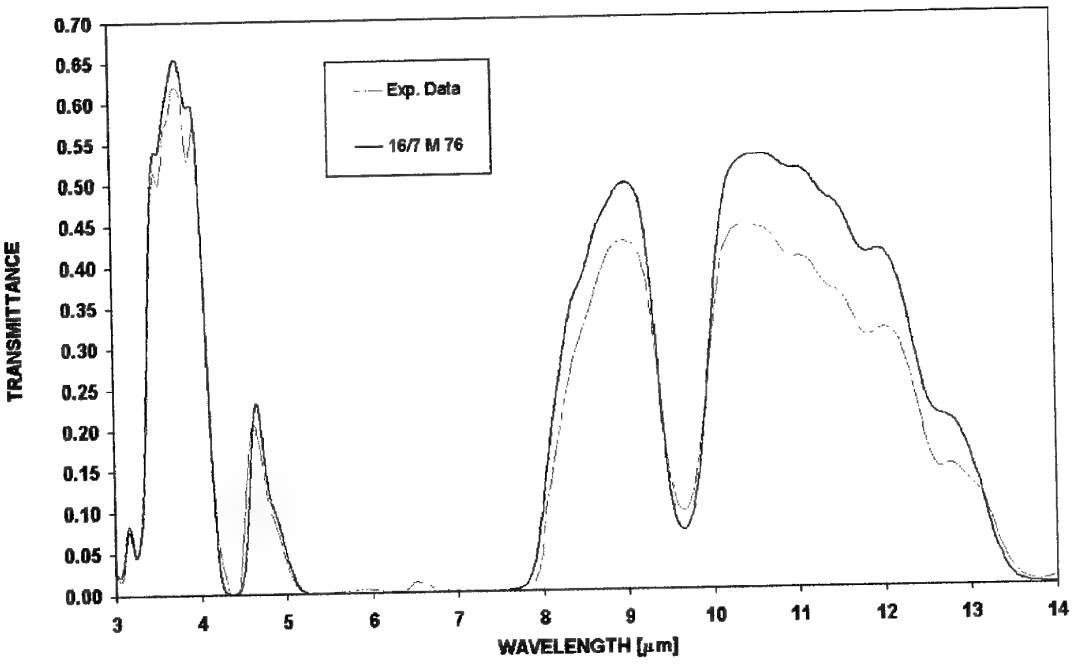

Figure 58: The measured transmittance (Exp. Data) compared to the prediction of MODTRAN 4.1 for zenith angle of 76° in the morning of 16/702.

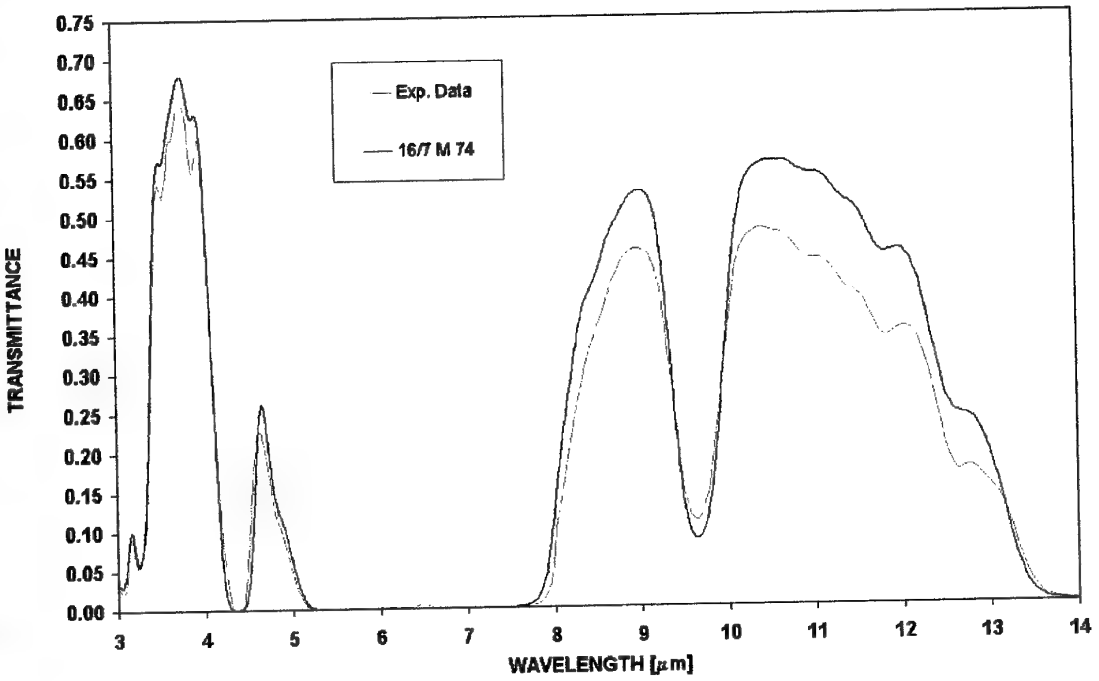

Figure 59: The measured transmittance (Exp. Data) compared to the prediction of MODTRAN 4.1 for zenith angle of 74° in the morning of 16/702.

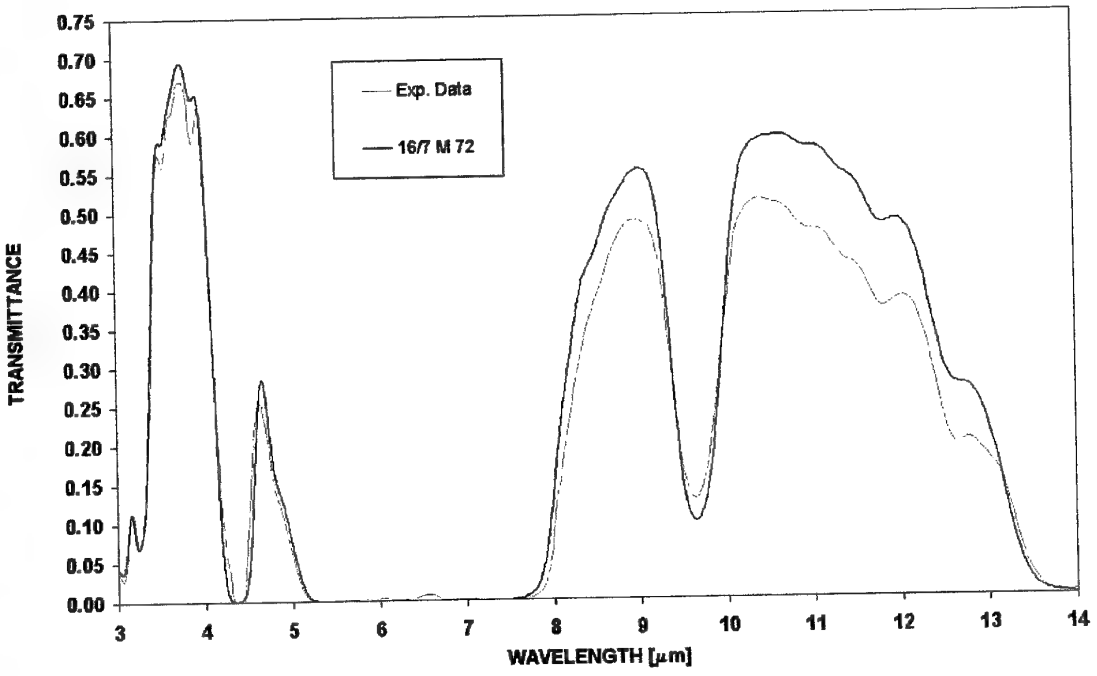

Figure 60: The measured transmittance (Exp. Data) compared to the prediction of MODTRAN 4.1 for zenith angle of 72° in the morning of 16/702.

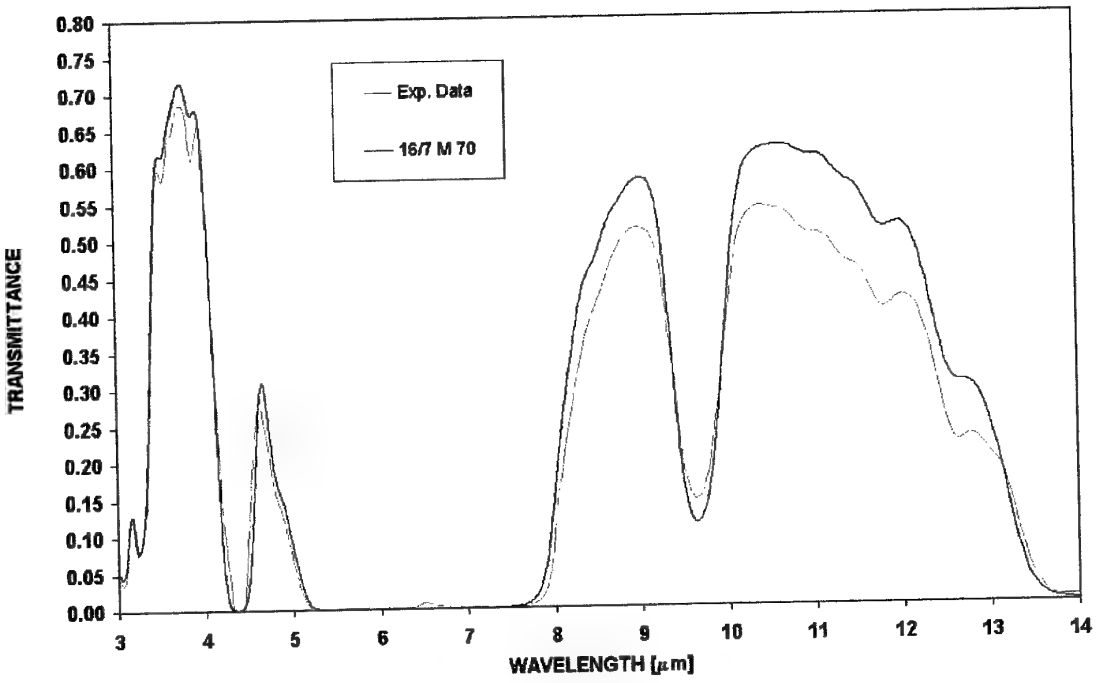

Figure 61: The measured transmittance (Exp. Data) compared to the prediction of MODTRAN 4.1 for zenith angle of 70° in the morning of 16/702.

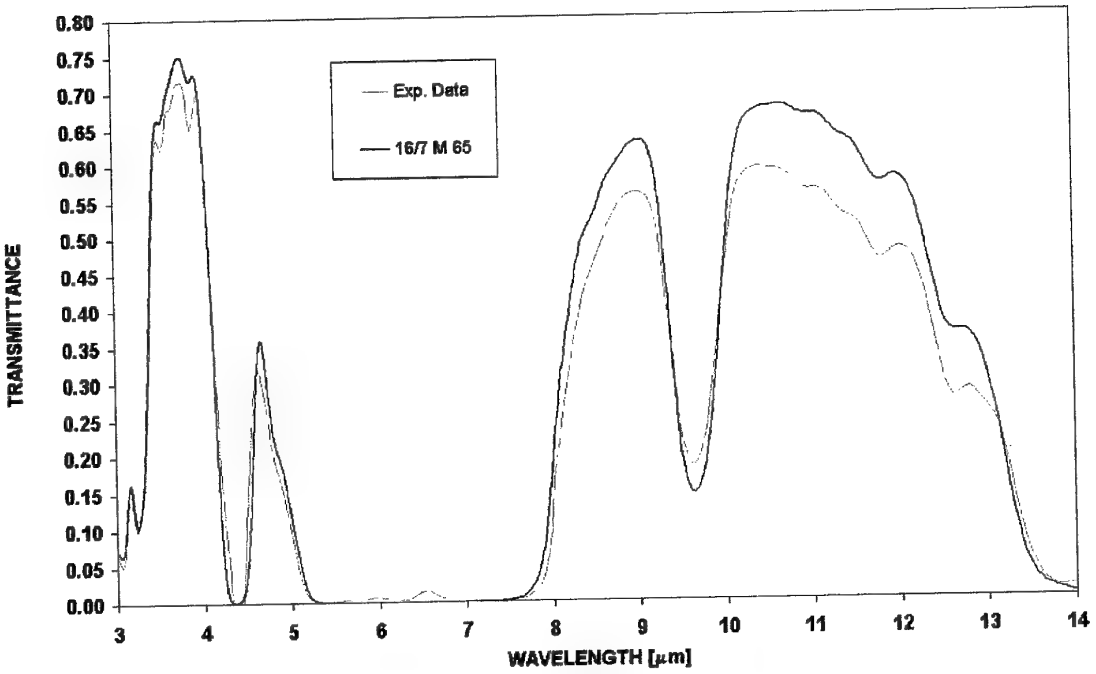

Figure 62: The measured transmittance (Exp. Data) compared to the prediction of MODTRAN 4.1 for zenith angle of 65° in the morning of 16/702.

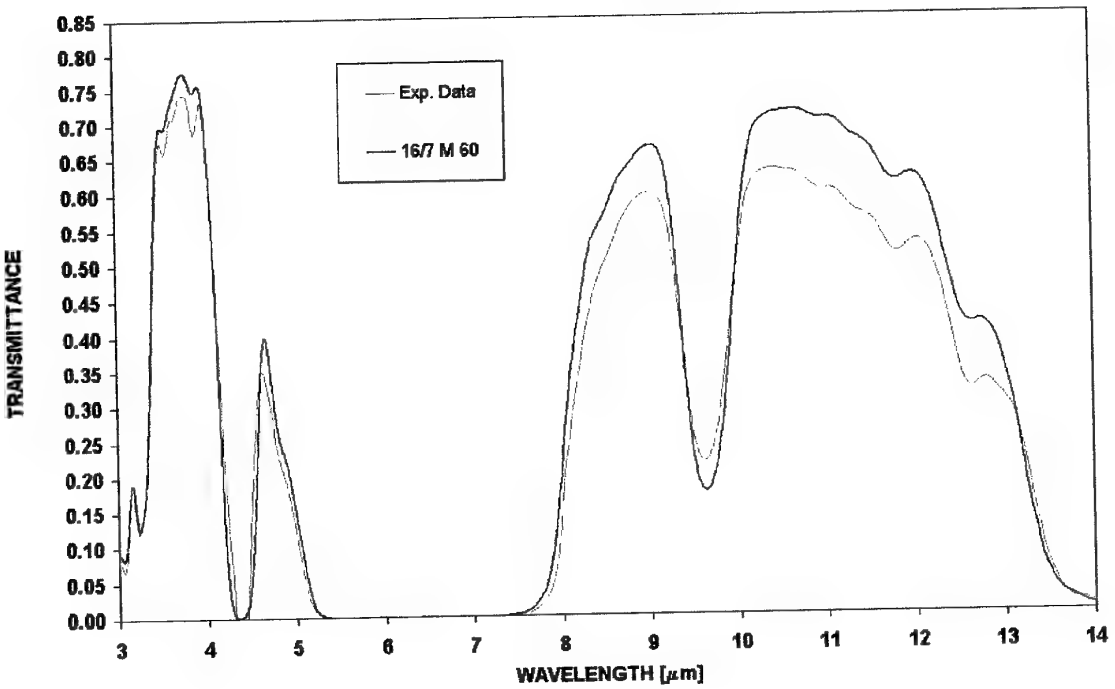

Figure 63: The measured transmittance (Exp. Data) compared to the prediction of MODTRAN 4.1 for zenith angle of 60° in the morning of 16/702.

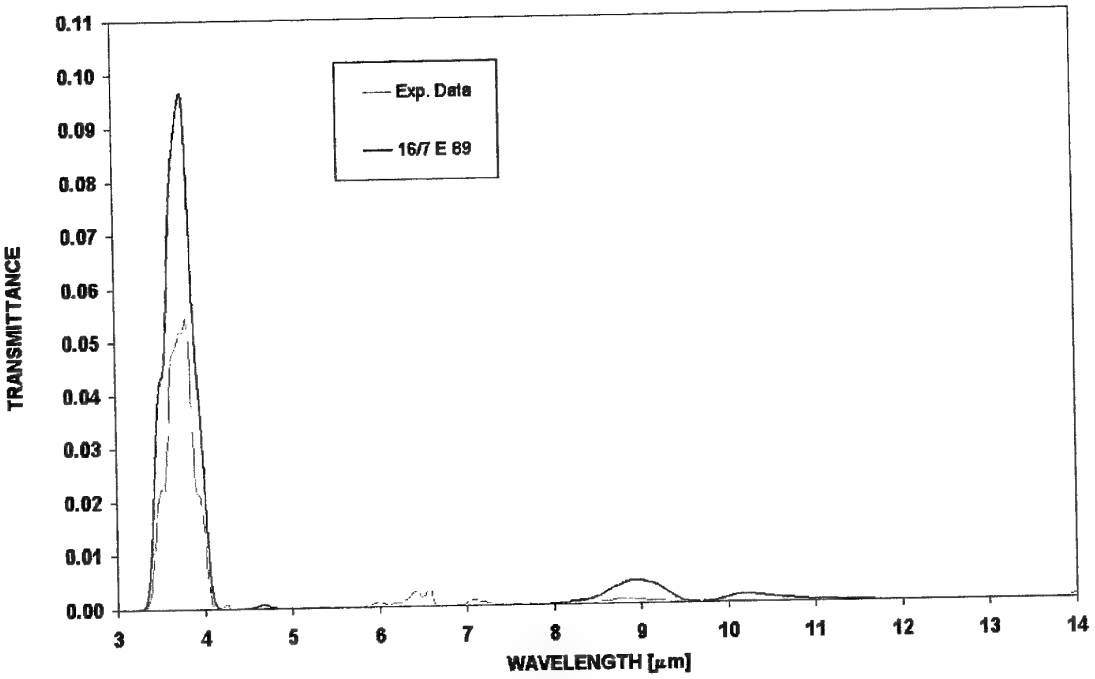

Figure 64: The measured transmittance (Exp. Data) compared to the prediction of MODTRAN 4.1 for zenith angle of 89° in the evening of 16/7/02

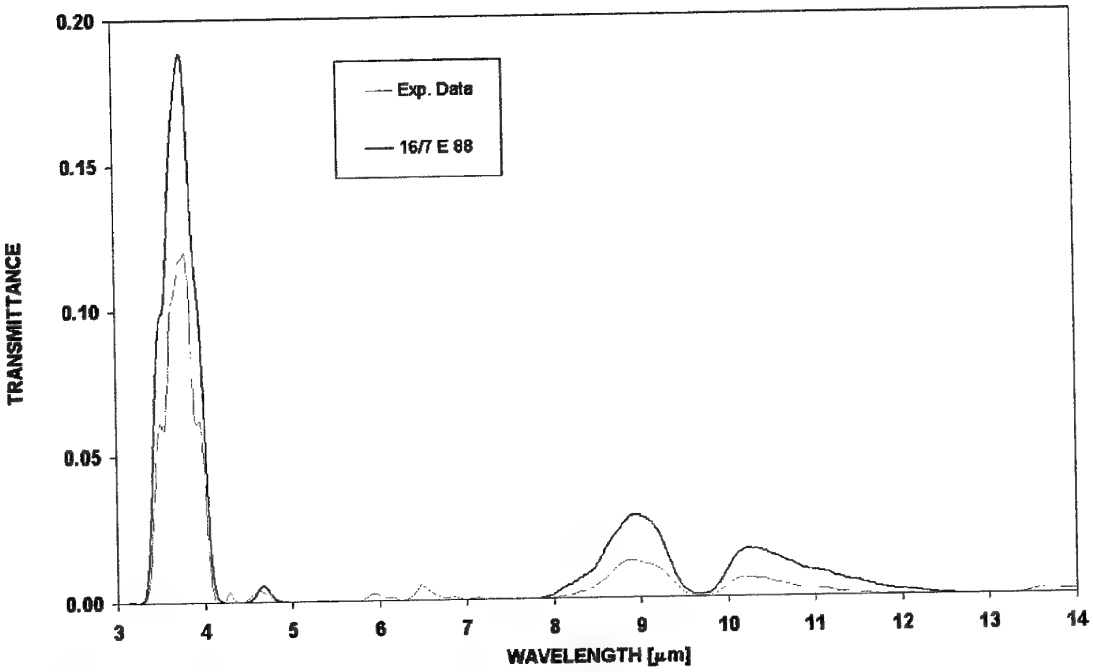

Figure 65: The measured transmittance (Exp. Data) compared to the prediction of MODTRAN 4.1 for zenith angle of 88° in the evening of 16/702.

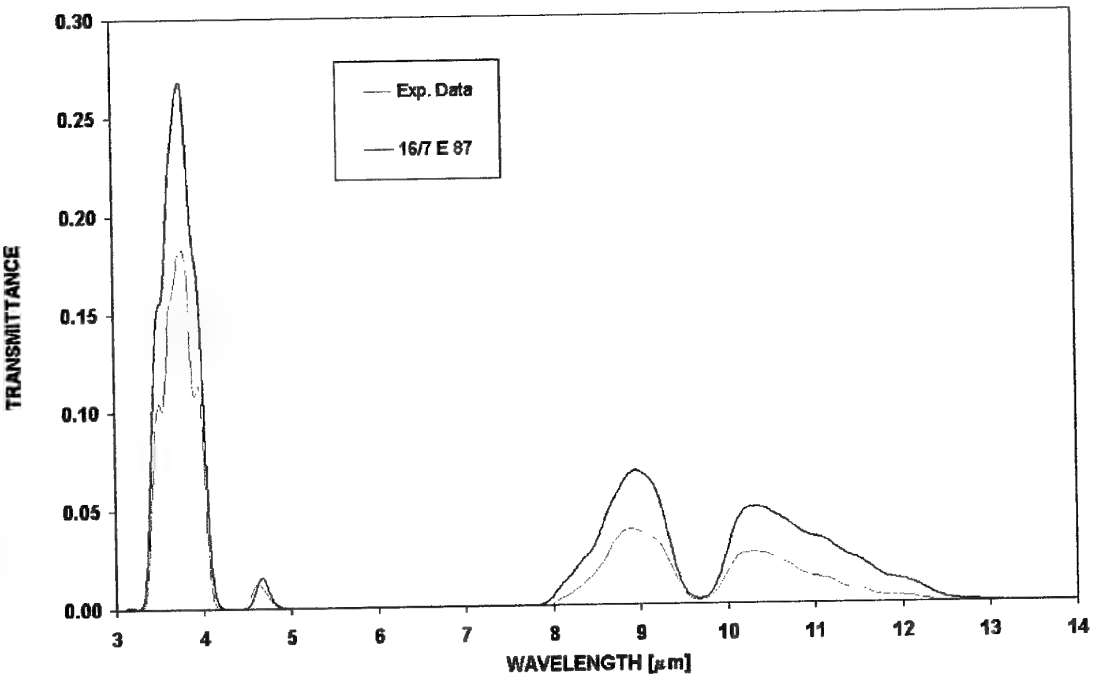

Figure 66: The measured transmittance (Exp. Data) compared to the prediction of MODTRAN 4.1 for zenith angle of 87° in the evening of 16/702.

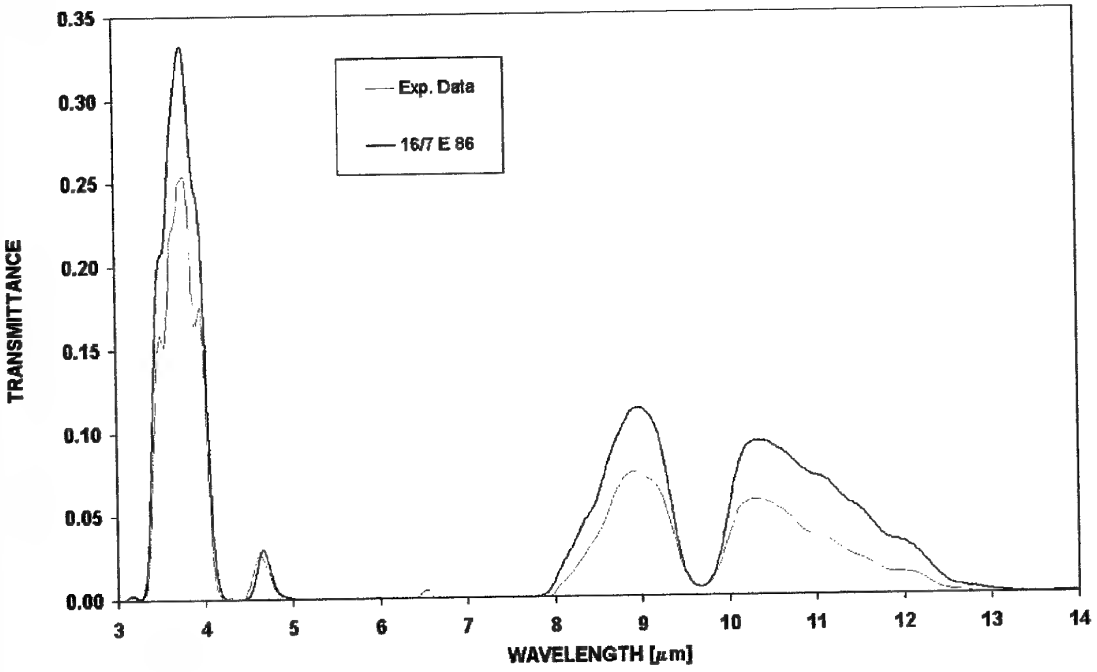

Figure 67: The measured transmittance (Exp. Data) compared to the prediction of MODTRAN 4.1 for zenith angle of 86° in the evening of 16/702.

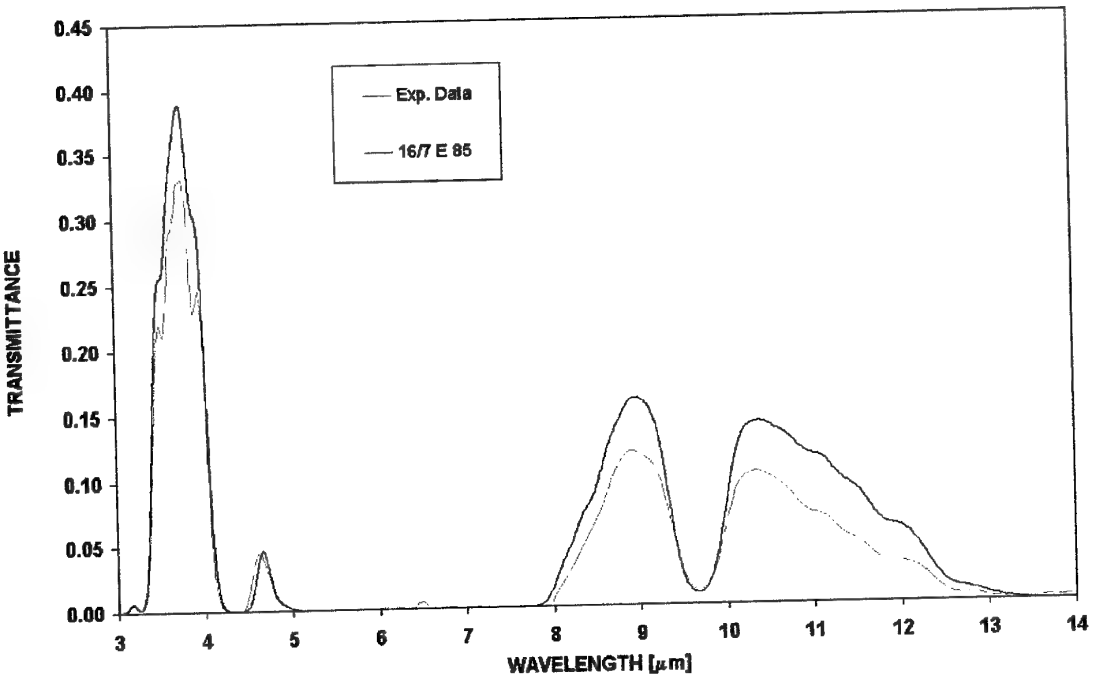

Figure 68: The measured transmittance (Exp. Data) compared to the prediction of MODTRAN 4.1 for zenith angle of 85° in the evening of 16/702.

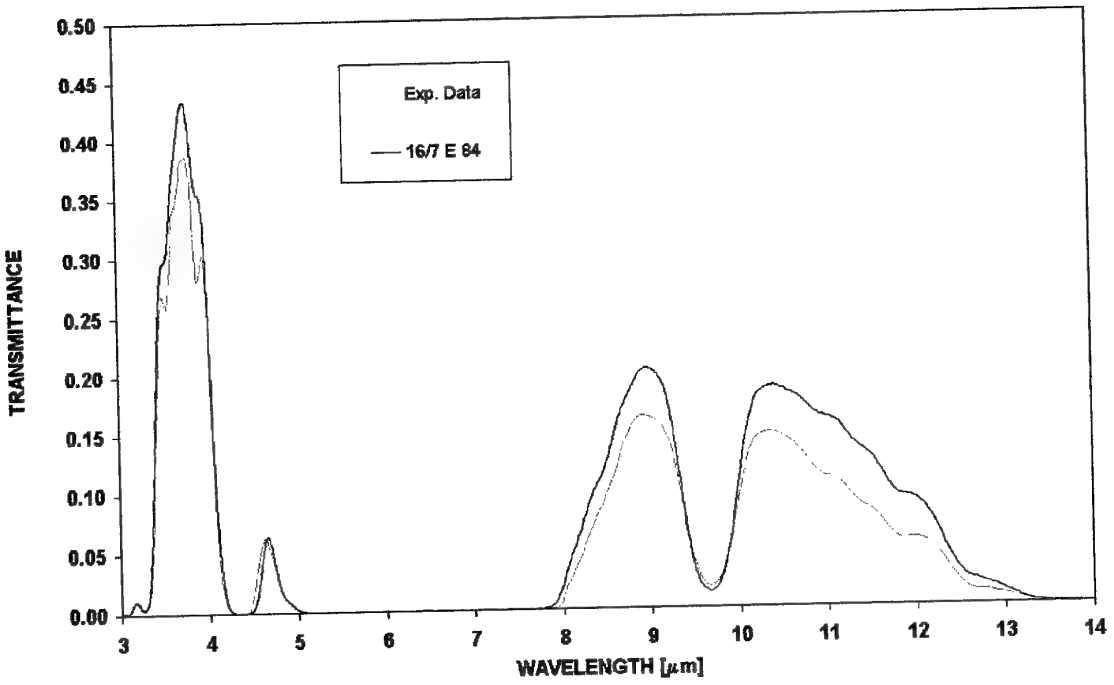

Figure 69: The measured transmittance (Exp. Data) compared to the prediction of MODTRAN 4.1 for zenith angle of 84° in the evening of 16/702.

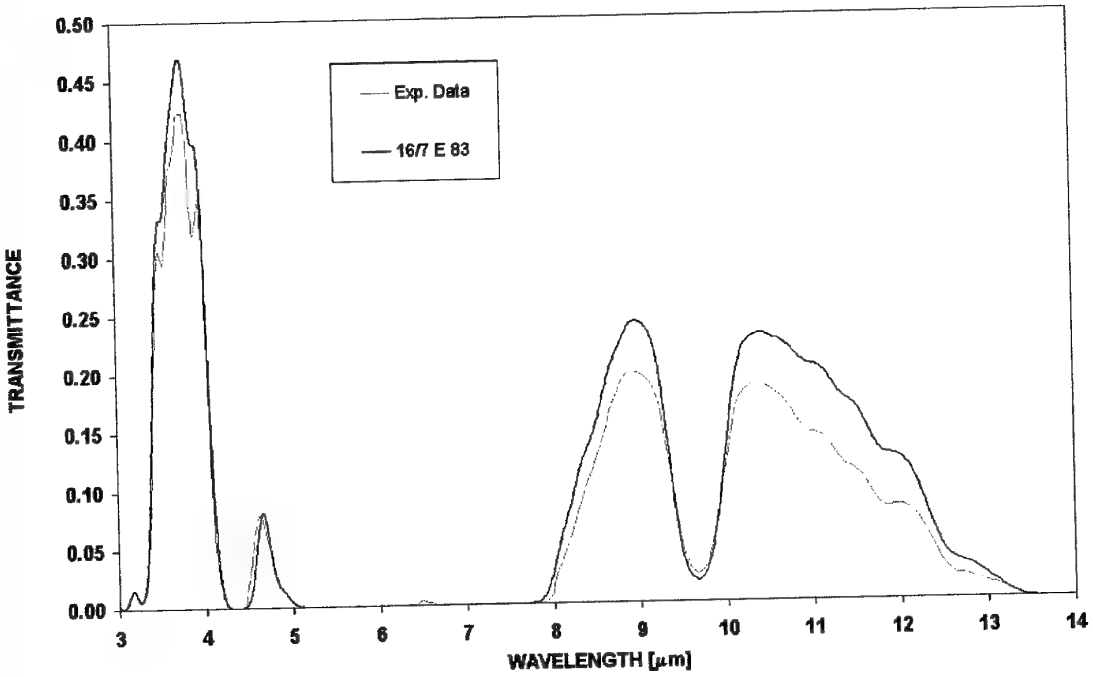

Figure 70: The measured transmittance (Exp. Data) compared to the prediction of MODTRAN 4.1 for zenith angle of 83° in the evening of 16/702.

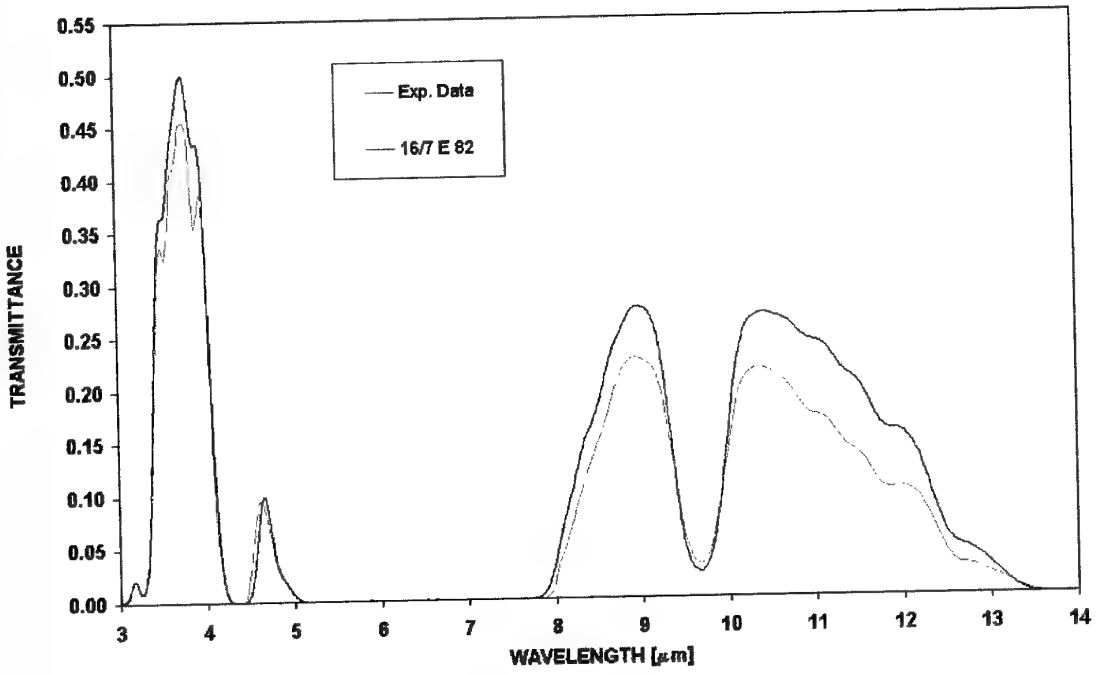

Figure 71: The measured transmittance (Exp. Data) compared to the prediction of MODTRAN 4.1 for zenith angle of 82° in the evening of 16/702.

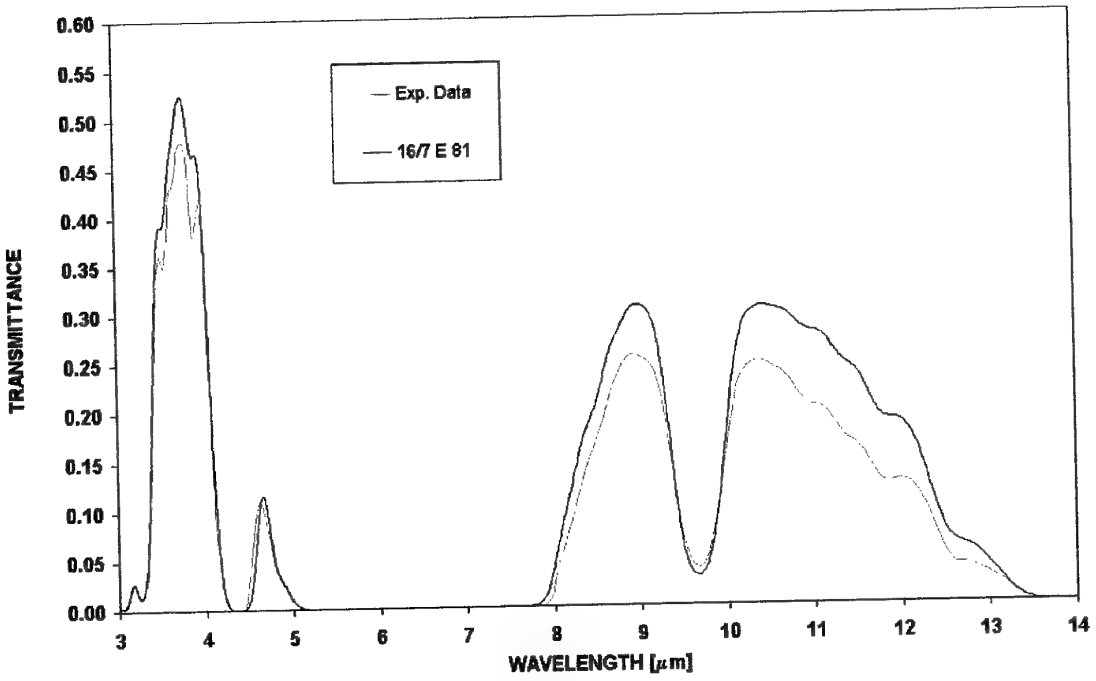

Figure 72: The measured transmittance (Exp. Data) compared to the prediction of MODTRAN 4.1 for zenith angle of 81° in the evening of 16/702.

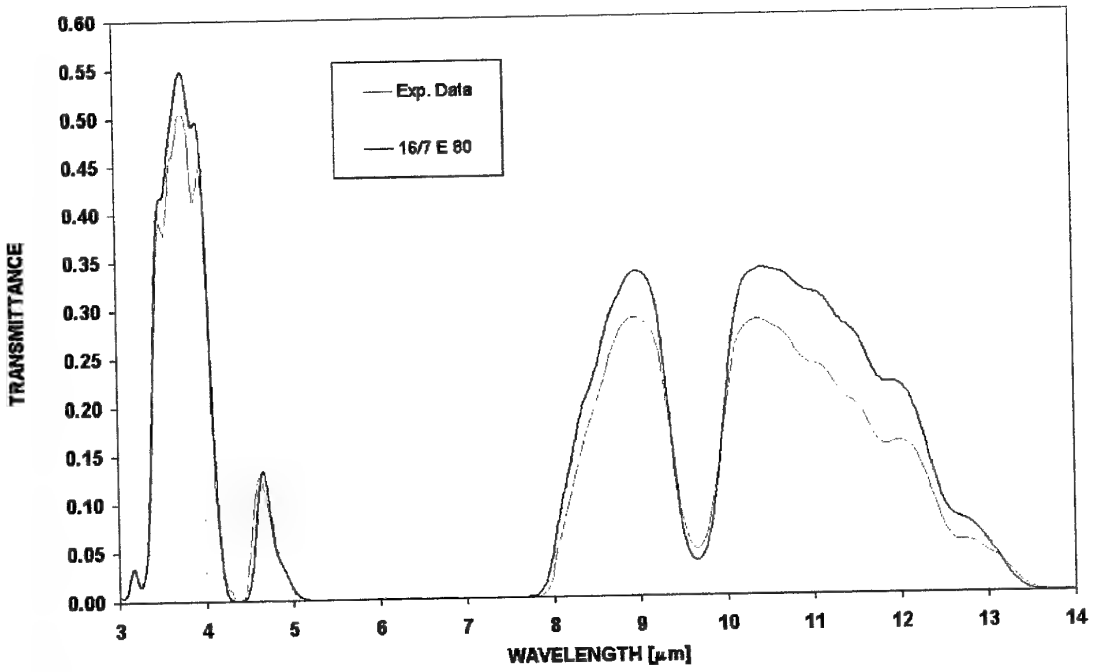

Figure 74: The measured transmittance (Exp. Data) compared to the prediction of MODTRAN 4.1 for zenith angle of 80° in the evening of 16/702.

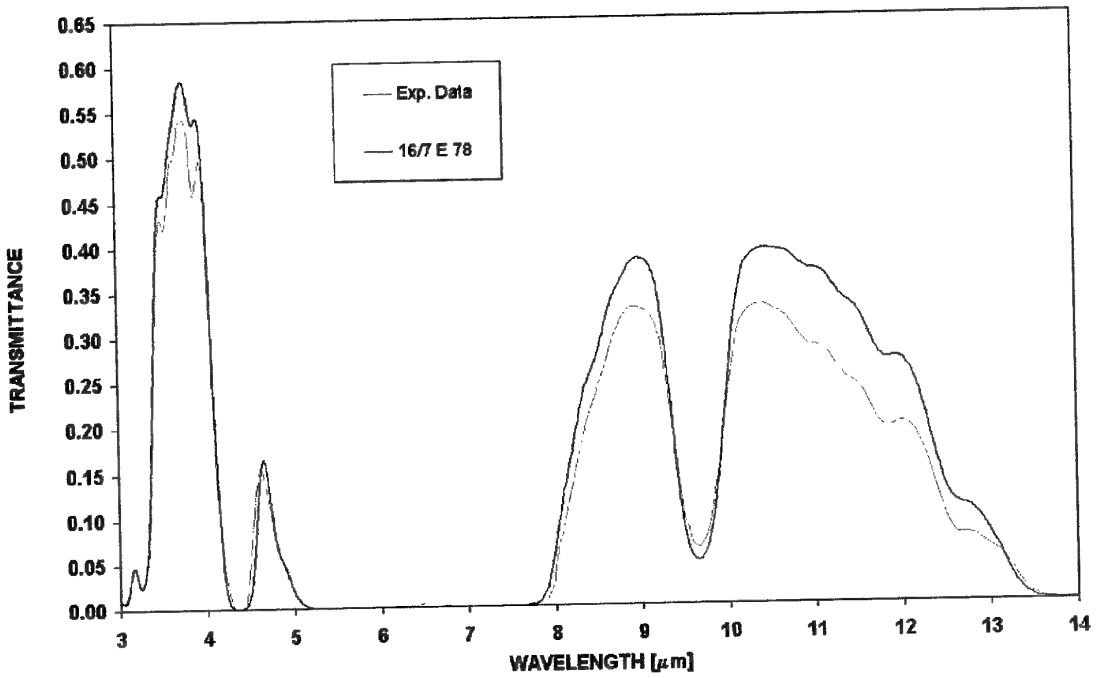

Figure 75: The measured transmittance (Exp. Data) compared to the prediction of MODTRAN 4.1 for zenith angle of 78° in the evening of 16/702.

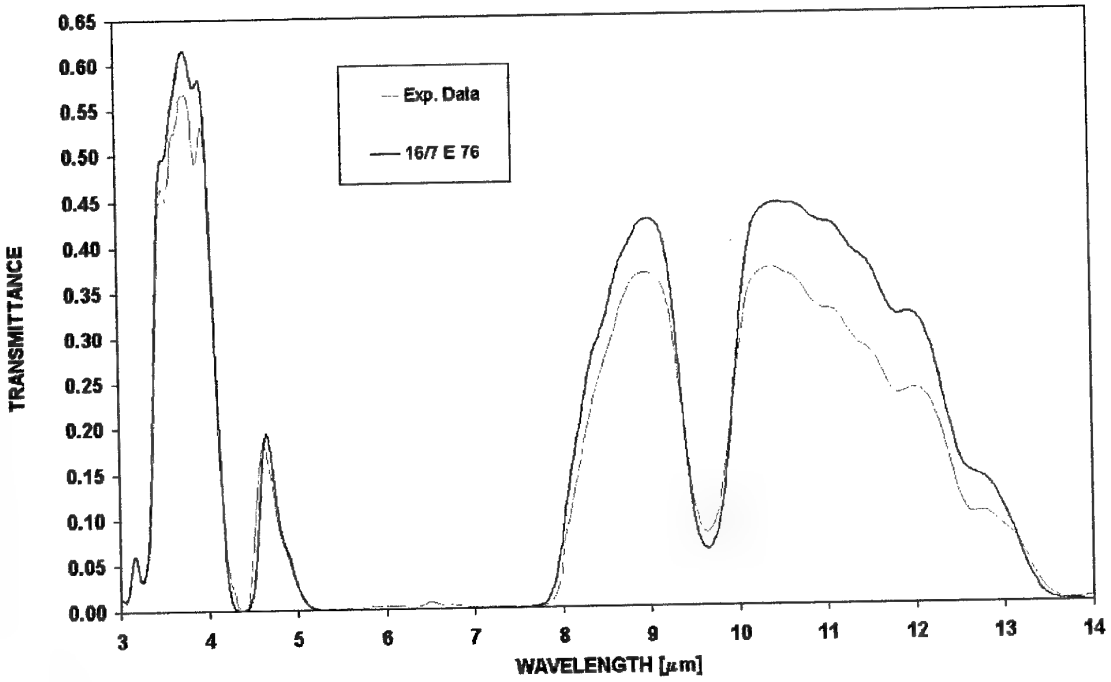

Figure 76: The measured transmittance (Exp. Data) compared to the prediction of MODTRAN 4.1 for zenith angle of 76° in the evening of 16/702.

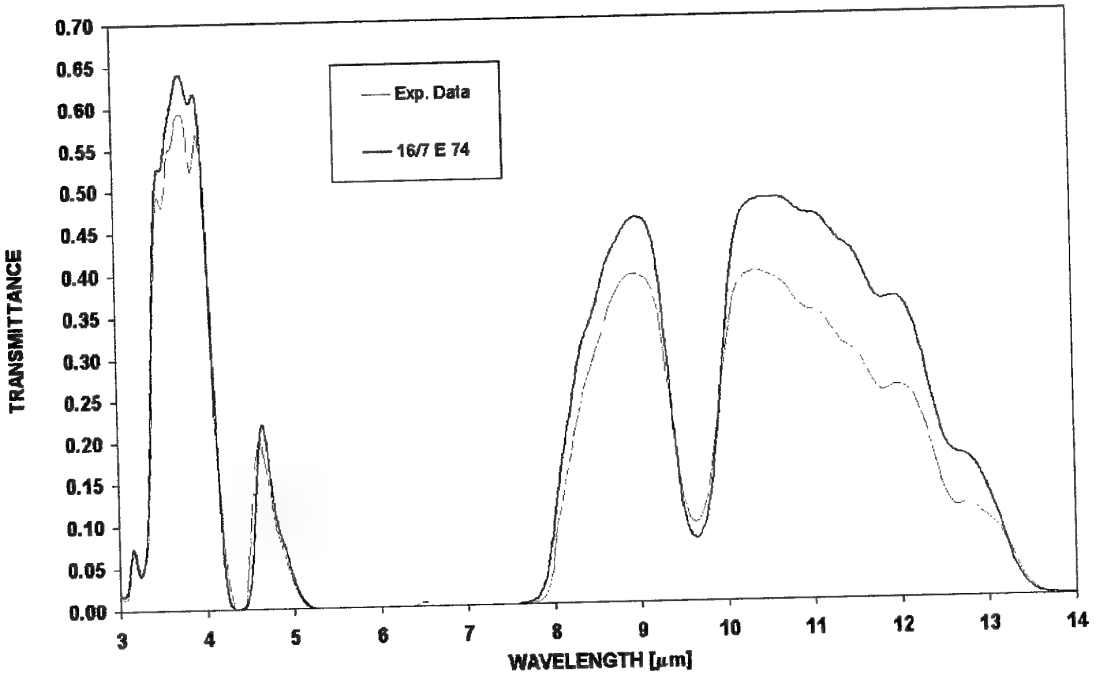

Figure 77: The measured transmittance (Exp. Data) compared to the prediction of MODTRAN 4.1 for zenith angle of 74° in the evening of 16/702.

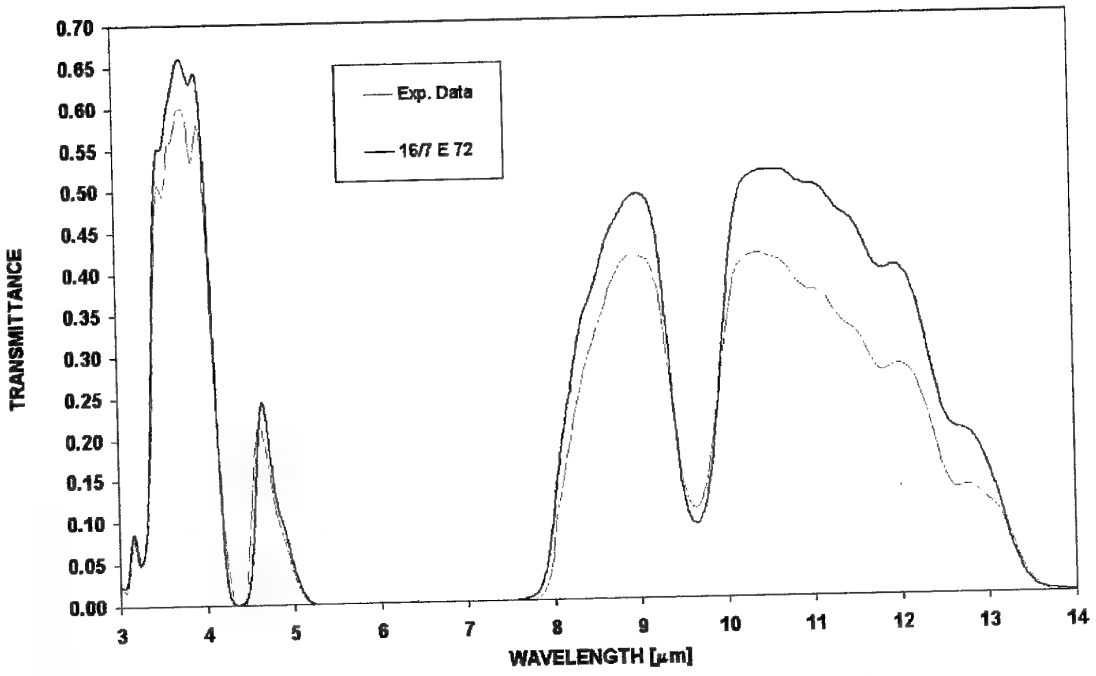

Figure 78: The measured transmittance (Exp. Data) compared to the prediction of MODTRAN 4.1 for zenith angle of 72° in the evening of 16/702.

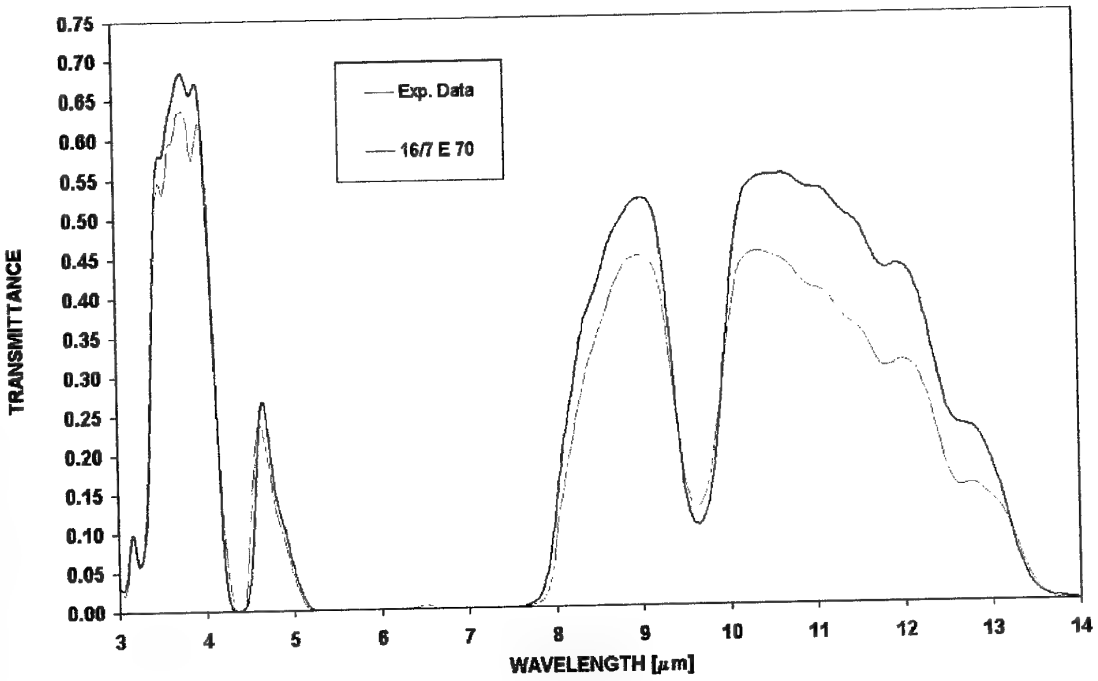

Figure 79: The measured transmittance (Exp. Data) compared to the prediction of MODTRAN 4.1 for zenith angle of 70° in the evening of 16/702.

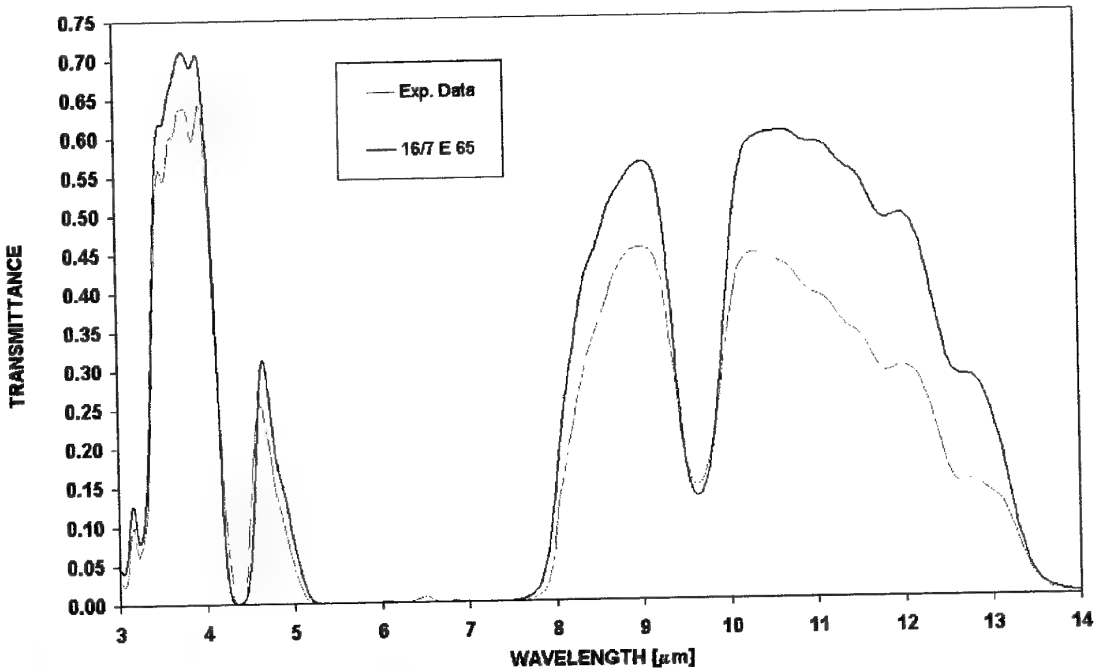

Figure 80: The measured transmittance (Exp. Data) compared to the prediction of MODTRAN 4.1 for zenith angle of 65° in the evening of 16/702.

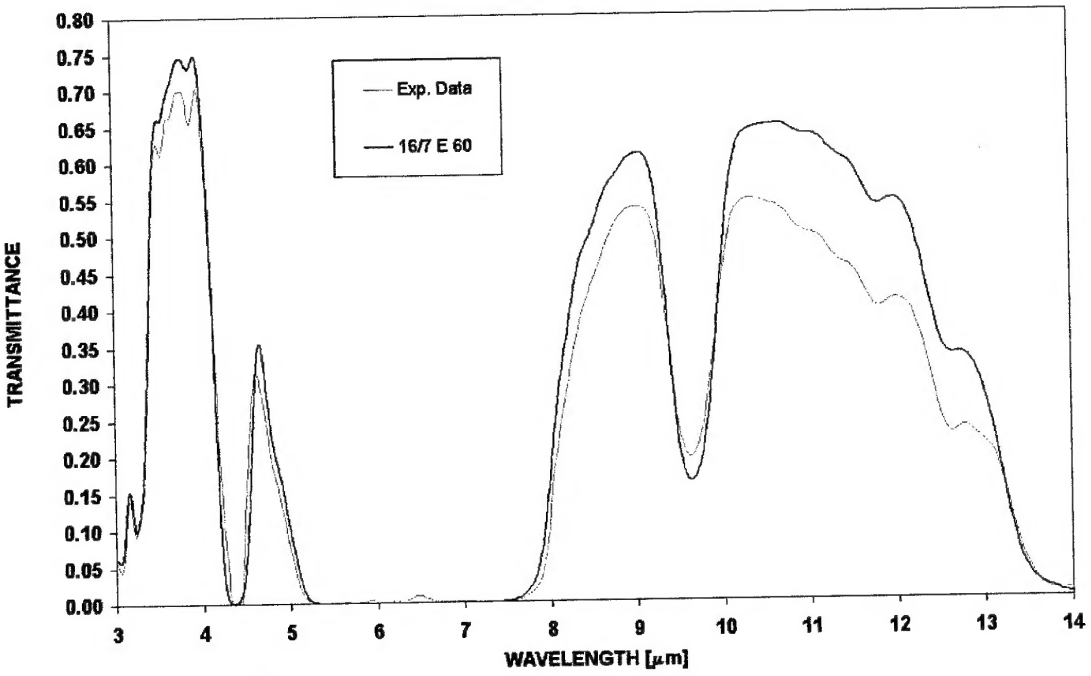

Figure 81: The measured transmittance (Exp. Data) compared to the prediction of MODTRAN 4.1 for zenith angle of 60° in the evening of 16/702.

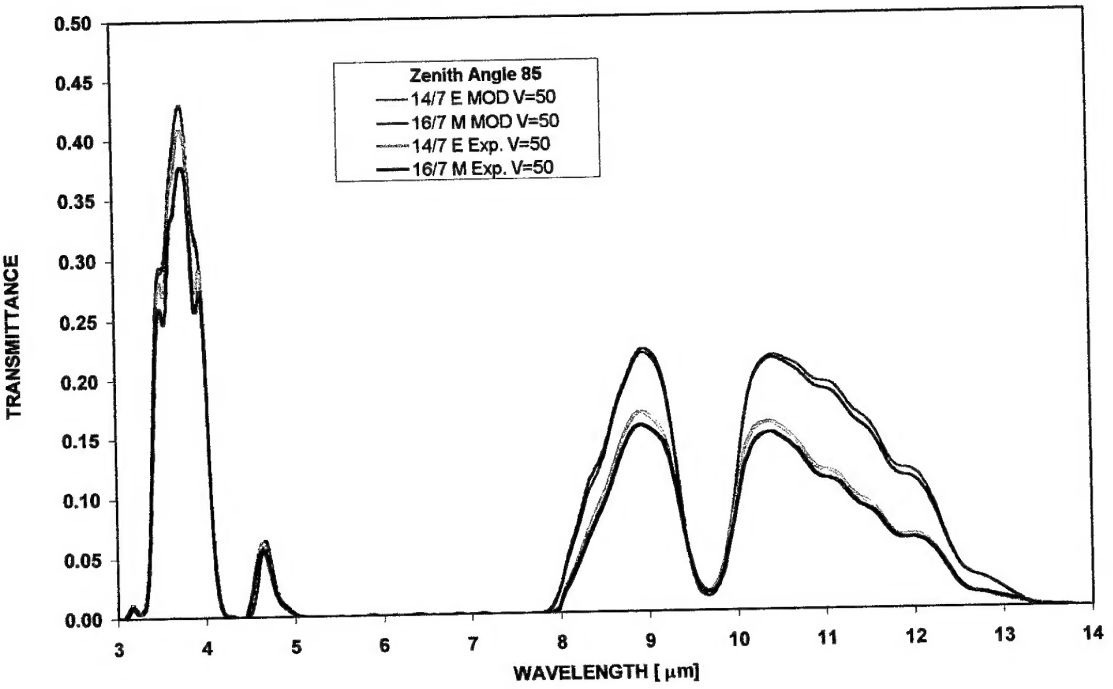

Figure 82: Comparison between the experimental data and the MODTRAN predictions for zenith angle of 85° in the evening of 14/7 and the morning of the 16/7.

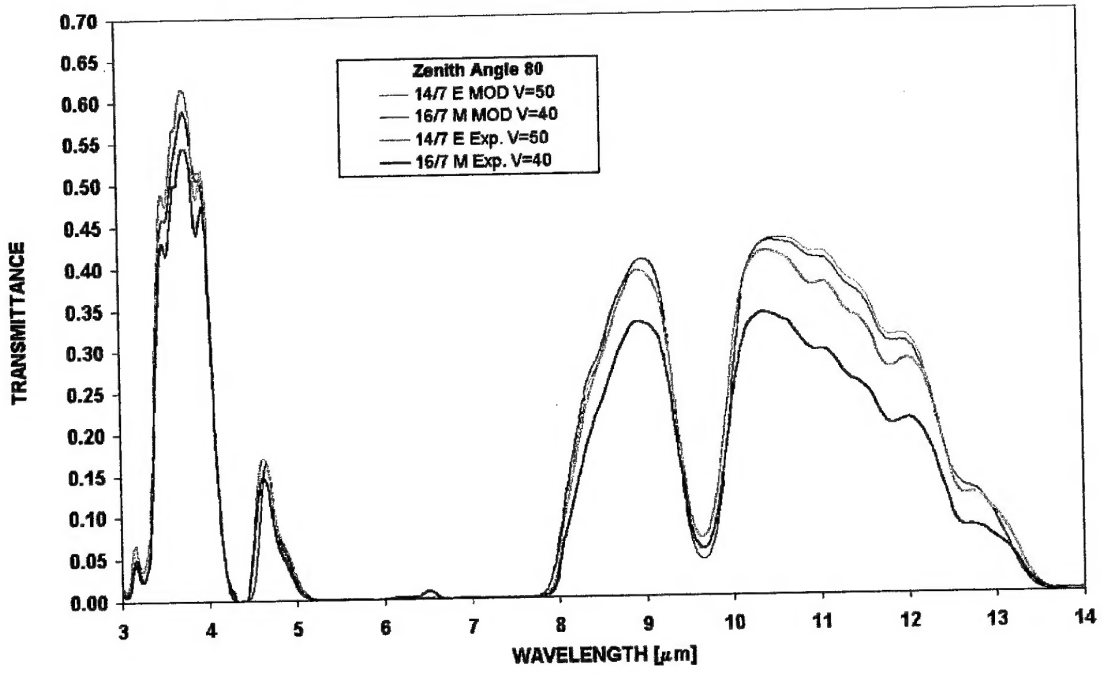

Figure 83: Comparison between the experimental data and the MODTRAN predictions for zenith angle of 80° in the evening of 14/7 and the morning of the 16/7.

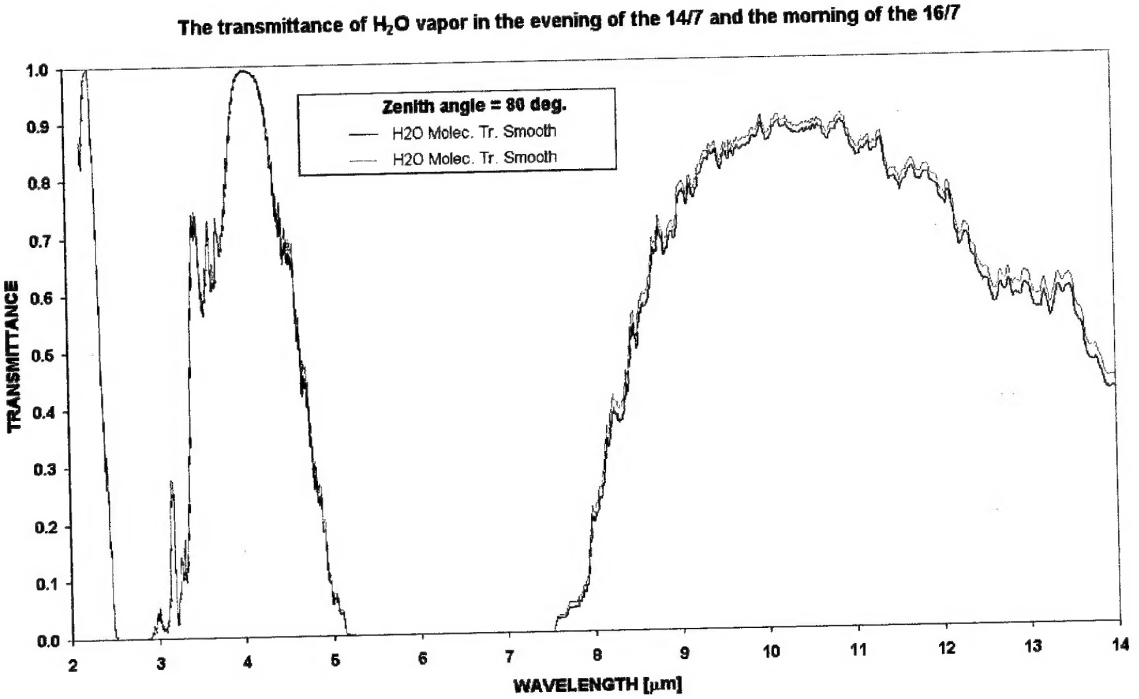

Figure 84: The predicted transmittance of water vapour for zenith angle of 80° in the evening of 14/7 and the morning of the 16/7.

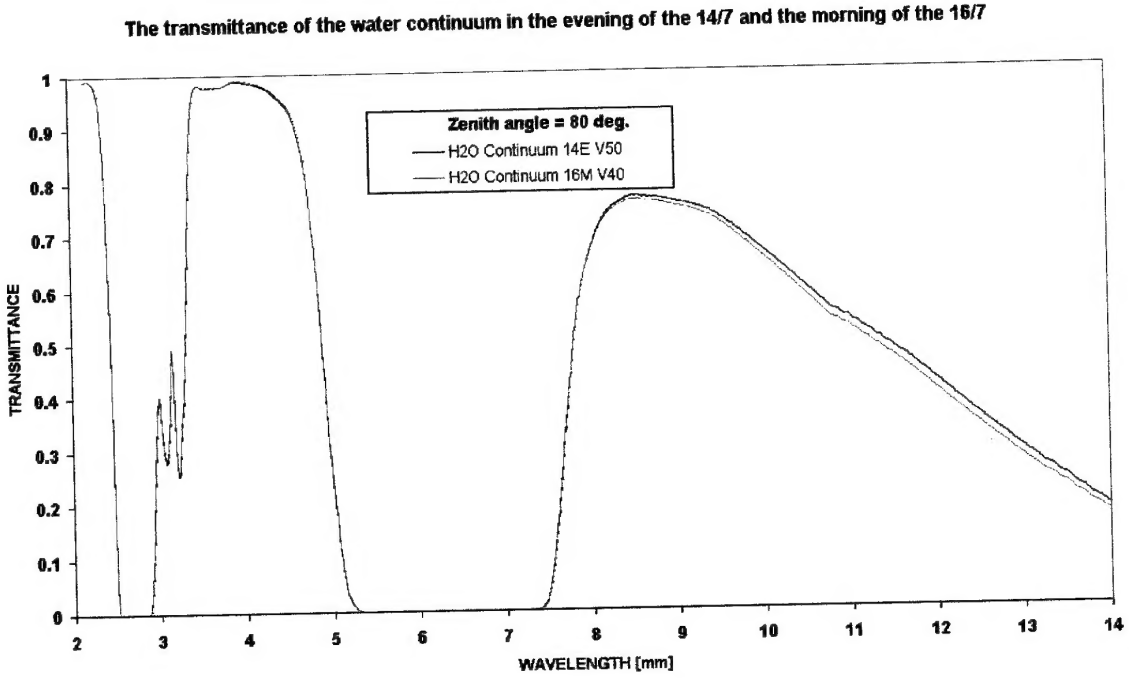

Figure 85: The predicted transmittance of water continuum for zenith angle of 80° in the evening of 14/7 and the morning of the 16/7.

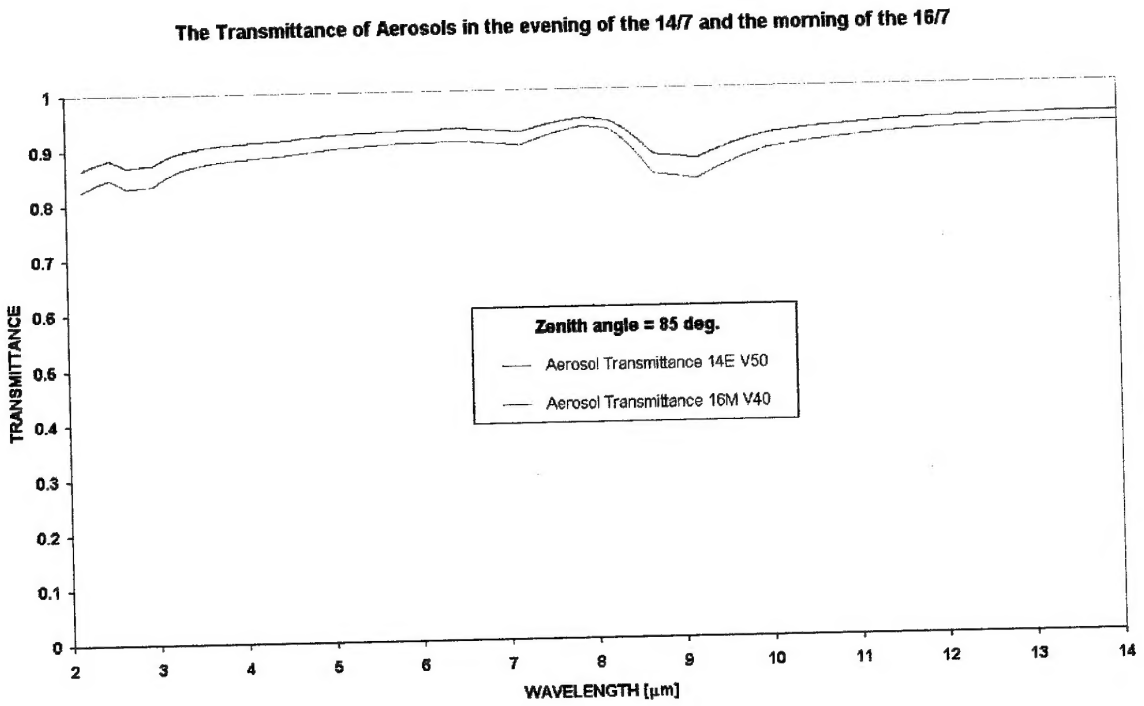

Figure 86: The predicted transmittance of the aerosols for zenith angle of 85° in the evening of 14/7 and the morning of the 16/7.

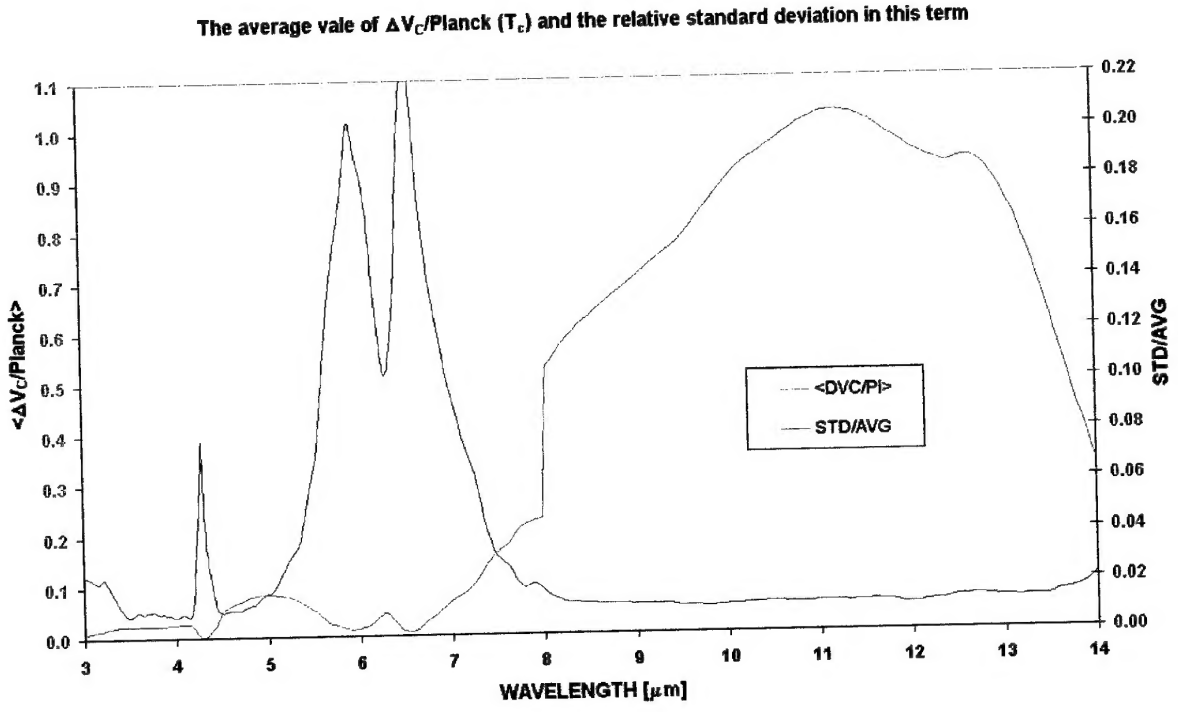

Figure 87: The average value of the term $\Delta V_c(\lambda)/\text{Planck}(T_c)$ and its relative error